A Numerical Investigation Of The Canonical Duality Method For Non-Convex Variational Problems

Haofeng Yu

Dissertation submitted to the Faculty of the
Virginia Polytechnic Institute and State University
in partial fulfillment of the requirements for the degree of

Doctor of Philosophy
in
Mathematics

Traian Iliescu, Chair
Jeff Borggaard
John Burns
Raffaella De Vita

September 19, 2011
Blacksburg, Virginia

Keywords: Duality, Non-convex Variational Problems, Semi-linear Equations, Global Optimization, Canonical Duality Theory, Canonical Dual Finite Element Method, Ericksen's Bar, Landau-Ginzburg Problem.

A Numerical Investigation Of The Canonical Duality Method For Non-Convex Variational Problems

Haofeng Yu

(ABSTRACT)

This thesis represents a theoretical and numerical investigation of the canonical duality theory, which has been recently proposed as an alternative to the classic and direct methods for non-convex variational problems. These non-convex variational problems arise in a wide range of scientific and engineering applications, such as phase transitions, post-buckling of large deformed beam models, nonlinear field theory, and superconductivity. The numerical discretization of these non-convex variational problems leads to global minimization problems in a finite dimensional space.

The primary goal of this thesis is to apply the newly developed canonical duality theory to two non-convex variational problems: a modified version of Ericksen's bar and a problem of Landau-Ginzburg type. The canonical duality theory is investigated numerically and compared with classic methods of numerical nature. Both advantages and shortcomings of the canonical duality theory are discussed. A major component of this critical numerical investigation is a careful sensitivity study of the various approaches with respect to changes in parameters, boundary conditions and initial conditions.

Dedication

To my wife Cedar and my lovely daughter Brooke. They are my strength and inspiration.

Acknowledgments

First of all, I would like to thank especially Dr. Iliescu for his consistent help and encouragement, without which this thesis couldn't be finished. The tremendous gratitude is also extended to my other committee members: Dr. Borggaard and Dr. Burns from the Department of Mathematics and Dr. De Vita from the Engineering Science and Mechanics Department at Virginia Tech.

I should give my thanks to Dr. Haskell for his kind suggestions and encouragement. I would also like to thank Dr. Gao for his help and lessons, both in academia and in life.

Thank you, the math department at Virginia Tech, for supporting me to finish my study and write this thesis.

Thank you, Blacksburg, Ruston and Ping Ding Shan, my three hometowns, for nurturing my body and soul.

Lastly, I am thankful to God. He has been the Light in my life during the dimmer moments.

Contents

1 Introduction **1**

1.1 Double-Well Structure 2

1.2 Classic and Direct Methods 4

1.3 Motivation and Outline of Thesis 6

2 Canonical Dual Theory **7**

2.1 Introduction to Duality 7

2.2 Traditional Duality and Duality Gap 8

2.3 Canonical Duality Theory and Perfect Duality 12

2.3.1 Canonical Duality Theory 12

2.3.2 Canonical Duality Formulation 16

3 Numerical Methods **20**

3.1 Numerical Methods for ODEs 20

3.2 Numerical Methods for PDEs 22

3.2.1 The Finite Difference Method (FDM) 22

3.2.2 The Finite Element Method (FEM) 23

3.3 Numerical Methods for Nonlinear Equations 25

3.3.1 Fixed Point (Picard) Iteration 26

3.3.2 Newton's Method 26

3.4 Numerical Methods for Optimization 27

4 A Numerical Investigation of A Modified Version of Ericksen's Bar 29

4.1 A Modified Version of Ericksen's Bar 30

4.2 Canonical Dual Methods for the Modified Version of Ericksen's Bar 33

4.3 The Soft Device 38

4.3.1 Theoretical Results 39

4.3.2 Numerical Examples 44

4.4 The Hard Device 63

4.4.1 Theoretical Results 64

4.4.2 Numerical Example 64

4.5 Summary 65

5 A Numerical Investigation of a Non-Convex Problem of Landau-Ginzburg Type 67

5.1 A Non-Convex Problem of Landau-Ginzburg Type 68

5.2 Canonical Dual Variational Principle 71

5.3 Canonical Dual Finite Element Method 73

5.4 Application to One-Dimensional Problems 78

5.4.1 Canonical Dual FEM Formulation 78

5.4.2 Standard Numerical Methods 79

5.4.3 Numerical Results 81

5.5 Application to Two-Dimensional Problems 88

5.5.1 Canonical Dual FEM Formulation 89

5.5.2 Standard Numerical Methods 91

5.5.3 Numerical Results 92

5.6 Summary 96

6 Summary and Future Work 97

Bibliography **100**

List of Figures

1.1 Fine layered micro-structures in phase transitions and twinning in solids [94]. 1

1.2 Effect of driving force f_u on potential diagrams $J(u)$: (a) $f_u > f_c$; (b) $f_u = f_c$; (c) $f_u = 0$; (d) $f_u < 0$. The horizontal axis is the u-axis. The vertical axis is the J-axis. 4

2.1 Framework in linear systems [33]. 10

2.2 Framework in fully nonlinear systems [33]. 13

4.1 Plots of (a) non-convex $W(\gamma)$ for $\mu = 1.5$, $\nu = 4$, $\alpha = 1.5$; (b) its derivative $\sigma = W'(\gamma)$; (c) double-well energy $W(\gamma)$; and (d) its non-monotone derivative $\sigma = W'(\gamma)$ for $\mu = 1$, $\nu = 3$, $\alpha = 2.5$. 32

4.2 Dual algebraic curves $\sigma(\zeta) - \mu\alpha = \pm(\zeta + \mu)\sqrt{2\nu^{-1}\zeta + \alpha^2}$: (a) $\mu = 1, \nu = 4, \alpha = 0.5\,(\eta < 0)$; (b) $\mu = 1.5, \nu = 4, \alpha = 1.5\,(\eta > 0)$. The vertical axis is the h-axis. 36

4.3 Plot of $\sigma = W'(\gamma)$ against γ for $\mu = 1.5, \nu = 4, \alpha = 1.5$ together with the Maxwell line (dashed) at $\sigma = \mu\alpha = 2.25$, which cuts off two equal closed areas from the σ curve. 38

4.4 Example 4.1A - Solutions by the FPI-FDM using various mesh sizes: $h = 0.1,\ 0.05,$ and 0.025. 47

4.5 Example 4.1A - NM-FDM vs the FPI-FDM. 48

4.6 Example 4.1A - Forces in the modified version of Ericksen's bar. 48

4.7 Example 4.1A - Dual (4.25) and primal solutions (4.47) with $t = 0.1$. Also shown in (b) is the FPI-FDM solution u_0. The horizontal axis is the x-axis for both plots. The vertical axis is (a) the ζ-axis and (b) the u-axis. 49

4.8 Example 4.1B - Forces in the modified version of Ericksen's bar. 50

4.9 Example 4.1B - Dual (4.25) and primal solutions (4.47) with $t = 1$. Also shown in (b) is the FPI-FDM solution u_0. The horizontal axis is the x-axis for both plots. The vertical axis is (a) the ζ-axis and (b) the u-axis. 50

4.10 Example 4.1C - Forces in the modified version of Ericksen's bar. 51

4.11 Example 4.1C - Dual (4.25) and primal solutions (4.47) with $t = 2$. Also shown in (b) is the FPI-FDM solution u_0. The horizontal axis is the x-axis for both plots. The vertical axis is (a) the ζ-axis and (b) the u-axis. 52

4.12 Example 4.2 - Forces in the modified version of Ericksen's bar. 52

4.13 Example 4.2 - Dual (4.25) and primal solutions (4.47). Also shown in (b) is the FPI-FDM solution u_0. The horizontal axis is the x-axis for both plots. The vertical axis is (a) the ζ-axis and (b) the u-axis. 53

4.14 Example 4.3 - Forces in the modified version of Ericksen's bar. 54

4.15 Example 4.3 - Dual (4.25) and primal solutions (4.47). The horizontal axis is the x-axis for both plots. The vertical axis is (a) the ζ-axis and (b) the u-axis. 54

4.16 Example 4.3 - Plot of the primal solutions $\bar{u}_i$, $i = 1, 2, 3$, and the smooth solution u_s, together with the FPI-FDM solution u_0. The horizontal axis is the x-axis; the vertical axis is the u-axis. 55

4.17 Example 4.3 - Intermediate FPI-FDM iterative solutions for the fourth, fifth and sixth iterations (second and third columns for $x = 0.5, 0.9$, respectively), and $(u_x)^k(x)$ (indicated by the dots), along with the energy density curve $E(u_x)$. The left-hand column shows the corresponding solutions for $x \in [0, 1]$. 56

4.18 Example 4.3 - Dual solutions ζ_i, $i = 1, 2, 3$ from Fig. 4.15(a), with integrand functions $E(u_x)$ against u_x at $x = 0.4, 0.62, 0.7, 0.8, 0.9$. 57

4.19 Example 4.3 - The integrand function of P_s vs u_x (solid curve) and the integrand function of P_s^d vs ζ (dashed curve) at different locations: (a) $x = 0.62$; (b) $x = 0.7$; (c) $x = 0.8$; (d) $x = 0.9$. 58

4.20 Example 4.4 - Forces in the modified version of Ericksen's bar. 59

4.21 Example 4.4 - Dual (4.25) and primal solutions (4.47). The horizontal axis is the x-axis for both plots. The vertical axis is (a) the ζ-axis and (b) the u-axis. 59

4.22 Example 4.4 - Intermediate FPI-FDM iterative solutions (second and third columns for $x = 0.2, 0.8$, respectively), and $(u_x)^k(x)$ (indicated by the short vertical red lines), along with the energy density curve $E(u_x)$. The left-hand side column shows the corresponding solutions for $x \in [0, 1]$. 60

4.23 Example 4.5 - Forces in the modified version of Ericksen's bar. 61

4.24 Example 4.5 - Dual (4.25) and primal solutions (4.47). The horizontal axis is the x-axis for both plots. The vertical axis is (a) the ζ-axis and (b) the u-axis. 61

4.25 Example 4.5 - Multiple solutions. 62

4.26 Example 4.6 - Dual (4.25) and primal solutions (4.47) : (a) dual solutions ζ_i, $i = 1, 2, 3$, for $\sigma(1) = 2.0549$; (b) primal solutions $\bar{u}_1$, and the FPI-FDM solution u_0. The horizontal axis is the x-axis for both plots. The vertical axis is (a) the ζ-axis and (b) the u-axis. 65

5.1 Effect of driving force f_u on potential diagrams $J(u)$ given by (5.9). The horizontal axis is the u-axis. The vertical axis is the J-axis. 70

5.2 The singular elliptic curve of dual solutions for equation (5.23). 74

5.3 Example 5.1 - Solutions obtained by: (a) FPI-FDM; (b) NM-FDM; (c) NS-FDM; (d) canonical dual FEM using various mesh sizes, compared with the exact solution u_0. 83

5.4 Example 5.1 - Exact solution and numerical approximations (FPI-FDM, NM-FDM, NS-FDM and Dual FEM). 84

5.5 Example 5.2 - Exact solution and numerical approximations (FPI-FDM, NM-FDM, NS-FDM and Dual FEM). 85

5.6 Example 5.3 - Exact solution and numerical approximations (FPI-FDM, NM-FDM, NS-FDM and Dual FEM). 86

5.7 Example 5.4 - For different initial guesses, the FPI-FDM yields multiple solutions, u_1, u_2 and u_3. The canonical dual FEM yields a unique solution u_{min}, which is a global minimizer. 87

5.8 Sample two-dimensional mesh for the canonical dual FEM. 89

5.9 Sample two-dimensional mesh for the FPI-FDM. 92

5.10 Example 5.5 - Exact solution u, multiple solutions $\bar{u}_1, \bar{u}_2$ by the FPI-FDM and global minimizer solution $\bar{u}$ by the canonical dual FEM. 93

5.11 Example 5.6 - Exact solution u, multiple solutions $\bar{u}_1, \bar{u}_2$ by the FPI-FDM and global minimizer solution $\bar{u}$ by the canonical dual FEM. 94

5.12 Example 5.7 - Multiple solutions $\bar{u}_1, \bar{u}_2$ and $\bar{u}_3$ by the FPI-FDM and global minimizer solution $\bar{u}$ by the canonical dual FEM. 95

List of Tables

4.1 Summary of the numerical examples for the soft device. 63

5.1 Example 5.1 - Profiles of the four numerical methods tested: FPI-FDM, NM-FDM, NS-FDM, and Dual FEM. For various mesh sizes h, the number of iterations, the total execution time and the error are listed. 82

5.2 Example 5.2 - Profiles of the four numerical methods tested: FPI-FDM, NM-FDM, NS-FDM, and Dual FEM. The number of iterations, the total execution time and the error are listed. 86

5.3 Example 5.3 - Profiles of the four numerical methods tested: FPI-FDM, NM-FDM, NS-FDM, and Dual FEM. The number of iterations, the total execution time and the error are listed. 87

Chapter 1

Introduction

Both convex and non-convex phenomena arise naturally from real-life systems. While convex problems can be relatively easier to solve using classical convex analysis, non-convex problems are generally more complicated. Fig. 1.1 shows experimental observations of phase transitions and twinning in solids, which reveal fine layered micro-structures; this is an example of non-convex problems [94]. Unfortunately, many problems in modern mechanics, science, and economics require

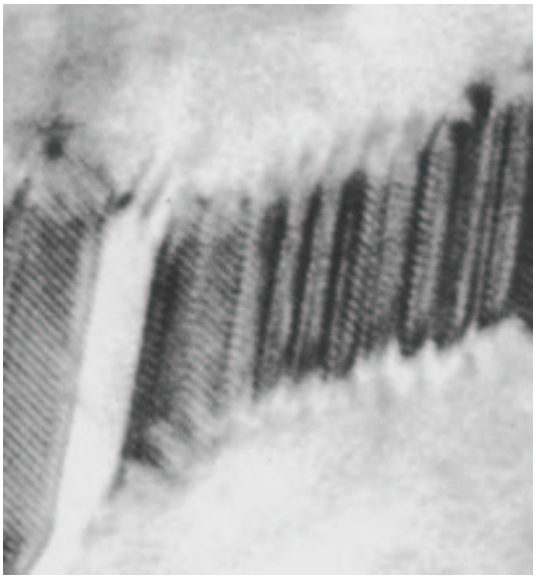

Figure 1.1: Fine layered micro-structures in phase transitions and twinning in solids [94].

the consideration of non-convexity for their accurate mathematical modeling.

In this thesis, the author focuses on a problem of non-convex type, namely, a primal problem ($\mathcal{P}$),

in the form of:

$$(\mathcal{P}): \quad P(u) = \frac{1}{2}\langle u, Au\rangle + W(u) - \langle u, f\rangle, \tag{1.1}$$

where the feasible space $\mathcal{U}_k$ is a convex subset of a normed space $\mathcal{U}$ with non-empty interior; $A : \mathcal{U} \to \mathcal{U}^*$ is a linear, self-adjoint operator such that $A = A^*$, which maps each $u \in \mathcal{U}$ into its dual space $\mathcal{U}^*$; the bilinear form $\langle u, u^*\rangle : \mathcal{U} \times \mathcal{U}^* \to \mathbb{R}$ puts $\mathcal{U}$ and $\mathcal{U}^*$ in duality; $W : \mathcal{U} \to \mathbb{R}$ is a given function(al), either convex or non-convex; $f \in \mathcal{U}^*$ is a given input; and $P(u) : \mathcal{U}_k \to \mathbb{R}$ represents the total cost (energy) function.

In the case that the non-convex function in (1.1) is Gâteaux differentiable, the stationary (or criticality) condition $DP(u) = 0$ leads to a governing equation [31]

$$Au + DW(u) = f, \tag{1.2}$$

where $DW(u)$ represents the Gâteaux derivative of $W(u)$ at u. Finding all critical points of the non-convex function $P(u)$, especially identifying the one with minimal (maximal) cost (potential) has been investigated in numerous studies (specific examples are given in Section 1.1) and may provide new insight into natural phenomena, like the one in Fig. 1.1.

1.1 Double-Well Structure

In non-convex mechanics and variational problems, where $\mathcal{U}$ is an infinite dimensional function space, the state variable u is a field function, and $A: \ U \to U^*$ is usually a partial differential operator over a given space domain $\mathbb{R}^n$. In this case, the governing equation (1.2) is a so-called *semi-linear equation*, which plays an important role in materials science and physics including ferroelectricity, liquid crystals, ferromagnetism, ferroelectricity, and superconductivity [36]. For example, in traditional Landau-Ginzburg theory of the second-order ferroelectric transformations, the Landau potential $W(u)$ can be reduced to a *double-well* function

$$W(u) = \frac{1}{2}\alpha\left(\frac{1}{2}|u|^2 - \beta\right)^2, \tag{1.3}$$

where $\alpha,\ \beta > 0$ are material constants.

When A vanishes, the primal problem $(\mathcal{P})$ is reduced to:

$$(\mathcal{P}_w): \quad P(u) = W(u) - \langle u, f\rangle. \tag{1.4}$$

Accordingly, its Euler-Lagrange equation is

$$DW(u) = f. \tag{1.5}$$

This type of problems appear in many physical systems such as hysteresis and phase transitions, non-convex optimal design and control, nonlinear bifurcation and stability analysis of finite deformation theory, nonlinear elasticity with residual strain, post-buckling of large deformed structures, such as Ericksen's bar problem [22], the twinning of crystals [23], the Azimuthal shear problem [46], etc.

If $A = -\Delta$ is simply the Laplacian operator and $W(u)$ is defined in (1.3), then (1.2) leads to a second-order *partial differential equation* (PDE), which is similar to the second-order Landau-Ginzburg equation [97, 33, 36]:

$$-\Delta u + \alpha \left(\frac{1}{2}|u|^2 - \beta \right) u = f. \tag{1.6}$$

If $A = -\Delta + curl\ curl$, then (1.2) is similar to the Cahn-Hilliard equation for liquid crystals [21]. In phase transitions of shape memory alloys, each local minimizer of W corresponds to a certain phase state of the material and each local maximizer characterizes the critical conditions (points) that lead to phase transitions [36]. In unilateral post-bifurcation analysis of beam contact problems, the solution of the post-buckling state is usually a local minimizer [33].

In dynamical systems, if $A = k_0\partial_{tt} - \Delta$, then (1.2) is the well-known Sine-Gordon equation [60]:

$$k_0\ddot{u}(t) - \Delta u = sin(u) + f. \tag{1.7}$$

This equation appears in many branches of physics, such as the theory of dislocations in metal and Josephson junctions [36]. In the one-dimensional case, it is similar to the Duffing equation in the real domain [97]:

$$k_0\ddot{u}(t) - \alpha u(t)(\lambda - \frac{1}{2}u(t)^2) = f. \tag{1.8}$$

It has been shown that even for this simple one-dimensional *ordinary differential equation* (ODE) [36], an analytic solution is very difficult to obtain. Furthermore, the equation is extremely sensitive to the parameters λ, α, the input (external force) f, and the initial condition $u(0)$.

Mathematically speaking, the so-called chaotic phenomena in nonlinear dynamics are mainly due to the non-convexity of the total energy $P(u)$ in (1.1). Very small perturbations of the system's initial conditions and parameters may lead the system to different local minimizers with significantly different performance characteristics [36]. To illustrate this, we consider the double-well potential (1.3), since it is structurally simple. Its total energy associated with the semi-linear equation (1.2) is

$$P(u) = \int_\Omega \left[\frac{1}{2}\alpha \left(\frac{1}{2}|u|^2 - \lambda \right)^2 - u(f - Au) \right] \mathrm{d}\Omega. \tag{1.9}$$

The changing of f modifies the shape of the energy density curve. To see the influence of the driving force f and the reaction force Au on the critical points of the non-convex energy $P(u)$, we

let $J(u) = \frac{1}{2}\alpha(\frac{1}{2}u^2 - \lambda)^2 - uf_u$ be the so-called energy density, where $f_u = f - Au$. The graph of the energy density $J(u)$ is shown in Fig. 1.2, where f_c is a certain critical force (similar to graphs in [36]).

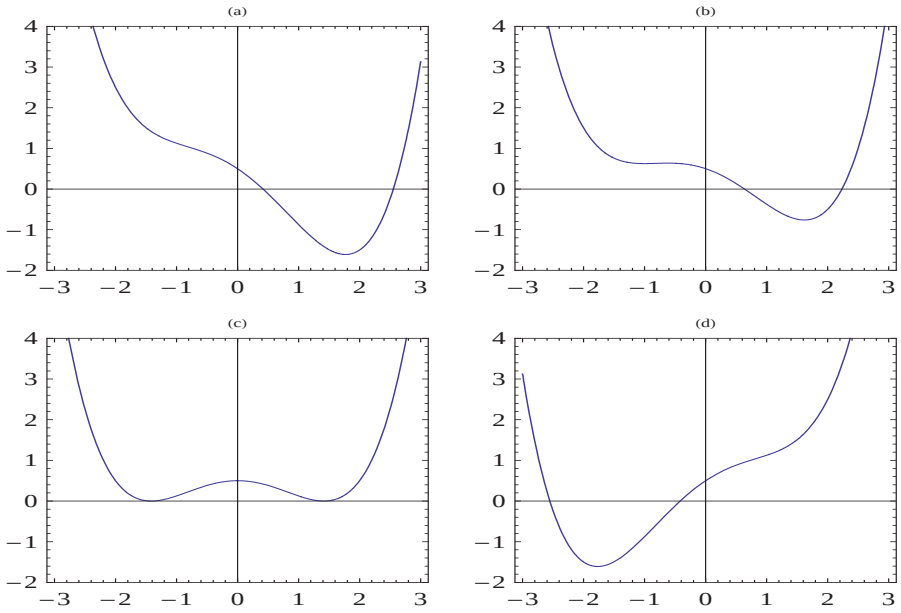

Figure 1.2: Effect of driving force f_u on potential diagrams $J(u)$: (a) $f_u > f_c$; (b) $f_u = f_c$; (c) $f_u = 0$; (d) $f_u < 0$. The horizontal axis is the u-axis. The vertical axis is the J-axis.

Decreasing f_u results in changes in the relative depths of the two minimizers of $J(u)$ and in the height of the local maximizer. The value u, at which the minimizer(s) occur, shifts slightly with f_u. For $f_u > f_c$, the results demonstrate that the potential energy surface has a single potential well (tilts to the right) that is a global minimizer, whereas for $f_u = f_c$, another potential well starts to appear and for $f_u = 0$ it has a double potential well that has two equal local minimizers with a local maximizer in-between. When $f_u < 0$, there a single potential well (tilts to the left) that is a global minimizer. Since the force field f_u depends on the state u (and sometime also on time t), any numerical error at each iteration may lead the state u to very different critical points of the non-convex action $P(u)$. This may be one of the main reasons why traditional perturbation analysis and direct approaches can sometimes fail for non-convex systems.

1.2 Classic and Direct Methods

Classic Methods The calculus of variations has generated numerous results since the 19th century, due to the pioneering work by Bernoulli, Euler, Lagrange, Riemann, Weierstrass, Jacobi,

Hamilton, etc. The methods used in these works are known as *classic* methods. More or less, all these methods include finding zeros of the "derivative" of the functional, in this case, $\mathcal{P}' = 0$, known as the *Euler-Lagrange equation* and then studying the positivity of the second variation around solutions of the Euler-Lagrange equation. There are many necessary and sufficient conditions addressing these issues, such as the Weierstrass, Legendre and Jacobi conditions, etc. [16, 75].

There are numerous ways to solve the induced Euler equations, both linear and nonlinear, both analytical and numerical. More details were discussed by Aubin and Ekeland [5], Ambrosetti and Malchiodi [2], Strang [84], and Hoffman [55]. In this thesis, several numerical approaches for the approximations of the solution of the Euler equation are used. These approximations include numerical methods for ODEs (the nonlinear shooting method), numerical methods for PDEs (the finite difference method and the finite element method), numerical methods for nonlinear equations (the fixed point iteration and Newton's method), and numerical methods for optimization (Quasi-Newton algorithms).

Direct Methods More recently, many different types of optimization problems have attracted the attention of researchers because of their relevance in modern science and technology. Optimal control problems governed by ODEs or PDEs, optimal design problems, shape optimization problems, nonlocal variational problems, and even more classical local variational principles have been analyzed and examined, both analytically and numerically, in the last decades [9, 13, 16, 23, 26, 27, 61, 66, 83, 88].

These studies have led to new developments in optimization theory. The direct methods, especially the relaxation methods, for solving non-convex variational problem have been discussed extensively during this period [85, 65, 73]. The direct methods deal directly with the functional. In a finite dimensional space, to locate the minima, they first try to find a minimizing sequence belonging to a compact set, and then extract a convergent subsequence, which by continuity of the function necessarily converges to a minimum. The idea of the direct method is to reproduce this analysis in the infinite dimensional case, to find such minimizing sequences in a bounded and closed set, and to ensure that the functional P is lower semi-continuous. More details can be found in [16]. It is known that in nonlinear/non-convex variational problems, traditional direct methods can provide only upper bound approaches to the solution. As a result, the so-called relaxation method can be used mainly for finding the global minimizer of the non-convex energy. However, in post-bifurcation analysis and phase transitions, local maximizers usually play a more important role [36]. In this case, the relaxation method for solving non-convex variational problems with three or more phases (potential wells) is more challenging.

1.3 Motivation and Outline of Thesis

Seeing the difficulties and limitations in the classic and direct methods, in this thesis, we take a different approach - we study duality theories for non-convex variational problems. This new research field involves a combination of theoretical analysis in mathematical modeling of natural systems, finite deformation theory, material science, nonlinear PDEs, global optimization, variational methods, dynamical systems, numerical algorithms and scientific computations [33, 48]. It will be shown in the later chapters that, while the problems mentioned in the earlier sections are difficult to solve, from a canonical "dual" perspective, they may be more straightforward.

The primary goal of this thesis is to apply this newly developed canonical duality theory to two non-convex variational problems: a modified version of Ericksen's bar and a problem of Landau-Ginzburg type. This so-called canonical duality theory is investigated numerically and compared with classic methods of numerical nature. A major component of this critical numerical investigation is a careful sensitivity study of the various approaches with respect to changes in parameters, boundary conditions and initial conditions.

The rest of the thesis is organized as follows: In Chapter 2, we review the duality theory, both the traditional Lagragian duality and the canonical duality theory. In Chapter 3, we review several standard numerical methods: the nonlinear shooting method, the finite difference method, the finite element method, the fixed point (Picard) method, Newton's method and optimization techniques. These methods will be used either to facilitate the application of the canonical dual method or to be compared with classic methods. Chapter 4 will focus on the application of the canonical duality theory to a modified version of Ericksen's bar problem. The results obtained with the canonical duality theory will be compared with those obtained with classic methods of numerical flavor. Both advantages and shortcomings of the canonical duality theory will be discussed. A particular emphasis will be put on the sensitivity of the proposed approaches with respect to changes in parameters, boundary conditions and initial conditions. Chapter 5 will focus on the application of the canonical duality theory to a problem of Landau-Ginzburg type. A canonical dual finite element method based on the canonical duality theory will be proposed for solving the nonlinear/non-convex problem. We will also solve the problem by using classic methods of numerical nature, for the purpose of comparison. A careful sensitivity study to test the robustness of the proposed methods with respect to changes in parameters, boundary conditions and initial conditions will also be carried out. Both pros and cons of the canonical dual method will be discussed. In Chapter 6, we will summarize the contributions of this thesis and comment on open problems and future research directions.

Chapter 2

Canonical Dual Theory

Seeing the difficulties and limitations in the classic and direct methods, in this thesis, we seek a different approach - a canonical duality theory. It is an indirect, dual approach, which has been recently developed and comprises a *canonical dual transformation*, a *pure complementary energy principle* and a *triality theory* [28, 31]. In this chapter, first, we introduce the concept of duality, then review the traditional Lagrangian duality, and finally present the canonical duality theory. Thus, a theoretical foundation for the applications presented in later chapters is laid down.

2.1 Introduction to Duality

The concept of *duality* is one of the most successful ideas in modern science. It is pervasive and important in natural phenomena, particularly, in physics and mathematics [29]. Roughly speaking, duality is the product of the interaction that takes place between the paired components of an elementary system. In physics, these components are position and momentum; displacement and force; strain and stress, etc. While these properties take different shapes and forms within each system, they invariably retain their basic nature [29]. In mathematics, duality is a mathematical involution that has numerous meanings and appears in different branches: geometric dualities, contra-variant dualities, analytic dualities, etc. In this thesis, we will focus on analytic duality, where problems are solved by considering the dual description of functions and operators. For convex system, classical duality theory in convex analysis can be found in, e.g., [74, 84, 81, 19, 56]. For con-convex systems, a so-called canonical duality theory was proposed by Gao (see [33]).

In mathematics, it is often desirable to express a functional relationship $F(u)$ as a different function (its dual or conjugate), whose argument is the derivative of $F(u)$, rather than u . If we let $u^* = dF/du$ be the argument of this new function, then this new function is called the *Legendre Transform*

of the original function, named after Adrien-Marie Legendre. In a broader setting, this derivative can be generalized to the Gâteaux derivative. Then, by the definition introduced in [33], a Gâteaux differentiable function $F : \mathcal{U}_a \to \mathbb{R}$ is said to be a *canonical function* on $\mathcal{U}_a$ if its Gâteaux derivative $DF : \mathcal{U}_a \to \mathcal{U}_a^* \subset \mathcal{U}$ is a one-to-one mapping from $\mathcal{U}_a$ onto its range $\mathcal{U}_a^*$. Thus, if $F(u)$ is a canonical function, the duality relation $u^* = DF(u)$ is invertible on $\mathcal{U}_a \times \mathcal{U}_a^*$, and its Legendre conjugate $F^* : \mathcal{U}_a^* \to \mathbb{R}$ can be defined uniquely by the classical Legendre transformation

$$F^*(u^*) = \{\langle u, u^* \rangle - F(u) \mid \ DF(u) = u^*, \ \ u \in \mathcal{U}_a\}. \tag{2.1}$$

The duality pair (u, u^*) is called the *canonical duality pair* on $\mathcal{U}_a \times \mathcal{U}_a^*$ if and only if the *duality relations*

$$u^* = DF(u) \ \ \Leftrightarrow \ \ u = DF^*(u^*) \ \ \Leftrightarrow \ \ F(u) + F^*(u^*) = \langle u, u^* \rangle \tag{2.2}$$

hold on $\mathcal{U}_a \times \mathcal{U}_a^*$.

Note that the Legendre Transform is not the only technique that can be used to form duality. Other techniques, such as *Fenchel Transform* and the canonical dual transformation, which is the central theme of the thesis, will be studied in the rest of the chapter. Though different transformations may lead to different duality pairs, there is one thing in common - they all form a system, the primal and the dual. The theory of duality can be said to be the study of the intrinsic relations between the pair, which has important implications in this thesis - the pair provides us both primal and dual perspectives on the problem.

2.2 Traditional Duality and Duality Gap

Clarke-Ekeland-Lasry Duality [36] is based on a dual action form and was originally given by Clarke in 1985 [15]. It was further developed for the case of convex Hamiltonian systems in the generalized formulation due to Ekeland and Lasry (see [20]). Next, we briefly describe it.

We let $F(u) = \langle u, f \rangle - W(u)$, and assume that $W(u)$ is convex. Therefore, $F(u)$ is concave, a canonical function. The primal function $P(u) = \frac{1}{2}\langle u, Au \rangle + W(u) - \langle u, f \rangle$ in (1.1) can be written in the so-called action form [20]:

$$P(u) = \frac{1}{2}\langle u, Au \rangle - F(u). \tag{2.3}$$

We shall use the notation $F^\sharp$ to denote the *Fenchel inf-conjugate* of F, defined by

$$F^\sharp(u^*) = \inf_{u \in \mathcal{U}_a} \{\langle u, u^* \rangle - F(u)\}.$$

Clearly, $F^\sharp : \mathcal{U}^* \to \mathbb{R} \cup \{-\infty\}$ is always concave, upper semi-continuous. If $F(u)$ is also concave, upper semi-continuous, then the following *Fenchel inf-duality relations* hold on $\mathcal{U}_a \times \mathcal{U}_a^*$:

$$u^* \in \partial^+ F(u) \ \ \Leftrightarrow \ \ u \in \partial^+ F^\sharp(u^*) \ \ \Leftrightarrow \ \ F(u) + F^\sharp(u^*) = \langle u, u^* \rangle, \tag{2.4}$$

where $\partial^+ F = -\partial^-(-F(u))$ is called the *super-differential* of F, corresponding to the sub-differential ∂^- in convex analysis. The duality pair $(u, u^*) \in \mathcal{U}_a \times \mathcal{U}_a^*$ is called a *Fenchel inf-duality pair* if the Fenchel inf-duality relations (2.4) hold on $\mathcal{U}_a \times \mathcal{U}_a^*$. Thus, in the case that $W(u)$ is convex, the first dual action form can be presented as

$$P^c(u) = \frac{1}{2}\langle u, Au\rangle - F^\sharp(Au).$$

The dual action principle says that if F is concave, then $\bar{u}$ is a critical point of P if and only if all the $\bar{u}^c \in \bar{u} + \text{Ker } A$ are critical points of P^c, and the *complementarity condition*

$$P(\bar{u}) + P^c(\bar{u}^c) = 0 \quad \forall \bar{u}^c \in \bar{u} + \text{Ker } A \tag{2.5}$$

holds, where Ker $A = \{u \in \mathcal{U} |\ \ Au = 0\}$ represents the kernel of A. However, if $F(u)$ is non-concave, the Fenchel-Young inequality

$$F^\sharp(u^*) \leq \langle u, u^*\rangle - F(u)$$

leads to

$$\theta = P(\bar{u}) + P^c(\bar{u}^c) \geq 0.$$

The nonzero $\theta > 0$ is called the *duality (or complementarity) gap*. This duality gap shows that the Clarke dual action principle does not hold for non-convex problems. Similar to the complementarity condition (2.5), the dual action form P^c is called the *complementary action*, and the duality gap is referred to to the complementarity gap in [33]. The complementary formulation has been a classical concept in engineering mechanics and physics for about one century, where a problem is said to be a complementary problem when it is equivalent to the primal problem without any duality gap (see Gao and Strang [49, 33]).

Lagrangian Duality [36] is based on the factorization of the self-adjoint (symmetric) operator

$$A = \Lambda^* K \Lambda,$$

where $\Lambda : \mathcal{U} \to \mathcal{Y}$ is a so-called *geometrical operator*, which maps each configuration $u \in \mathcal{U}$ into a so-called *intermediate space* $\mathcal{Y}$ and the symmetric *constitutive operator* K links $\mathcal{Y}$ with its dual space $\mathcal{Y}^*$. Let $\langle \xi; \varsigma \rangle$ denote the bilinear form in $\mathcal{Y} \times \mathcal{Y}^*$. The balance operators $\Lambda^* : \mathcal{Y}^* \to \mathcal{U}^*$ can be defined by

$$\langle \Lambda u; \xi^* \rangle = \langle u, \Lambda^* \xi^* \rangle,$$

which maps each dual intermediate variable $\xi^* \in \mathcal{Y}^*$ back to the dual configuration space $\mathcal{U}^*$. By the definition of the canonical function, if the operator $K : \mathcal{Y}_a \to \mathcal{Y}_a^*$ is invertible, then the quadratic function $\bar{U}(\xi) = \frac{1}{2}\langle \xi; K\xi \rangle$ is a canonical function on $\mathcal{Y}_a$. Moreover, if the feasible space $\mathcal{U}_k$ can be written in the canonical form (see [33])

$$\mathcal{U}_k = \{u \in \mathcal{U}_a |\ \ \Lambda u \in \mathcal{Y}_a\},$$

then, based on the trio-factorization $A = \Lambda^* K \Lambda$, the primal function P in (2.3) can be written in the *canonical form*

$$\min\{P(u) = \bar{U}(\Lambda u) - F(u) |\ \ u \in \mathcal{U}_k\}. \tag{2.6}$$

The criticality condition $DP(\bar{u}) = 0$, i.e., the semi-linear equation (1.2) in this case can be reformulated as

$$\Lambda^* D_\Lambda \bar{U}(\Lambda u) - DF(\bar{u}) = 0,$$

where $D_\Lambda \bar{U}(\Lambda u)$ denotes the Gâteaux derivative of $\bar{U}$ with respect to $\xi = \Lambda u$. In terms of the canonical duality pairs (u, u^*) and (ξ, ς), this semi-linear equation can be split into the so-called *trio-canonical forms*

$$\begin{aligned} &\text{(a) geometrical equations: } \xi = \Lambda u, \\ &\text{(b) duality relations:} \qquad \xi^* = D\bar{U}(\xi), \ \ u^* = DF(u), \\ &\text{(c) balance equation:} \qquad u^* = \Lambda^* \xi^*. \end{aligned} \tag{2.7}$$

Now it is convenient to introduce a unified framework of linear systems (see Fig. 2.1) proposed by Strang [84]. The problem (2.6) is said to be geometrically linear (nonlinear) if the geometrical

$$\begin{array}{ccccc} u \in \ \mathcal{U} & \longleftarrow & \langle u\ ,\ u^* \rangle & \longrightarrow & \mathcal{U}^* \ni u^* \\ \Lambda \downarrow & & & & \uparrow \Lambda^* \\ \xi \in \ \mathcal{Y} & \longleftarrow & \langle \xi\ ;\ \xi^* \rangle & \longrightarrow & \mathcal{Y}^* \ni \xi^* \end{array}$$

Figure 2.1: Framework in linear systems [33].

operator Λ is linear (nonlinear); the problem is said to be physically (or constitutively) linear (nonlinear) if both duality relations are linear (nonlinear); the problem is said to be *fully nonlinear* if it is both geometrically and physically nonlinear (see [33, 32]). The development of the $\Lambda^*\Lambda$-operator theory was initiated by von Neumann in 1932, and was subsequently extended and put into a more general setting in the studies of complementary variational principles by Noble and Sewell [68], Tonti [92], Arthurs [3], Oden and Reddy [70], and Sewell [81]. In Strang's textbook [84], the trio-factorization $A = \Lambda^* K \Lambda$ for linear operators can be understood through continuous theories for discrete systems. For nonlinear operators A, the trio-factorization and canonical forms in both non-convex and non-conservative systems were presented in [33].

The trio-canonical forms (2.7) serve as a framework for the classical Lagrangian duality theory in geometrically linear systems. Through the classical Lagrangian $L : \mathcal{U}_a \times \mathcal{Y}_a^* \to \mathbb{R}$

$$L(u, \xi^*) = \langle \Lambda u; \xi^* \rangle - \bar{U}^*(\xi^*) - F(u), \tag{2.8}$$

the canonical dual function $P^*:\mathcal{Y}_k^*\subset\mathcal{Y}_a^*\to\mathbb{R}$ can be defined by

$$P^*(\varsigma)=\{L(u,\varsigma)|\ \ D_uL(u,\varsigma)=0,\ u\in\mathcal{U}_a\}=F^*(\Lambda^*\varsigma)-\bar{U}^*(\varsigma) \tag{2.9}$$

on the dual feasible space $\mathcal{Y}_k^*=\{\varsigma\in\mathcal{Y}_a^*|\ \ \Lambda^*\varsigma\in\mathcal{U}_a^*\}$ (see [33]).

Mono-Duality[33] In geometrically linear static systems, where the canonical function $\bar{U}(\xi)$ is usually convex and $F(u)$ is concave, the total potential $P(u)$ is convex, and $L(u,\varsigma)$ is a saddle function on $\mathcal{U}_a\times\mathcal{Y}_a^*$. The saddle Lagrange duality theory leads to the classical min-max duality theory in convex systems:

$$\inf P(u)=\inf_{u\in\mathcal{U}_a}\sup_{\varsigma\in\mathcal{Y}_a^*}L(u,\varsigma)=\sup_{\varsigma\in\mathcal{Y}_a^*}\inf_{u\in\mathcal{U}_a}L(u,\varsigma)=\sup_{\varsigma\in\mathcal{Y}_k^*}P^*(\varsigma).$$

Bi-Duality[33] In geometrically linear dynamical systems and game theory, both $\bar{U}(\xi)$ and $F(u)$ are usually convex. In this case, the canonical function $P(u)=\bar{U}(\xi)-F(u)$ is the so-called total action in dynamical systems, which is a d.c. function (i.e., a difference of convex functions). The Lagrangian (2.8) associated with the d.c. function $P(u)$ is a so-called *super- (or ∂^+-) Lagrangian* (see [33]), i.e., $L(u,\varsigma)$ is concave in each of its variables u and ς and if $(\bar{u},\bar{\varsigma})$ is a critical point of $L(u,\varsigma)$, then the following inequality holds

$$L(u,\bar{\varsigma})\le L(\bar{u},\bar{\varsigma})\ge L(\bar{u},\varsigma)\ \ \forall(u,\varsigma)\in\mathcal{U}_a\times\mathcal{Y}_a^*.$$

Clearly, the Hamiltonian

$$H(u,\varsigma)=\langle\Lambda u;\varsigma\rangle-L(u,\varsigma)=F^*(\Lambda^*\varsigma)+\bar{U}^*(\varsigma)$$

associated with a super Lagrangian $L(u,\varsigma)$ is always convex in each of its variables. This might be the reason why most people prefer the convex Hamiltonian $H(u,\varsigma)$ instead of the super-Lagrangian $L(u,\varsigma)$ in dynamical systems. The super-Lagrangian leads to a so-called *bi-duality theory* [33], i.e., if $(\bar{u},\bar{\varsigma})$ is a critical point of a super-Lagrangian Ξ, then either

$$\inf_{u\in\mathcal{U}_k}P(u)=\Xi(\bar{u},\bar{\varsigma})=\inf_{\varsigma\in\mathcal{Y}_k^*}P^*(\varsigma),$$

or

$$\sup_{u\in\mathcal{U}_k}P(u)=\Xi(\bar{u},\bar{\varsigma})=\sup_{\varsigma\in\mathcal{Y}_k^*}P^*(\varsigma).$$

This bi-duality theory plays an important role in d.c. programming [33].

In the problem $(\mathcal{P})$ considered in this thesis, since the function $W(u)$ is non-convex, it turns out that $F(u)$ is no longer a canonical function, and the duality relation is not one-to-one. Thus, the

Legendre transformation of the non-convex function F cannot be uniquely defined [81]. In this case, the *Fenchel-Young Inequality* for the non-convex function F also produces a nonzero duality gap between the primal function and its classical Lagrangian dual function.

During the last three decades, many modified versions of the Fenchel-Rockafellar duality have been proposed. One so-called relaxation method in non-convex mechanics (Dacorogna [16]; Atai and Steigmann [4]), can be used to solve the relaxed convex problems. However, due to the duality gap, these relaxed solutions are not equivalent to the real solutions. Tremendous efforts have been recently focused on finding the so-called perfect duality theory (i.e., without a duality gap) in global optimization. Some important concepts have been developed in global optimization and variational inequalities (Ekeland [18]; Toland [91]; Auchmuty [6, 7]; Singer [82]; Thach *et al* [89]; Tuy [95]; Rubinov *et al* [78]; Gasimov [52]; Goh and Yang [56], Rubinov and Gasimov [77], etc.). Generally speaking, the main difficulty is due to the fact that the Legendre conjugate of a general non-convex function is usually multi-valued. As Ekeland [20] pointed out, the question of finding general methods and theory for solving non-convex problems remains open.

2.3 Canonical Duality Theory and Perfect Duality

Generally, in mathematics, a canonical form (often called normal form) of an object is a standard presentation. A canonical form is required to have two essential properties. Every object under consideration must have exactly one canonical form, and two objects that have the same canonical form must be the same up to some equivalence. The uniqueness requirement is sometimes relaxed, allowing the forms to be unique up to order of terms. A canonical form not only classifies every class, but gives a distinguished (canonical) representative.

2.3.1 Canonical Duality Theory

The *canonical duality theory* and the trio-canonical forms in non-convex (geometrically nonlinear) systems were studied by Gao and Strang [49] in large deformation variational/boundary value problems governed by non-smooth duality relations (constitutive laws), where $A = 0$ and the primal problem $(\mathcal{P})$ takes the following stationary variational form:

$$(\mathcal{P}_{\text{sta}}): \quad P(u) = \check{W}(\Lambda(u)) - \langle u, f\rangle \ \ \rightarrow \text{sta} \ \ \forall u \in \mathcal{U}_k, \tag{2.10}$$

in which the notation $P(u) \rightarrow \text{sta}\ \forall u \in \mathcal{U}_k$ stands for finding all stationary points of P over the feasible space $\mathcal{U}_k$; the internal energy $\check{W}(\xi)$ is a convex functional of the canonical (geometric) strain tensor ξ; for a given input f, the external energy $F(u) = \langle u, f\rangle$ is a linear functional; and the geometrical measure $\Lambda(u)$ is a quadratic tensor function of the state variable u. In the case

that $\Lambda(u)$ is Gâteaux differentiable, we have the following decomposition [50]:

$$\Lambda(u) = \Lambda_t(u)u + \Lambda_c(u), \tag{2.11}$$

where $\Lambda_t(u) = D\Lambda(u)$ denotes the Gâteaux derivative of $\Lambda(u)$ with respect to u, and $\Lambda_c = \Lambda(u) - \Lambda_t(u)u$ is the so-called *complementary operator* of Λ_t. Through the decomposition (2.11), Gao and Strang discovered that the duality gap existing in classical Lagrange duality theory can be naturally recovered by the so-called *complementary gap function* defined by

$$G(u, \varsigma) = -\langle \Lambda_c(u); \varsigma \rangle. \tag{2.12}$$

Therefore, they proved that the original non-convex problem (2.10) is equivalent to the following constrained *complementary variational problem*:

$$(\mathcal{P}^c_{\text{sta}}): \quad \begin{cases} P^c(u, \varsigma) = \check{W}^\sharp(\varsigma) + G(u, \varsigma) \quad \to \text{sta} \ \ \forall \varsigma \in \mathcal{Y}^*_a, \\ \quad s.t. \ \ \Lambda^*_t(u)\varsigma = f, \end{cases} \tag{2.13}$$

where the balance operator $\Lambda^*_t(u)$ is the adjoint operator of Λ_t defined by the duality pairing $\langle \Lambda_t(u)u; \varsigma \rangle = \langle u, \Lambda^*_t(u)\varsigma \rangle$, and $\check{W}^\sharp(\varsigma)$ is the Fenchel super-conjugate:

$$\check{W}^\sharp(\varsigma) = \sup\{\langle \xi; \varsigma \rangle - \check{W}(\xi) | \ \ \xi \in \mathcal{Y}_a\}.$$

Gao and Strang further proved that if $(\bar{u}, \bar{\varsigma})$ is a critical point of the extended Lagrangian

$$\Xi(u, \varsigma) = \langle \Lambda(u); \varsigma \rangle - \check{W}^\sharp(\varsigma) - \langle u, f \rangle, \tag{2.14}$$

then the complementarity condition $P(\bar{u}) + P^c(\bar{u}, \bar{\varsigma}) = 0$ holds. Moreover, if $G(\bar{u}, \bar{\varsigma}) \geq 0$, then $(\bar{u}, \bar{\varsigma})$ is a saddle point of $\Xi(u, \varsigma)$ and $\bar{u}$ is a global minimizer of $P(u)$. Their original work on duality theory in finite field theory leads to a unified framework in *fully nonlinear canonical systems* (see Fig. 2.2).

$$\begin{array}{ccccc} u \in \ \mathcal{U} & \longleftarrow \langle u \ , \ u^* \rangle \longrightarrow & \mathcal{U}^* \ni u^* \\ \Lambda_t + \Lambda_c = \Lambda \ \Big\downarrow & & \Big\uparrow \ \Lambda^*_t = (\Lambda - \Lambda_c)^* \\ \xi \in \ \mathcal{Y} & \longleftarrow \langle \xi \ ; \ \xi^* \rangle \longrightarrow & \mathcal{Y}^* \ni \xi^* \end{array}$$

Figure 2.2: Framework in fully nonlinear systems [33].

The **Key Idea** of this canonical dual transformation [33] is to choose a certain (geometrically reasonable) operator $\xi = \Lambda(u) : \mathcal{U}_a \to \mathcal{Y}_a$ such that a given non-convex function $P(u)$ can be written

in the canonical form $P(u) = \Phi(u, \Lambda(u))$, where $\Phi(u, \xi) : \mathcal{U}_a \times \mathcal{Y}_a \to \mathbb{R}$ is a canonical function in each of its variables (see [32]). Very often, $\Phi(u, \xi) = \bar{W}(\xi) - F(u)$. Since both $\bar{W} : \mathcal{Y}_a \to \mathbb{R}$ and $F : \mathcal{U}_a \to \mathbb{R}$ are canonical functions, their Legendre conjugates can be uniquely defined via the classical Legendre transformation. Thus, the extended Lagrangian

$$\Xi(u, \varsigma) = \langle \Lambda(u); \varsigma \rangle - \bar{W}^*(\varsigma) - F(u) \tag{2.15}$$

is well defined on $\mathcal{U}_a \times \mathcal{Y}_a^*$. Then, by using the so-called Λ-*canonical dual transformation* (see [33])

$$F^\Lambda(\varsigma) = \{\langle \Lambda(u); \varsigma \rangle - F(u) | \quad \Lambda_t^*(u)\varsigma - DF(u) = 0, \ \ u \in \mathcal{U}_a\}, \tag{2.16}$$

the canonical dual function of the non-convex $P(u)$ can be well defined by

$$P^d(\varsigma) = \{\Xi(u, \varsigma) | \ \ D_u \Xi(u, \varsigma) = 0, \ \ u \in \mathcal{U}_a\} = F^\Lambda(\varsigma) - \bar{W}^*(\varsigma). \tag{2.17}$$

In the case that F is linear and Λ is quadratic, the Λ-conjugate $F^\Lambda(\varsigma)$ is equivalent to the complementary gap function, i.e.,

$$F^\Lambda(\varsigma) = \{G(u, \varsigma) | \ \ \Lambda_t^*(u)\varsigma = f, \ \ u \in \mathcal{U}_a\}.$$

An Example of Canonical Duality To illustrate the idea, we consider a very simple example, a non-convex optimization in $\mathbb{R}^n$:

$$\min_{\mathbf{x} \in \mathbb{R}^n} P(\mathbf{x}) = \frac{1}{2}\alpha \left(\frac{1}{2}|\mathbf{x}|^2 - \lambda \right)^2 - \mathbf{x}^T f. \tag{2.18}$$

The criticality condition $DP(\mathbf{x}) = 0$ leads to a coupled nonlinear algebraic equation system in $\mathbb{R}^n$

$$\alpha \left(\frac{1}{2}|\mathbf{x}|^2 - \lambda \right) \mathbf{x} = f, \tag{2.19}$$

which is usually difficult to solve analytically for all roots, and to determine which solution is a global minimizer of P (2.18). However, by the canonical dual transformation, this problem can be easily solved. Since $W(\mathbf{x}) = \frac{1}{2}\alpha(\frac{1}{2}|\mathbf{x}|^2 - \lambda)^2$ is a double-well energy, if we choose $\xi = \Lambda(\mathbf{x}) = \frac{1}{2}\mathbf{x}^2 - \lambda \in \mathbb{R}$, then $\check{W}(\xi) = \frac{1}{2}\alpha\xi^2$ is a canonical (quadratical) function. Its Legendre conjugate is simply given by $\check{W}^*(\varsigma) = \frac{1}{2}\alpha^{-1}\varsigma^2$. For the quadratic operator $\Lambda(x) : \mathbb{R}^n \to \mathbb{R}$, its Gâteaux differential is simply $\Lambda_t(x) = \mathbf{x}^T$. Thus, the complementary operator can be given by $\Lambda_c(\mathbf{x}) = (\frac{1}{2}|\mathbf{x}|^2 - \lambda) - \mathbf{x}^T\mathbf{x} = -\frac{1}{2}|\mathbf{x}|^2 - \lambda$. The extended Lagrangian for this non-convex optimization problem is

$$\Xi(x, \varsigma) = (\frac{1}{2}|\mathbf{x}|^2 - \lambda)\varsigma - \frac{1}{2}\alpha^{-1}\varsigma^2 - \boldsymbol{x}^T\mathbf{f}. \tag{2.20}$$

For a fixed $\varsigma \in \mathbb{R}$, the partial criticality condition $D_{\mathbf{x}}\Xi(\mathbf{x}) = 0$ leads to the canonical balance equation

$$\Lambda_t^*(\mathbf{x})\varsigma = \mathbf{x}\varsigma - \mathbf{f} = 0. \tag{2.21}$$

With this condition, the complementary energy P^c in problem (2.13) takes the following form:

$$P^c(\mathbf{x}, \varsigma) = \frac{1}{2}\alpha^{-1}\varsigma^2 + (\frac{1}{2}|\mathbf{x}|^2 + \lambda)\varsigma,$$

where $G(\mathbf{x}, \varsigma) = (\frac{1}{2}|\mathbf{x}|^2+\lambda)\varsigma = -\Lambda_c(\mathbf{x})\varsigma$ is the complementary gap function. For each nonzero $\varsigma \neq 0$, the canonical balance equation (2.21) gives $\mathbf{x} = \mathbf{f}/\varsigma$. Substituting this into the extended Lagrangian Ξ, the canonical dual function of P can be obtained by the canonical dual transformation

$$\begin{aligned} P^d(\varsigma) &= \{\Xi(\mathbf{x}, \varsigma)| \ D_u\Xi(\mathbf{x}, \varsigma) = 0\} \\ &= -\frac{\mathbf{f}^T\mathbf{f}}{2\varsigma} - \frac{1}{2}\alpha^{-1}\varsigma^2 - \lambda\varsigma \quad \forall \varsigma \neq 0. \end{aligned} \tag{2.22}$$

The critical points of this canonical function solve the following dual equation

$$(\alpha^{-1}\varsigma + \lambda)\varsigma^2 = \frac{1}{2}\mathbf{f}^T\mathbf{f}. \tag{2.23}$$

For any given parameters α, λ and the vector $\mathbf{f} \in \mathbb{R}^n$, this cubic algebraic equation has at most three roots satisfying $\varsigma_1 > 0 > \varsigma_2 \geq \varsigma_3$, and each of these roots leads to a critical point of the non-convex function P, i.e., $\mathbf{x}_i = \mathbf{f}/\varsigma_i, \ \ i = 1, 2, 3$. It was shown by Gao in [33] that $\mathbf{x}_1$ is a global minimizer of P, while $\mathbf{x}_2$ is a local minimizer and $\mathbf{x}_3$ is a local maximizer. For the global minimizer $\mathbf{x}_1$, we have the saddle duality relation (so-called *tri-duality* or *triality* in [33])

$$P(\mathbf{x}_1) = \min_{\mathbf{x}\in\mathbb{R}^n} P(\mathbf{x}) = \max_{\varsigma>0} P^d(\varsigma) = P^d(\varsigma_1).$$

For the local extrema, the bi-duality relations

$$P(\mathbf{x}_2) = \min P(\mathbf{x}) = \min P^d(\varsigma) = P^d(\varsigma_2),$$

and

$$P(\mathbf{x}_3) = \max P(\mathbf{x}) = \max P^d(\varsigma) = P^d(\varsigma_3),$$

hold in the neighborhoods of $(\mathbf{x}_2, \varsigma_2)$ and $(\mathbf{x}_3, \varsigma_3)$.

In mathematical physics, the canonical duality relation $\varsigma = D\bar{W}(\xi)$ is usually called the constitutive law. The one-to-one duality relation between each canonical dual pair ensures the existence of the geometrical measure $\xi = \Lambda(u)$ and the canonical form of functional. Extensive applications of this canonical dual transformation method have been given in non-convex continuous systems, and some analytical solutions of non-convex/non-smooth boundary value problems have been obtained (see [30, 32]). The generalization of this method to non-smooth global optimization problems that is suitable for arbitrary nonlinear operator Λ was made in [32].

2.3.2 Canonical Duality Formulation

Recall the non-convex problem proposed in the beginning of the thesis:

$$(\mathcal{P}): \quad P(u) = \frac{1}{2}\langle u, Au\rangle + W(u) - \langle u, f\rangle.$$

The canonical duality theory for solving this primal problem in infinite dimensional systems has been recently established, and applications have been made to post-buckling analysis of non-convex beam models [34], non-smooth/non-convex/nonconservative dynamics [35], as well as the Landau-Ginzburg equation in super-conductivity. The numerical discretization of these non-convex variational problems leads to non-convex global optimization problems, where A is usually a large-scale symmetric matrix.

In order to formulate an explicit dual problem, we assume that the operator $A : \mathcal{U}_a \subset \mathcal{U} \to \mathcal{U}_a^* \subset \mathcal{U}^*$ is invertible. Thus, for each given input $f \in \mathcal{U}_a^*$, the function $F : \mathcal{U}_a \to \mathbb{R}$, defined by

$$F(u) = \langle u, f\rangle - \frac{1}{2}\langle u, Au\rangle,$$

is a canonical function on $\mathcal{U}_a$, since its Gâteaux derivative $u^* = DF(u) = f - Au$ is one-to-one mapping from $\mathcal{U}_a$ onto the range $\mathcal{U}_a^*$. It turns out that (u, u^*) is a (Legendre) canonical duality pair on $\mathcal{U}_a \times \mathcal{U}_a^*$. We further assume that for the given non-convex function $W(u) : \mathcal{U}_a \to \mathbb{R}$, there exists a geometrical operator $\Lambda(u) : \mathcal{U} \to \mathcal{Y}_a$, which maps each $u \in \mathcal{U}_a$ into another metric space $\mathcal{Y}$, such that the non-convex function $W(u)$ can be written in the canonical form $W(u) = \check{W}(\Lambda(u))$, where $\check{W}(\xi)$ is a canonical function defined on a subset $\mathcal{Y}_a \subset \mathcal{Y}$. By the definition of the canonical function, $\check{W} : \mathcal{Y}_a \to \mathbb{R}$ is Gâteaux differentiable, and the duality relation $\varsigma = D\check{W} : \mathcal{Y}_a \to \mathcal{Y}_a^* \subset \mathcal{Y}^*$ is invertible. Let $\langle *; * \rangle : \mathcal{Y} \times \mathcal{Y}^* \to \mathbb{R}$ denote the bilinear form on $\mathcal{Y} \times \mathcal{Y}^*$. Then, the Legendre conjugate function $\check{W}^* : \mathcal{Y}_a^* \to \mathbb{R}$ of the canonical function $\check{W}$ can be obtained uniquely by the classical Legendre transformation

$$\check{W}^*(\varsigma) = \{\langle \xi; \varsigma\rangle - \check{W}(\xi) |\ D\bar{W}(\xi) = \varsigma,\ \ \xi \in \mathcal{Y}_a\}. \tag{2.24}$$

Furthermore, the Legendre canonical duality relations

$$\varsigma = D\check{W}(\xi) \ \ \Leftrightarrow \ \ \xi = D\check{W}^*(\varsigma) \ \ \Leftrightarrow \ \ \check{W}(\xi) + \check{W}^*(\varsigma) = \langle \xi; \varsigma\rangle \tag{2.25}$$

hold on $\mathcal{Y}_a \times \mathcal{Y}_a^*$. Thus, the pair (ξ, ς) is also a Legendre canonical dual pair on $\mathcal{Y}_a \times \mathcal{Y}_a^*$.

For simplicity, we first limit our attention to scalar-valued quadratic operators $\Lambda : \mathcal{U} \to \mathcal{Y}$

$$\Lambda(u) = \frac{1}{2}|u|^2 - \lambda, \tag{2.26}$$

where $|*|$ is an Euclidean norm, and $\lambda \in \mathbb{R}$ is a constant. Also, by using the so-called *sequential canonical dual transformation method* developed in [33, 32], the results of this thesis may be generalized to any so-called *canonical polynomial operator* $\Lambda(u)$ (see [28, 33]. Finally, we assume that

the feasible set $\mathcal{U}_k$ can be written as

$$\mathcal{U}_k = \{u \in \mathcal{U}_a |\ \ \Lambda(u) \in \mathcal{Y}_a\}.$$

Since we are interested in finding all critical points of the non-convex function $P(u)$ over the feasible space $\mathcal{U}_k$, in terms of the canonical function $\check{W}$ and the geometrical measure $\xi = \Lambda(u)$, the primal minimization problem $(\mathcal{P})$ should be rewritten in the canonical stationary variational form $(\mathcal{P}_{\rm sta})$:

$$\begin{aligned}(\mathcal{P}_{\rm sta}): \qquad & P(u) = \check{W}(\Lambda(u)) - F(u) \\ & = W(u) + \frac{1}{2}\langle u, Au\rangle - \langle u, f\rangle \quad \to \text{sta}\ \ \forall u \in \mathcal{U}_k. \end{aligned} \tag{2.27}$$

The criticality condition $DP(\bar{\mathbf{u}}) = 0$ leads to the following canonical equation

$$\left(A + D_\Lambda \check{W}(\Lambda(\bar{\mathbf{u}}))I\right)\bar{\mathbf{u}} = f, \tag{2.28}$$

where $D_\Lambda \check{W}$ is the Gâteaux derivative of $\check{W}(\Lambda(u))$ with respect to $\Lambda(u)$, and I is an identity matrix. Clearly, the canonical equation (2.28) is essentially equivalent to the semi-linear equation (1.2). However, by the canonical dual transformation, a complete set of solutions of this nonlinear system can be obtained via the canonical duality formulation. In Gao's monograph [33], the following theorem claims a perfect zero duality gap.

Theorem 2.1 (Perfect Duality Formulation [36]). *Suppose that, for a given $f \in \mathcal{U}_a^*$, the dual feasible space*

$$\mathcal{Y}_k^* = \{\varsigma \in \mathcal{Y}_a^* |\ \ (A + \varsigma I)\ \textit{is invertible and}\ (A+\varsigma I)^{-1} f \in \mathcal{U}_a\ \ \} \tag{2.29}$$

is not empty. Then, the problem

$$(\mathcal{P}_{\rm sta}^d): \quad P^d(\varsigma) = -\frac{1}{2}\langle (A+\varsigma I)^{-1} f, f\rangle - \lambda\varsigma - \check{W}^*(\varsigma) \quad \to \text{sta}\ \ \forall \varsigma \in \mathcal{Y}_k^* \tag{2.30}$$

is canonically (perfectly) dual to the primal problem $(\mathcal{P}_{\rm sta})$ in the sense that if $\bar{u} \in \mathcal{U}_k$ is a solution of the primal stationary problem $(\mathcal{P}_{\rm sta})$ given in equation (2.10), then $\bar{\varsigma} = D_\Lambda \check{W}(\Lambda(\bar{u}))$ is a solution of the dual problem $(\mathcal{P}_{\rm sta}^d)$ and

$$P(\bar{u}) = P^d(\bar{\varsigma}). \tag{2.31}$$

Theorem 2.1 shows that there is no duality gap between the primal problem $(\mathcal{P}_{\rm sta})$ and its canonical dual problem $(\mathcal{P}_{\rm sta}^d)$. In other words, it ensures the equivalence between primal and dual problems, given the criteria of invertibility is satisfied. Since the criticality condition of P^d is an algebraic equation with only one unknown $\varsigma \in \mathbb{R}$, the canonical dual problem $(\mathcal{P}_{\rm sta}^d)$ has a finite number of critical points in $\mathcal{Y}_k^*$. All these dual solutions $\bar{\varsigma}_i$ $(i = 1, 2, ...)$ form a subset of $\mathcal{Y}_k^*$, which is denoted by

$$\mathcal{Y}_s^* = \{\bar{\varsigma} \in \mathcal{Y}_k^* |\ \ D\check{W}^*(\bar{\varsigma}) + \lambda = \frac{1}{2} f^T (A + \bar{\varsigma} I)^{-2} f\}. \tag{2.32}$$

In [33], Gao proposed the following theorem to address the completeness issue and claimed that the dual solution set $\mathcal{Y}_s^*$ leads to a complete set of solutions of the primal problem $(\mathcal{P}_{\rm sta})$.

Theorem 2.2 (Complete Solution Set [36]). *Suppose that the assumption in Theorem 2.1 holds. Thus, for every solution $\bar{\varsigma} \in \mathcal{Y}_s^*$, the vector $\bar{\mathbf{u}}$ defined by*

$$\bar{\mathbf{u}}(\bar{\varsigma}) = (A + \bar{\varsigma} I)^{-1} f \tag{2.33}$$

solves the primal problem $(\mathcal{P}_{\rm sta})$. Conversely, every solution $\bar{\mathbf{u}}$ of the primal problem $(\mathcal{P}_{\rm sta})$ can be written in the form (2.33) for some dual solution $\bar{\varsigma} \in \mathcal{Y}_s^*$.

Theorem 2.2 shows that, by the canonical dual transformation, a complete set of solutions to the non-convex primal problem is obtained as

$$\mathcal{U}_s = \{\bar{u} \in \mathcal{U}_k |\ \ \bar{u} = (A + \bar{\varsigma}(\bar{u}) I)^{-1} f \ \ \forall \bar{\varsigma} \in \mathcal{Y}_s^*\}. \tag{2.34}$$

For the given non-convex problem $(\mathcal{P})$, each solution $\bar{u} \in \mathcal{U}_s$ could be only a local extremum point (either local minimizer or local maximizer) of the non-convex function $P(u)$. In order to determine the global minimizers and local extremes of P, we introduce the following subsets:

$$\mathcal{Y}_+^* = \{\varsigma \in \mathcal{Y}_k^* |\ \ (A + \varsigma I) \text{ is positive definite}\}, \tag{2.35}$$

$$\mathcal{Y}_-^* = \{\varsigma \in \mathcal{Y}_k^* |\ \ (A + \varsigma I) \text{ is negative definite}\}. \tag{2.36}$$

By the triality theory proposed in [43, 28, 33], the global minimizers and maximizers of the primal problem $(\mathcal{P}_{\rm sta})$ and the dual problem $(\mathcal{P}_{\rm sta}^d)$ are discussed in the following theorem.

Theorem 2.3 (Global Minimizer and Maximizer [36]). *Suppose that the canonical function $\breve{W}(\xi)$ is convex on $\mathcal{Y}_a$. For each dual solution $\bar{\varsigma} \in \mathcal{Y}_s^*$, we let $\bar{u}(\bar{\varsigma}) = (A + \bar{\varsigma} I)^{-1} f$.*

If $\bar{\varsigma} \in \mathcal{Y}_+^*$, then $\bar{\varsigma}$ is a global maximizer of P^d on $\mathcal{Y}_+^*$, while $\bar{\mathbf{u}}(\bar{\varsigma})$ is a global minimizer of P on $\mathcal{U}_k$, and

$$P(\bar{u}) = \min_{u \in \mathcal{U}_k} P(u) = \max_{\varsigma \in \mathcal{Y}_+^*} P^d(\varsigma) = \ P^d(\bar{\varsigma}). \tag{2.37}$$

Moreover, the dual solution set $\mathcal{Y}_s^*$ has at most one element $\bar{\varsigma} \in \mathcal{Y}_+^*$.

If $\bar{\varsigma} \in \mathcal{Y}_-^*$, then $\bar{\varsigma}$ and the associated $\bar{u}$ are local critical points of P^d and P, respectively. In this case, $\bar{u}$ is a local maximizer of $P(u)$ on its neighborhood [1] $\mathcal{U}_r \subset \mathcal{U}_k$ if and only if $\bar{\varsigma}$ is a local maximizer of P^d on its neighborhood $\mathcal{Y}_r^* \subset \mathcal{Y}_k^*$, and

$$P(\bar{u}) = \max_{u \in \mathcal{U}_r} P(u) = \max_{\varsigma \in \mathcal{Y}_r^*} P^d(\varsigma) = P^d(\bar{\varsigma}). \tag{2.38}$$

This theorem is interesting in that it seems that we are able to separate the global minimizer and maximizer into different domains. Therefore, it implies that, instead of finding all the solutions

[1] The sub-space $\mathcal{U}_r \subset \mathcal{U}_k$ is said to be the neighborhood of the critical point $\bar{u}$ if $\bar{u}$ is the only critical point of P on $\mathcal{U}_r$. The definition for the neighborhood $\mathcal{Y}_r^* \subset \mathcal{Y}_k^*$ is similar.

and running an exhaustive comparison to identify extremality, we may find the specific extreme solution in its corresponding domain, given that these domains are separated.

To end this chapter, note that the canonical duality theory works directly with the functional of interest, instead of its "derivative." Therefore, it may be interpreted as a direct method. This is not exactly the case since, by the canonical dual transformation, we actually work with a dual form of the primal functional. Once the canonical dual transformation is employed, traditional techniques in convex analysis may be used.

Chapter 3

Numerical Methods

Since the main goal of this thesis is to perform a careful numerical investigation of the canonical dual method presented in Chapter 2 and compare the corresponding numerical results with those obtained by using standard numerical methods, various numerical methodologies are used throughout the thesis. These include: (i) numerical methods for ODEs, (ii) numerical methods for PDEs, (iii) numerical methods for nonlinear equations, and (iv) numerical methods for optimization. Given the variety of numerical methods frequently employed in this thesis, we *summarize* them in this chapter. Each methodology represents a well-developed research field in its own. It is thus not reasonable to attempt an exhaustive presentation for each of them. Instead, we will briefly introduce the numerical methods used in Chapters 4 and 5, emphasizing those features specifically displayed in our numerical experiments. For further details, such as the study of stability and order of convergence of these numerical methods, we refer the reader to classic surveys that we reference in the sequel.

3.1 Numerical Methods for ODEs

A basic introduction to the subject is given in classic textbooks, such as [12, 14]. The problem that needs to be approximated numerically is the following *Initial Value Problem* (IVP):

$$u^{(n)}(t) = f(t, u^{(1)}, u^{(n-1)}) \quad \forall t \in [0, \infty), \tag{3.1}$$

$$u(0) = u_0^0,\ u^{(1)}(0) = u_0^1,\ \ldots, u^{(n-1)}(0) = u_0^{n-1}. \tag{3.2}$$

The goal of numerical methods for ODEs such as (3.1)-(3.2) is to approximate the exact solution u (which generally cannot be computed analytically) at a sequence of points in the computational

domain $[0, \infty)$:

$$0 = t_0 < t_1 < \ldots < t_m < \ldots \tag{3.3}$$

Another type of problem, which will be of particular interest to us, is the *Boundary Value Problem (BVP)*. We consider a second-order BVP ($n = 2$), since this will be the case of interest to us:

$$u''(x) = f(x, u, u') \qquad \forall\, x \in [a, b], \tag{3.4}$$
$$u(a) = u_0, \tag{3.5}$$
$$u(b) = u_1. \tag{3.6}$$

One of the popular numerical methods for approximating the solution to the BVP (3.4)-(3.6) is the *nonlinear shooting method* [55, 12, 53]. This method is centered around the following idea: it transforms the BVP into a system of first-order ODEs, which can be solved by standard numerical methods for IVPs, like the Runge-Kutta method. The boundary condition on one side of the computational solution domain can be used as initial condition for the newly formed IVP; however, the other boundary condition cannot be used as initial condition. The IVP can then be solved by assuming an additional initial condition, and the solution at the other boundary can be compared to the known boundary condition not yet used. Thus, an iterative approach, called *shooting* is employed to vary the assumed initial condition until the specified boundary condition is satisfied [55]. Specifically, instead of solving the BVP (3.4)-(3.6) directly, one can consider the following second-order IVP:

$$u''(x) = f(x, u, u') \qquad \forall\, x \in [a, b], \tag{3.7}$$
$$u(a) = u_0, \tag{3.8}$$
$$u'(a) = t. \tag{3.9}$$

We then choose the parameter $t = t_k$ in a manner to ensure that

$$\lim_{k \to \infty} u(b, t_k) = u(b) = u_1, \tag{3.10}$$

where $u(x, t_k)$ denotes the solution to the IVP (3.7)-(3.9) with $t = t_k$, and $u(x)$ denotes the solution to the BVP (3.4)-(3.6). Note that the IVP (3.7)-(3.9) with a parameter t satisfying (3.10) is equivalent to the original BVP (3.4)-(3.6).

To implement the nonlinear shooting method (equations (3.7)-(3.10)) numerically, we use the following algorithm (Algorithm 11.2 in [12]) to approximate the solution of the nonlinear BVP (3.4)-(3.6). For simplicity, we only briefly sketch this algorithm below.

Algorithm - Nonlinear Shooting Method
Input: endpoints a and b; boundary conditions u_0 and u_1; number of subintervals N; tolerance ϵ; maximum number of subintervals M.

Output: approximations $W_{1,i}$ to $u(x_i)$; $W_{2,i}$ to $u'(x_i)$ for each $i = 0, 1, ..., N$.

Step 1 Set step size $h = (b - a)/N$; Let $k = 1$.

Step 2-6 **While** $k \leq M$

Apply Runge-Kuttta method to solve (3.7)-(3.10).

End While

Step 7- 9 Test for accuracy. If $|W_{1,n} - u_1| < \epsilon$, then output.

3.2 Numerical Methods for PDEs

For simplicity and clarity of the presentation, we consider the following PDE to illustrate the numerical methodology:

$$-\Delta u = f \qquad \text{in } \Omega \tag{3.11}$$
$$u = g \qquad \text{on } \partial\Omega, \tag{3.12}$$

where $\Omega \subset \mathbb{R}^d,\ d = 1, 2$, is the computational domain, $f : \Omega \to \mathbb{R}$ is the forcing term, $g : \partial\Omega \to \mathbb{R}$ yields the boundary conditions, and $u : \Omega \to \mathbb{R}$ is the solution that we need to approximate numerically.

For simplicity, we only consider the one-dimensional case:

$$\Omega = [0, 1]. \tag{3.13}$$

We emphasize, however, that our presentation carries over with very few changes to the two-dimensional and three-dimensional cases. Thus, the PDE (3.11)-(3.12) becomes

$$-u'' = f \qquad \text{in } [0, 1], \tag{3.14}$$
$$u(0) = u_0, \qquad u(1) = u_1. \tag{3.15}$$

3.2.1 The Finite Difference Method (FDM)

A basic introduction to the *Finite Difference Method (FDM)* is given in classic textbooks, such as [87, 53].

The FDM algorithm proceeds as follows: First, we divide the interval $[0, 1]$ into N subintervals of equal lengths:

$$0 = x_0 < x_1 < \ldots < x_{N-1} < x_N = 1, \tag{3.16}$$

where $x_i = i\,h$, with $h = \dfrac{1}{N}$, $i = 0, 1, \ldots, N$. The goal of the FDM is to approximate the exact solution u of (3.14)-(3.15) (which in general cannot be computed analytically) at the discrete points x_i, $i = 1, \ldots, N-1$. This is achieved by solving the discretized version of (3.14)-(3.15):

$$\frac{-u_{i-1} + 2\,u_i - u_{i-1}}{h^2} = f(x_i) \qquad i = 1, \ldots, N-1 \tag{3.17}$$

$$u_0 = u_0, \qquad u_1 = u_1, \tag{3.18}$$

in which the second-order differential operator is approximated (up to order $\mathcal{O}(h^2)$) by a finite difference term

$$-u''(x_i) \approx \frac{-u_{i-1} + 2\,u_i - u_{i-1}}{h^2}. \tag{3.19}$$

The system in (3.17)-(3.18) can be written as a linear system of algebraic equations

$$\mathbf{A}\,\mathbf{u} = \mathbf{b}, \tag{3.20}$$

in which the matrix A and the right-hand side vector $\mathbf{b}$ have the following form

$$\mathbf{A} = \begin{pmatrix} 2 & -1 & & & \\ -1 & 2 & -1 & & \\ & \ldots & \ldots & \ldots & \\ & & -1 & 2 & -1 \\ & & & -1 & 2 \end{pmatrix}, \qquad \mathbf{b} = \begin{pmatrix} h^2 f(x_1) + u_0 \\ h^2 f(x_2) \\ \ldots \\ h^2 f(x_{N-2}) \\ h^2 f(x_{N-1}) + u_N \end{pmatrix}. \tag{3.21}$$

The boundary conditions (3.18) are incorporated in the linear system (3.21) by modifying the corresponding entries in $\mathbf{b}$ accordingly. Since the matrix $\mathbf{A}$ resulting from the FDM discretization of PDEs (not necessarily the simple PDE (3.11)-(3.12) considered here) is generally sparse, iterative methods are generally used to solve the linear system (3.18). For a survey of iterative methods, the reader is refereed to [79, 17, 57, 93]. In this thesis, we mainly use the linear solver, LinearSolve, of Mathematica, which automatically switches among various modern matrix computation techniques depending on the matrix given.

3.2.2 The Finite Element Method (FEM)

There are so many good books on the *Finite element Method* (FEM), covering theoretical aspects, implementation issues, or both [25, 63, 86, 8].

This section represents just a modest attempt at summarizing the most important properties of the FEM, highlighting those features that are displayed in the following chapters. We also mention that one of the main strengths of the FEM is its ability to treat complex computational geometries.

Obviously, this is most easily illustrated in two and three dimensions. For clarity of exposition, however, we choose to use the same one-dimensional example as that employed in the previous subsection, i.e., the PDE in (3.14)-(3.15). Furthermore, to simplify the FEM presentation, we replace the non-homogeneous Dirichlet boundary conditions (3.15) with homogeneous ones:

$$u(0) = 0, \qquad u(1) = 0. \tag{3.22}$$

We emphasize that there is no loss of generality in considering the homogeneous boundary conditions in (3.22). Indeed, this can be achieved through a simple change of variables (the lifting procedure). Thus, the PDE considered in this section reads:

$$-u'' = f \qquad \text{in } [0,1] \tag{3.23}$$

$$u(0) = 0, \qquad u(1) = 0. \tag{3.24}$$

The FEM starts by considering the weak formulation of (3.23)-(3.24), which follows by multiplying (3.23) by a smooth test function v, integrating this product over the domain $[0,1]$, integrating by parts, and using the homogeneous boundary condition (3.24):

$$(f, v) = (-u'', v) \tag{3.25}$$

$$= (u', v') \qquad \forall \text{ smooth } v, \tag{3.26}$$

where $(f_1, f_2) = \int_0^1 f_1(x) f_2(x) dx$ denotes the inner product of two generic scalar functions f_1 and f_2. The smoothness of the test function v required by the integration by parts in the weak formulation (3.26) is $v \in H^1([0,1])$, where $H^1([0,1])$ is the Sobolev space of functions defined on $[0,1]$ that have a square integrable derivative (see, e.g., [25]). We emphasize that one of the main differences between the FDM and the FEM is the type of PDE formulation they consider: the FDM works directly with the original classical formulation of the PDE (3.14), whereas the FEM works with the weak formulation (3.26).

The next step in the FEM discretization is the choice of the functional space in which both the FEM approximation and the test function live. One obvious practical condition that the FEM space $X^h \subset H^1([0,1])$ needs to satisfy is that it should be finite dimensional. Furthermore, in the FEM, X^h consists of piecewise polynomial functions:

$$x^h := span\{\phi_1, \phi_2, \ldots, \phi_N\}, \tag{3.27}$$

where $\phi_i,\ i = 1, 2, ..., N$, are the local finite element basis functions. For example, the linear finite element basis functions read

$$\phi_i(x) = \begin{cases} \frac{x - x_{i-1}}{x_i - x_{i-1}} & x_{i-1} \le x < x_i \\ \frac{x_{i+1} - x}{x_{i+1} - x_i} & x_{i-1} \le x < x_i \\ 0 & otherwise. \end{cases} \tag{3.28}$$

We note that the computational domain in (3.28) (the interval $[0,1]$) was divided into a non-uniform partition

$$0 = x_0 < x_1 < \cdots < x_{N-1} < x_N = 1. \tag{3.29}$$

The next step in the FEM procedure is the Galerkin projection, which consists of the weak formulation (3.26) in which the functional space is the finite dimensional space X^h defined in (3.27):

$$(u_h', v_h') = (f, v_h) \quad \forall v_h \in X^h. \tag{3.30}$$

Since the finite element approximation u_h belongs to X^h, (3.27) implies that

$$u_h(x) = \sum_{j=1}^{N-1} u_j \phi_j(x). \tag{3.31}$$

Plugging (3.31) in (3.30) and choosing $v_h := \phi_i,\ i = 1, 2, ..., N$, yields the following linear system:

$$\mathbf{A}\mathbf{u} = \mathbf{b}, \tag{3.32}$$

where $u := (u_1, u_2, \ldots, u_N)$ is the vector of finite element unknowns, $\mathbf{A} = (a_{ij})$, with $(a_{ij}) = (\phi_j', \phi_i')$, is the stiffness matrix, and $\mathbf{b} = (b_i)$, with $b_i = (f, \phi_i)$ is the load vector. The local integrals in the entries of $\mathbf{A}$ and $\mathbf{b}$ are computed by first mapping the local intervals to a reference element (the interval $[-1, 1]$ in the one-dimensional case), and then using Gauss quadrature. We emphasize that, since the finite element basis functions have a compact support (ϕ_i is non-zero only in $[x_{i-1}, x_{i+1}]$), the matrix $\mathbf{A}$ is sparse. Thus, as in the FDM case, iterative linear solvers should to be used.

Remark 1. *For one-dimensional problems, when the mesh points are uniformly spaced, the FEM with linear basis functions and the FDM are equivalent. Indeed, in this case the linear systems that we need to solve for the two numerical methods are almost the same. In general, however, FDM and FEM produce different numerical results.*

3.3 Numerical Methods for Nonlinear Equations

A good survey of numerical methods for nonlinear equations, including both theoretical and computational aspects, is given in, e.g., [64].

The general problem that needs to be solved is the following: Find $\mathbf{u} \in \mathbb{R}^n$ such that

$$\mathbf{F}(\mathbf{u}) = \mathbf{0}, \tag{3.33}$$

where $\mathbf{F} : \mathbb{R}^{\mathbf{n}} \to \mathbb{R}^{\mathbf{n}}$ is a nonlinear function.

The most common approach used in the numerical approximation of $\mathbf{u}$, the solution of (3.33), is to linearize the nonlinear function F and then solve the resulting linear problem. Next, we present two of the most popular such approaches, which we employ in the following chapters.

3.3.1 Fixed Point (Picard) Iteration

The fixed point iteration (FPI), also know as the *Picard iteration*, proceeds by rewriting (3.33) as

$$\mathbf{\Phi}(\mathbf{y}) = \mathbf{y}. \tag{3.34}$$

Thus, a solution $\mathbf{x}$ of (3.33) is a fixed point $\mathbf{y}$ for (3.34). The FPI consists of the following iterative process: Let $\mathbf{y} \in \mathbb{R}^n$ (the initial guess) be given. For each $k = 1, 2, ...$, given $\mathbf{y}^{k-1} \in \mathbb{R}^n$, let $\mathbf{y}^k$ be

$$\mathbf{y}^k = \mathbf{\Phi}(\mathbf{y}^{k-1}). \tag{3.35}$$

One can prove that, if $\mathbf{\Phi}$ is a *contraction*, then

$$\mathbf{y}^k \to \alpha, \text{ when } k \to \infty, \tag{3.36}$$

where α is the fixed point of $\mathbf{\Phi}$. We remind that $\mathbf{\Phi} : \mathbb{R}^n \to \mathbb{R}^n$ is a contraction if there exists a constant $0 < \gamma < 1$ such that

$$\|\mathbf{\Phi}(\mathbf{a}) - \mathbf{\Phi}(\mathbf{b})\| \leq \|\mathbf{a} - \mathbf{b}\| \quad \forall \mathbf{a}, \mathbf{b} \in \mathbb{R}^n. \tag{3.37}$$

The proof of the convergence of the FPI (3.35) can be found in, e.g., [64, 53].

We note that one of the main positive features of the FPI (3.35) is its robustness with respect to initial guesses $\mathbf{y}^0$. Indeed, it can be shown that for fairly general nonlinear functions $\mathbf{F}$, the FPI (3.35) converges for all initial guess $\mathbf{y}^0$. The trade-off, however, is that the FPI (3.35) generally converges only linearly, and thus has a relatively slow convergence.

3.3.2 Newton's Method

An alternative to the FPI is *Newton's method* (NM). NM is also an iterative process, which starts with an initial guess $\mathbf{x}^0 \in \mathbb{R}^n$ and, assuming that $\mathbf{x}^{k-1}$ is given, computes the next iterate $\mathbf{x}^k$ for each $k = 1, 2, 3, ...$ This computation of the next iterate $\mathbf{x}^k$ is based on the linearization of the nonlinear function $\mathbf{F}$. Indeed, ideally we would like the next iterate $\mathbf{x}^k$ to satisfy $\mathbf{F}(\mathbf{x}^k) = \mathbf{0}$. Since this equation is nonlinear, however, we first linearize it by using a first-order Taylor expansion around the previous iterate, $\mathbf{x}^{k-1}$:

$$\mathbf{0} = \mathbf{F}(\mathbf{x}^k) \approx \mathbf{F}(\mathbf{x}^{k-1}) + \mathbf{F}'(\mathbf{x}^{k-1})(\mathbf{x}^k - \mathbf{x}^{k-1}), \tag{3.38}$$

where $\mathbf{F}(\mathbf{x}^{k-1}) := \left(\frac{\partial F_i}{\partial x_j}(\mathbf{x}^{k-1})\right)_{1 \leq i,j \leq n}$ is the Jacobian matrix of $\mathbf{F}$ at $\mathbf{x}^{k-1}$.

Solving the linear (in $\mathbf{x}^k$) equation

$$\mathbf{F}'(\mathbf{x}^{k-1})(\mathbf{x}^k - \mathbf{x}^{k-1}) = -\mathbf{F}(\mathbf{x}^{k-1}) \tag{3.39}$$

yields the new iterate $\mathbf{x}^k$.

One of the most important positive features of NM (3.39) is its quadratic convergence. Indeed, one usually notices in practical computations that NM (3.39) is significantly faster than the FPI (3.35), which only converges linearly. There is, however, a caveat. NM is very sensitive with respect to the initial guess $\mathbf{x}^0$: if $\mathbf{x}^0$ is close to the exact solution, then NM converges quadratically; if, however, $\mathbf{x}^0$ is not close enough to $\mathbf{x}$, then NM can actually fail to converge. We emphasize that this phenomenon is not only of theoretical concern - we can observe it in practical computations, as we will later see in Chapters 4 and 5.

3.4 Numerical Methods for Optimization

Note that by Theorems 2.1 - 2.3, the dual formulation of the non-convex primal problem $\mathcal{P}_{sta}$ (2.10) leads to an optimization problem, which can be solved using numerical methods. An excellent introduction to numerical methods for optimization is given in Nocedal and Wright [69].

In this thesis, we will use quasi-Newton methods to perform the optimization. Quasi-Newton methods, like steepest descent, require only the gradient of the objective function to be supplied at each iterate. By measuring the changes in gradients, they construct a model of the objective function that is good enough to produce super-linear convergence. In contrast, another popular optimization method, Newton's method, assumes that the function to be minimized can be locally approximated as a quadratic function near the stationary point, and uses the first and second derivatives (gradient and Hessian) to find the stationary point. Although Newton's methods have quadratic convergence, the Hessian matrix of second derivatives of the function to be minimized needs to be computed at each iterate. In quasi-Newton methods, however, the Hessian matrix need not be computed. Instead, the Hessian is updated by analyzing successive gradient vectors. Therefore, quasi-Newton methods are sometimes more efficient than Newton's method, and this is one reason why quasi-Newton method is used in this thesis. The other reason is that, in the numerical optimizing process, the local convexity of the objective function is implicitly guaranteed. This property is important to the application of Theorem 2.2, of which local convexity is required.

There are many variants of quasi-Newton methods. Among them, a popular one is the the BFGS method, named for its discoverers Broyden, Fletcher, Goldfarb, and Shanno. A brief description of the BFGS algorithm is given below. For a detailed discussion of the BFGS method, the reader is referred to Section 8.1 in [69].

Algorithm - BFGS Method
Let f be the objective function. The starting point $\mathbf{x}^0$, convergence tolerance $\epsilon > 0$, and inverse Hessian approximation $\boldsymbol{H}_0$ are given. For simplicity, we choose $\boldsymbol{H}_0$ to be the identity matrix. Let

$k = 0$.

While $\| \bigtriangledown f_k \| > \epsilon$

Compute search direction

$$\boldsymbol{\rho}_k = -\boldsymbol{H}_k \bigtriangledown f_k \tag{3.40}$$

Set $\mathbf{x}_{k+1} = \mathbf{x}_k + \alpha_k \boldsymbol{\rho}_k$, where α_k is computed from a line search procedure to satisfy the Wolfe conditions (Chapter 3 in [69]);

Define $\boldsymbol{s}_k = \mathbf{x}_{k+1} - \mathbf{x}_k$ and $\boldsymbol{y}_k = \bigtriangledown f_{k+1} - \bigtriangledown f_k$;

Compute $\boldsymbol{H}_{k+1}$ by means of BFGS formula

$$\boldsymbol{H}_{k+1} = \left(\boldsymbol{I} - \frac{s_k y_k^T}{y_k^T s_k} \right) \boldsymbol{H}_k \left(\boldsymbol{I} - \frac{y_k s_k^T}{y_k^T s_k} \right) + \frac{s_k s_k^T}{y_k^T s_k}; \tag{3.41}$$

Let k= k+1;

End While

Each iteration can be performed at a cost of $O(n^2)$ arithmetic operations. The algorithm is robust with a super-linear rate of convergence. Note that in the BFGS updating formula (3.41), $\boldsymbol{H}_{k+1}$ is positive whenever $\boldsymbol{H}_k$ is (see page 199 in [69]).

Chapter 4

A Numerical Investigation of A Modified Version of Ericksen's Bar

In Chapter 1, we have introduced a general primal problem of the form

$$(\mathcal{P}): \qquad P(u) = \frac{1}{2}\langle u, Au\rangle + W(u) - \langle u, f\rangle. \tag{4.1}$$

The criticality condition $DP(u) = 0$ for the variational problem $(\mathcal{P})$ leads to the governing equation

$$Au + DW(u) = f. \tag{4.2}$$

When A vanishes, the primal problem $(\mathcal{P})$ is reduced to:

$$(\mathcal{P}_W): \qquad P(u) = W(u) - \langle u, f\rangle. \tag{4.3}$$

In this chapter, we work with a modified version of Ericksen's bar in nonlinear elasticity [22], which is structurally similar to the form $(\mathcal{P}_W)$, with u being replaced by u_x. Both the non-convex variational problems and the associated boundary-value problems are studied using Ericksen's soft and hard devices. The strain-energy function is a general fourth-order polynomial in a suitable measure of strain, which provides a convenient model for the study of phase transitions. Because of the non-convex (double-well) structure of the term $W(u)$, we expect the problem $(\mathcal{P}_W)$ to have non-unique stationary point solutions. On the basis of the canonical duality theory introduced in Chapter 2, the nonlinear differential equation for the non-convex, non-homogeneous variational problem, here with either mixed or Dirichlet boundary conditions, is converted into an algebraic equation, which can, in principle, be solved to obtain a complete set of solutions. Another important outcome of the canonical duality theory is the identification and characterization of the local energy extrema and the global energy minimizer.

For the soft loading device, criteria for the existence, uniqueness, smoothness and multiplicity of solutions are presented and discussed. We will illustrate the difficulty of capturing nonsmooth solution and identifying extrema with standard numerical methods discussed in Chapter 3. The results illustrate the important fact that smooth analytic or numerical solutions of a nonlinear mixed boundary-value problem might not be minimizers of the associated potential variational problem. From a dual perspective, the convergence (or non-convergence) of the standard numerical methods is explained and numerical examples are provided. For the hard loading device, the canonical duality theory is applied directly to obtain the minimizing solution. The standard numerical methods are used to show that smooth analytic or numerical solutions of a nonlinear Dirichlet boundary-value problem might not be minimizers of the associated potential variational problem.

The rest of the chapter is organized as follows. In Section 4.1, we present a modified version of Ericksen's bar. In Section 4.2, the canonical dual transformation is employed to obtain a pure complementary energy functional for both soft and hard device problems. In Section 4.3, the triality theory provides local and global extremality conditions for non-convex problems for the variational problem for the soft loading device. The existence of smooth solutions to the associated mixed boundary-value problem is discussed. In Section 4.4, the minimizing solution for the variational problem with hard loading device is given, based on the results proposed for the soft device. Section 4.5 contains some concluding remarks.

4.1 A Modified Version of Ericksen's Bar

Experimental observations of phase transitions and twinning in solids reveal fine layered microstructure in many configurations (see Fig. 1.1). In the last thirty years, a considerable theoretical effort has been aimed at understanding such phenomena. This has been based mainly on finding minimizers of an energy functional that incorporates a non-convex elastic strain-energy function as the material model, similar to the van der Waals double-well potential. The relevance of these ideas is clearly revealed by Derricks's analysis of the non-unique minimizers for an elastic bar with a non-monotone strain-stress relation [22, 94].

In this chapter, we revisit Ericksen's bar, which is treated as a one-dimensional smooth manifold covered by a material coordinate x, with x ranging over a closed, finite interval $I = [0, 1]$ and $\mathcal{U}$ a certain displacement space:

$$(\mathcal{P}_E): \quad \min_{u\in\mathcal{U}} \left\{ E = \int_0^1 W(u_x)dx - \sigma(1)u(1) \right\}. \tag{4.4}$$

Ericksen's bar provides a simple but convenient model for the study of phase transitions. For both soft and hard loading devices, Ericksen showed that the solutions obtained are meta-stable and

may have an arbitrary number of discontinuities. These discontinuities are phase interfaces, where transition between a pair of phases occurs. Thus, these interfaces are important for explaining experimental observations of hysteresis, which arises when the material points become trapped in meta-stable states [62, 96].

Following Ericksen's idea, we consider the two classic loading devices: soft and hard. To make the mixing of phases more dramatic, we introduce a distributed axial loading $f \in \mathcal{C}[0,1]$. For the soft device, the bar is fixed at the end $x = 0$, while the end $x = 1$ is subject to a given dead load $\sigma(1)$. Thus, we have a variational problem with mixed boundary conditions, which can be written as

$$(\mathcal{P}_s): \quad \min_{u\in\mathcal{U}_s}\left\{P_s(u) = \int_0^1 W(u_x)dx - \int_0^1 fu\mathrm{d}x - \sigma(1)u(1)\right\}, \tag{4.5}$$

where $u : [0,1] \to \mathbb{R}$ is the displacement function in a certain feasible function space, which we denote by $\mathcal{U}_s$ (to be defined in Section 4.3), and $W(u_x)$ is the strain energy per unit length, which here is taken to be non-convex, and u_x is a uniaxial measure of strain. The associated one-dimensional (first Piola-Kirchhoff) stress is

$$\sigma(x) = \frac{\partial W(u_x)}{\partial u_x}. \tag{4.6}$$

For the hard device, u is restricted to a certain feasible function space, $\mathcal{U}_h$ (to be defined in Section 4.4), such that

$$u(0) = 0,\ u(1) = d, \tag{4.7}$$

where d is a given constant. In this case, the variational problem can be written as

$$(\mathcal{P}_h): \quad \min_{u\in\mathcal{U}_h}\left\{P_h(u) = \int_0^1 W(u_x)\mathrm{d}x - \int_0^1 fu\mathrm{d}x\right\}. \tag{4.8}$$

For consistency with the classical theory of elasticity the energy and stress must vanish in the undeformed configuration and the extensional elastic modulus must be positive, i.e.,

$$W(0) = W'(0) = 0, \quad W''(0) > 0, \tag{4.9}$$

where a prime indicates a derivative of W with respect to u_x. For this purpose, it suffices to consider W to have the following fourth-order polynomial form:

$$W(\gamma) = \tfrac{1}{2}\mu\gamma^2 + \tfrac{1}{2}\nu\left(\tfrac{1}{2}\gamma^2 - \alpha\gamma\right)^2, \tag{4.10}$$

where γ is a (one-dimensional) measure of strain, and μ, ν and α are positive material constants (see Gao and Ogden [46]). For consistency with the notations in [46], in this section, the author uses γ for u_x. However, u_x is used throughout the rest of the chapter. This is the strain-energy

function they used in considering the azimuthal shear problem that yields multiple solutions, in which context γ is the local shear strain. The corresponding stress σ is given by

$$\sigma = W'(\gamma) = \gamma\left(\tfrac{1}{2}\nu\gamma^2 - \tfrac{3}{2}\nu\alpha\gamma + \mu + \nu\alpha^2\right). \tag{4.11}$$

For (4.10), the first two equations in (4.9) are satisfied, as is the third, since $W''(0) = \mu + \nu\alpha^2$ and we have $\mu > 0$ and $\nu > 0$. Moreover, as shown in [46], $W''(\gamma) \geq 0$ if $\nu\alpha^2 \leq 2\mu$, W is non-convex if $\nu\alpha^2 > 2\mu$, and has a double-well if $\nu\alpha^2 > 8\mu$. Fig. 4.1 shows both $W(\gamma)$ and $\sigma = W'(\gamma)$ for the latter two situations with representative values of μ, ν and α. Note, in particular, that σ is non-monotone in each case.

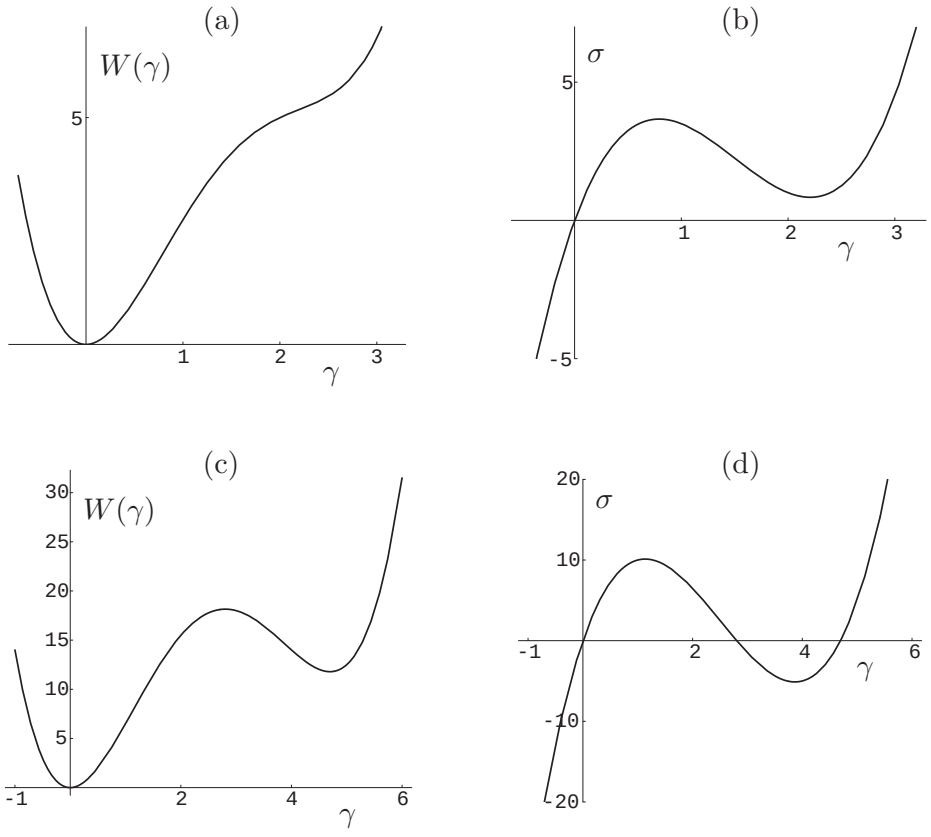

Figure 4.1: Plots of (a) non-convex $W(\gamma)$ for $\mu = 1.5$, $\nu = 4$, $\alpha = 1.5$; (b) its derivative $\sigma = W'(\gamma)$; (c) double-well energy $W(\gamma)$; and (d) its non-monotone derivative $\sigma = W'(\gamma)$ for $\mu = 1$, $\nu = 3$, $\alpha = 2.5$.

Here we have $\gamma = u_x$ and we take $\nu\alpha^2 > 2\mu$ so that the two variational problems above, $(\mathcal{P}_s)$ and $(\mathcal{P}_h)$, are non-convex problems involving the energy function (4.10). As discussed in the previous chapters, direct approaches and relaxation methods for solving nonlinear equilibrium equations

have been discussed extensively for more than thirty years [16, 28, 54, 76]. It is known that for nonlinear variational problems, traditional direct methods can provide only upper bounds to the solutions. In particular, the relaxation method based on the *Young measure* can be used for finding global minimizers of non-convex problems [67, 72, 71]. However, in the study of phase transitions, local extrema play an important role and cannot be ignored. Identification of the extrema of the variational problems $(\mathcal{P}_s)$ and $(\mathcal{P}_h)$ is a fundamentally difficult task in non-convex analysis, whether or not W has a double-well. The canonical duality theory appears as a possible way for addressing these issues. This is the major reason why we are interested in the canonical duality theory introduced in the first two chapters.

4.2 Canonical Dual Methods for the Modified Version of Ericksen's Bar

The canonical duality theory comprises three components: a canonical dual transformation, a pure complementary energy principle and a triality theory [28, 31]. The canonical dual transformation can be used to establish perfect dual problems in non-convex optimization and a pure complementary energy principle in nonlinear mechanics, while triality theory provides local and global extremality conditions for non-convex problems [31, 33, 50].

In this section, we apply the *canonical dual transformation* to $P_s(u)$ and $P_h(u)$ in order to obtain the associated pure complementary energy functionals following the method developed in [28, 31]. We define a two-component canonical strain measure $\boldsymbol{\xi}$ by

$$\boldsymbol{\xi} = (\varepsilon, \xi) = \left(\tfrac{1}{2}u_x^2,\ \tfrac{1}{2}u_x^2 - \alpha u_x\right) \in \mathbb{R}^2. \tag{4.12}$$

The canonical energy obtained by substituting for $\boldsymbol{\xi}$ in (4.10) is

$$U(\boldsymbol{\xi}) = \mu\varepsilon + \tfrac{1}{2}\nu\xi^2. \tag{4.13}$$

This is a convex (quadratic) function, which is well defined on the domain

$$\mathcal{E} = \{(\varepsilon, \xi) \in \mathcal{L}^1 \times \mathcal{L}^2 \ \big|\ \varepsilon(x) \geq 0,\ \ \xi(x) \geq -\tfrac{1}{2}\alpha^2,\ \ \forall x \in [0,1]\}, \tag{4.14}$$

where $\mathcal{L}^p$ is the space of Lebesgue integrable functions for $p \in [1, \infty)$ [1].

The canonical dual 'stress' vector

$$\boldsymbol{\zeta} = (\varsigma, \zeta) = U_{\boldsymbol{\xi}}(\boldsymbol{\xi}) = (\mu,\ \nu\xi) \in \mathbb{R}^2, \tag{4.15}$$

where $U_{\boldsymbol{\xi}}(\boldsymbol{\xi}) \equiv \partial U(\boldsymbol{\xi})/\partial\boldsymbol{\xi}$, is well defined on the dual space

$$\mathcal{S} = \{(\varsigma, \zeta) \in \mathcal{L}^\infty \times \mathcal{L}^2 \ \big|\ \varsigma(x) = \mu,\ \ \zeta(x) \geq -\tfrac{1}{2}\nu\alpha^2,\ \ \forall x \in [0,1]\ \}. \tag{4.16}$$

Thus, the complementary energy can be obtained by the Legendre transformation

$$U^*(\boldsymbol{\zeta}) = \{\boldsymbol{\xi}\cdot\boldsymbol{\zeta} - U(\boldsymbol{\xi}) \mid \ \boldsymbol{\zeta} = U\ (\boldsymbol{\xi})\} = \tfrac{1}{2}\nu^{-1}\zeta^2. \tag{4.17}$$

By replacing $W(u_x) = U(\boldsymbol{\xi})$ in $\mathcal{P}(u)$ by $\boldsymbol{\xi}\cdot\boldsymbol{\zeta} - U^*(\boldsymbol{\zeta})$, we obtain the Gao-Strang total complementary energy $\Xi(u,\zeta)$ [50] for this non-convex problem in the form

$$\begin{aligned}\Xi(u,\zeta) &= \int_0^1 [\boldsymbol{\xi}\cdot\boldsymbol{\zeta} - U^*(\boldsymbol{\zeta})]\mathrm{d}x - \int_0^1 fu\mathrm{d}x - \sigma(1)u(1)\\ &= \int_0^1 \left[\tfrac{1}{2}(u_x)^2(\zeta+\mu) - \alpha u_x\zeta - \tfrac{1}{2}\nu^{-1}\zeta^2\right]\mathrm{d}x - \int_0^1 fu\mathrm{d}x - \sigma(1)u(1).\end{aligned} \tag{4.18}$$

For a given $\boldsymbol{\zeta}\in\mathcal{S}$, the criticality condition $\delta_u\Xi(u,\zeta) = 0$, lead to the equation

$$\sigma_x + f = 0 \ \ \forall x\in(0,1), \tag{4.19}$$

with a natural boundary condition $\sigma|_{x=1} = \sigma(1) = \sigma_1$, where

$$\sigma = (\zeta+\mu)u_x - \alpha\zeta. \tag{4.20}$$

Note that if one replaces η by $\nu\xi$ in (4.20), with ξ given by (4.12), and then, with $\gamma = u_x$, σ is consistent with the expression for σ in (4.11).

Integrating (4.19) and applying the natural boundary condition $\sigma|_{x=1} = \sigma_1$, we obtain

$$\sigma(x) = \int_x^1 f(s)ds + \sigma(1). \tag{4.21}$$

Now use (4.19) to eliminate f from (4.18) and make the substitution $u_x = (\sigma+\alpha\zeta)/(\mu+\zeta)$ from (4.20) to obtain the pure complementary energy functional

$$P_s^d(\zeta) = -\frac{1}{2}\int_0^1 \left(\frac{(\sigma+\alpha\zeta)^2}{\mu+\zeta} + \nu^{-1}\zeta^2\right)\mathrm{d}x, \tag{4.22}$$

which is well defined on the dual feasible space

$$\mathcal{S}_a = \{\zeta\in\mathcal{L}^2 \,\big|\, \zeta(x)+\mu\neq 0,\ \ \zeta(x)\geq -\tfrac{1}{2}\nu\alpha^2,\ \ \forall x\in[0,1]\ \}. \tag{4.23}$$

Similarly, the pure complementary energy functional for the hard device is

$$P_h^d(\zeta) = -\frac{1}{2}\int_0^1 \left(\frac{(\sigma+\alpha\zeta)^2}{\mu+\zeta} + \nu^{-1}\zeta^2\right)\mathrm{d}x + \sigma(1)u(1), \tag{4.24}$$

which is also defined on $\mathcal{S}_a$. The criticality conditions for $P_s^d(\zeta)$ and $P_h^d(\zeta)$ with respect to ζ leads to the same *Dual Algebraic Equation* (DAE) for both (4.22) and (4.24), namely

$$(2\nu^{-1}\zeta + \alpha^2)(\mu+\zeta)^2 = (\sigma-\mu\alpha)^2. \tag{4.25}$$

It should be pointed out that the integrand of $\mathcal{P}^d(\zeta)$ has a singularity at $\zeta = -\mu$, which explains the exclusion $\zeta \neq -\mu$ in the definition of $\mathcal{S}_a$. In fact, it turns out that, in general, $\zeta = -\mu$ does not correspond to a critical point of $\mathcal{P}^d(\zeta)$. Exceptionally, we may have $\zeta(x) = -\mu$ for some $x \in (0,1)$, but this is always associated with $\sigma(x) = \mu\alpha$. It is therefore important to note that when (4.25) holds, the integrand in (4.22) can be written as

$$\alpha(\sigma + \alpha\zeta) + \nu^{-1}\zeta^2. \tag{4.26}$$

When $\zeta = -\mu$ (and $\sigma = \mu\alpha$), this reduces to $\nu^{-1}\mu^2$, and the singularity in the integrand is thereby removed.

The DAE (4.25) is very important in solving the modified version of Ericksen's bar in that its solutions can be calculated directly and can be ordered. These ordered solutions will then be converted to corresponding primal solutions. Thus, for the given parameters μ, ν, α, the three solutions of the cubic DAE (4.25) can be given as

$$\bar{\zeta}_1 = -\frac{1}{6}(\nu\alpha^2 + 4\mu) + \frac{1}{6}\left[\frac{(\nu\alpha^2 - 2\mu)^2}{\omega(\sigma)} + \omega(\sigma)\right], \tag{4.27}$$

$$\begin{aligned}\bar{\zeta}_2 = &-\frac{1}{6}(\nu\alpha^2 + 4\mu) - \frac{1}{12}\left[\frac{(\nu\alpha^2 - 2\mu)^2}{\omega(\sigma)} + \omega(\sigma)\right] \\ &+\frac{\mathrm{i}\sqrt{3}}{12}\left[\frac{(\nu\alpha^2 - 2\mu)^2}{\omega(\sigma)} - \omega(\sigma)\right],\end{aligned} \tag{4.28}$$

$$\begin{aligned}\bar{\zeta}_3 = &-\frac{1}{6}(\nu\alpha^2 + 4\mu) - \frac{1}{12}\left[\frac{(\nu\alpha^2 - 2\mu)^2}{\omega(\sigma)} + \omega(\sigma)\right] \\ &-\frac{\mathrm{i}\sqrt{3}}{12}\left[\frac{(\nu\alpha^2 - 2\mu)^2}{\omega(\sigma)} - \omega(\sigma)\right],\end{aligned} \tag{4.29}$$

where

$$\omega(\sigma) = 3\nu^{1/3}\left(2\beta^2 - \eta + 2\sqrt{\beta^2(\beta^2 - \eta)}\right)^{1/3}.$$

For convenience, we will use the following notations:

$$\beta = \mu\alpha - \sigma, \quad \eta = (\nu\alpha^2 - 2\mu)^3/27\nu. \tag{4.30}$$

If $\sigma \neq 0$, then $\omega(\sigma)$ is real if $\eta \leq \beta^2$, in which case there is only one real solution, namely (4.27). On the other hand, if $\eta > \beta^2$, then all three solutions are real and may be written as

$$\bar{\zeta}_1 = -\frac{1}{6}(\nu\alpha^2 + 4\mu) + \frac{1}{6}\left[\omega(\sigma) + \omega^{\mathrm{c}}(\sigma)\right], \tag{4.31}$$

$$\bar{\zeta}_2 = -\frac{1}{6}(\nu\alpha^2 + 4\mu) - \frac{1}{12}\left[\omega(\sigma) + \omega^{\mathrm{c}}(\sigma)\right] - \frac{\mathrm{i}\sqrt{3}}{12}\left[\omega(\sigma) - \omega^{\mathrm{c}}(\sigma)\right], \tag{4.32}$$

$$\bar{\zeta}_3 = -\frac{1}{6}(\nu\alpha^2 + 4\mu) - \frac{1}{12}\left[\omega(\sigma) + \omega^{\mathrm{c}}(\sigma)\right] + \frac{\mathrm{i}\sqrt{3}}{12}\left[\omega(\sigma) - \omega^{\mathrm{c}}(\sigma)\right], \tag{4.33}$$

where $\omega^{\mathrm{c}}(\sigma)$ is the complex conjugate of $\omega(\sigma)$, in which case $\omega(\sigma)\omega^{\mathrm{c}}(\sigma) = 1$.

For a graphical view of the *dual algebraic curve* (4.25), we let

$$h(\zeta) = \sigma - \mu\alpha = \pm(\mu + \zeta)\sqrt{2\nu^{-1}\zeta + \alpha^2}, \tag{4.34}$$

and plot $h(\zeta)$ in Fig. 4.2 below.

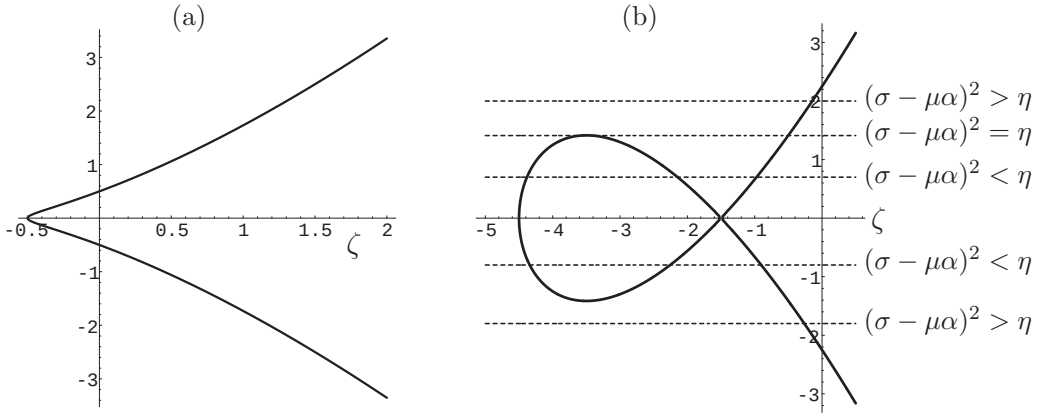

Figure 4.2: Dual algebraic curves $\sigma(\zeta) - \mu\alpha = \pm(\zeta+\mu)\sqrt{2\nu^{-1}\zeta + \alpha^2}$: (a) $\mu = 1, \nu = 4, \alpha = 0.5\,(\eta < 0)$; (b) $\mu = 1.5, \nu = 4, \alpha = 1.5\,(\eta > 0)$. The vertical axis is the h-axis.

We summarize the criteria for the solutions of the DAE (4.25), which is associated with the dual formulations.

Theorem 4.1 (Solutions of the DAE (4.25) **of the Dual Formulations [47]).** *Suppose that the body force f and the dead load σ_1 are given, $\sigma(x)$ is defined by* (4.21) *and $\beta(x) = \sigma(x) - \mu\alpha$.*

(i) If $\eta \le 0$ ($\nu\alpha^2 \le 2\mu$), then the DAE (4.25) *has a unique solution in the whole domain* $[0, 1]$.

(ii) If $\eta > 0$, then the DAE (4.25) *can have multiple solutions in* $[0, 1]$.

(a) If σ is such that $\beta^2 > \eta$, then the DAE (4.25) *has a unique real root $\bar{\zeta}_1(x) > -\mu$.*

(b) If $\beta^2 < \eta$ for some material point x, then it has multiple solutions, and (4.25) *has three real roots at x, ordered as*

$$\bar{\zeta}_1(x) \ge -\mu \ge \bar{\zeta}_2(x) \ge \bar{\zeta}_3(x) \ge -\tfrac{1}{2}\nu\alpha^2. \tag{4.35}$$

Proof. The main part of the proof is just a particular case of Theorem 3 in [46].

(i) This is intuitively true. Observe that for values of parameters such that $\eta < 0$ (i.e., $\nu\alpha^2 < 2\mu$), the plot of the DAE curve is shown in Fig. 4.2. For any value that $\beta(\zeta) = \mu\alpha - \sigma$ takes, it crosses the DAE curve only once, which is to say, there is a unique solution for any given σ.

(ii) As shown in Fig. 4.2(b), for $\eta > 0$ with $2\mu < \nu\alpha^2 < 8\mu$, the DAE (4.25) has at most three real solutions depending on $\sigma(x)$, $x \in (0,1)$. Specifically, if σ is such that $\beta^2 > \eta$, then the DAE (4.25) has a unique real root $\bar{\zeta}_1(x) > -\mu$. If $\beta^2 < \eta$ for some material point x, then the DAE (4.25) has multiple solutions. We prove here that the three real roots are ordered as above. We set $\omega = a + b\mathrm{i}$, where a and b are real, so that $\omega + \bar{\omega} = 2a$ and $\omega - \bar{\omega} = 2b\mathrm{i}$. Then

$$\bar{\zeta}_1 - \bar{\zeta}_2 = \tfrac{1}{2}(a - b/\sqrt{3}), \quad \bar{\zeta}_2 - \bar{\zeta}_3 = b/\sqrt{3}. \tag{4.36}$$

Without loss of generality, we may set $\sqrt{3}a \geq b \geq 0$, so that $\bar{\zeta}_1 \geq \bar{\zeta}_2 \geq \bar{\zeta}_3$.

Next, we note that

$$\begin{aligned} \bar{\zeta}_1 + \mu &= \tfrac{1}{6}[2a - (\nu\alpha^2 - 2\mu)], \\ \bar{\zeta}_2 + \mu &= \tfrac{1}{6}[\sqrt{3}b - a - (\nu\alpha^2 - 2\mu)], \\ \bar{\zeta}_3 + \tfrac{1}{2}\nu\alpha^2 &= \tfrac{1}{6}[2(\nu\alpha^2 - 2\mu) - a - \sqrt{3}b]. \end{aligned}$$

Since $\nu\alpha^2 > 2\mu$, it follows from the relation $\omega\bar{\omega} = a^2 + b^2 = (\nu\alpha^2 - 2\mu)^2$ that $\nu\alpha^2 - 2\mu \leq 2a$, so that $\bar{\zeta}_1 \geq -\mu$.

We also have

$$\nu\alpha^2 - 2\mu + a - \sqrt{3}b = \sqrt{a^2 + b^2} + a - \sqrt{3}b \geq \frac{2b}{\sqrt{3}} + \frac{b}{\sqrt{3}} - \sqrt{3}b = 0.$$

Hence $\bar{\zeta}_2 \leq -\mu$. Finally,

$$2(\nu\alpha^2 - 2\mu) - a - \sqrt{3}b = \frac{(\sqrt{3}a - b)^2}{2\sqrt{a^2 + b^2} + a + \sqrt{3}b} \geq 0,$$

and it follows that $\bar{\zeta}_3 \geq -\frac{1}{2}\nu\alpha^2$. □

We now introduce the Maxwell line, which plays an important role in phase transitions. For the given non-convex strain energy $W(\gamma)$, the so-called 'Maxwell line' in the $\gamma - \sigma$ space is the horizontal line that cuts the curve $\sigma = W'(\sigma)$ in such a way that the two closed areas so formed are equal, as depicted in Fig. 4.3, which is similar to Fig. 1 in [22]. For a detailed discussion of this with respect to the solutions $\bar{\zeta}_i$, $i = 1, 2, 3$, and the location of the corresponding solutions for γ on the curve, we refer to Theorem 5 in [46]. The relevance of the Maxwell line and the canonical dual space are shown in the theorem below. Its proof can be found in [47].

Theorem 4.2 (Maxwell Line - Theorem 1 in [47]). *Suppose that $W(\gamma)$ is the given non-convex strain energy such that $\sigma = W'(\sigma)$ is the associated first Piola-Kirchhoff stress. Let ζ be the canonical dual stress defined by the DAE* (4.25) *and suppose that $\eta > 0$. Then, the Maxwell line corresponds to the $\zeta-$axis in the dual algebraic curve space.*

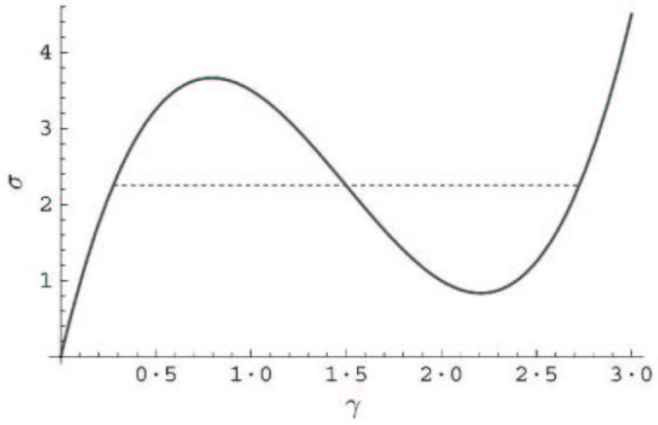

Figure 4.3: Plot of $\sigma = W'(\gamma)$ against γ for $\mu = 1.5, \nu = 4, \alpha = 1.5$ together with the Maxwell line (dashed) at $\sigma = \mu\alpha = 2.25$, which cuts off two equal closed areas from the σ curve.

Theorem 4.2 essentially says that the Maxwell line in the $\gamma - \sigma$ space can be defined as the $\zeta-$axis in the dual algebraic curve space

$$(2\nu^{-1}\zeta + \alpha^2)(\mu + \zeta)^2 = 0. \tag{4.37}$$

This was first found in the context of a pure azimuthal shear problem in nonlinear elasticity [46]. The canonical DAE (4.25) for general three-dimensional finite elasticity was proposed in [30]. Based on the dual solutions above, the non-convex variational problems $(\mathcal{P}_s)(4.5)$ and $(\mathcal{P}_h)(4.8)$ can be solved. Theorems 4.1 and 4.2 plays an important role in phase transitions of the modified version of Ericksen's bar, and may have broader implications in general non-convex analysis.

4.3 The Soft Device

Recall that for the soft device the bar is fixed at one end ($x = 0$), while the other end ($x = 1$) is subject to a given dead load. In this section, we first present theoretical results, including a complete set of solutions, for the mixed variational problem $(\mathcal{P}_s)$. Then, we compare the analytical solutions with numerical results obtained by using a fixed point iteration method together with a finite difference approximation.

4.3.1 Theoretical Results

For the soft device, the Ericksen's bar is fixed at the left end $x = 0$, while the right end at $x = 1$ is subject to a given dead load σ_1. Since the strain energy $W(\gamma)$ is configured to be a fourth-order polynomial function of $\gamma = u_x$, as defined in (4.10), the kinematically feasible space $\mathcal{U}_s$ can be defined as

$$\mathcal{U}_s = \{u \in \mathcal{L}(0,1) | u_x \in \mathcal{L}^4(0,1), u(0) = 0\}. \tag{4.38}$$

By replacing $W(u_x)$ with (4.10), the primal variational problem for the soft device (4.5) can be written in the form

$$(\mathcal{P}_s): \quad \min_{u \in \mathcal{U}_s} \left\{ P_s(u) = \int_0^1 \tfrac{1}{2}\mu {u_x}^2 + \tfrac{1}{2}\nu(\tfrac{1}{2}{u_x}^2 - \alpha u_x)^2 dx - \int_0^1 f u \mathrm{d}x - \sigma(1)u(1) \right\}, \tag{4.39}$$

The criticality condition $\delta P_s(u) = 0$ for (4.39) leads to the mixed boundary-value problem

$$(\text{BVP1}): \quad \sigma_x + f = 0, \tag{4.40}$$

where

$$\sigma = u_x \left(\tfrac{1}{2}\nu u_x^2 - \tfrac{3}{2}\nu\alpha u_x + \mu + \nu\alpha^2 \right), \tag{4.41}$$

with boundary conditions

$$u(0) = 0 \tag{4.42}$$

and

$$t \left(\tfrac{1}{2}\nu t^2 - \tfrac{3}{2}\nu\alpha t + \mu + \nu\alpha^2 \right) = \sigma(1), \tag{4.43}$$

where $\sigma(1)$ is prescribed and the notation $t = u_x(1)$ is used.

Note that for (BVP1), there could be at most three smooth solutions for $t = u_x(1)$ that satisfy the Neumann boundary condition, which is a third-order polynomial equation. In order to study smooth solutions of (BVP1), we consider a similar mixed boundary value problem

$$(\text{BVP2}): \quad \sigma_x + f = 0, \tag{4.44}$$

with boundary conditions

$$u(0) = 0 \tag{4.45}$$

and

$$u_x(1) = t, \tag{4.46}$$

with t one of the roots of the equation in (4.43). By 'smooth,' we mean here a solution that is once continuously differentiable, while 'nonsmooth' refers to a solution that is continuous and piecewise continuously differentiable.

Note that (BVP1) and (BVP2) differ only in the Neumann boundary condition at $x = 1$. Actually, the set of solutions of (BVP2) is a subset of that of (BVP1). This is true since, in (BVP2), we 'force' $u_x = t$, one of the three solutions of the cubic equation (4.41).

Let the material constants $\mu > 0, \nu > 0, \alpha > 0$, the distributed axial load $f(x)$ and the stress $\sigma(1)$ be given. Then, with β and η defined by (4.30), we give the following theorems, which are similar to the results derived in [46] for the azimuthal shear problem.

Theorem 4.3 (Closed-Form Solutions - Theorem 2 in [47]). *Given a body force f and an axial dead load σ_1, such that $\sigma(x)$ is defined by* (4.21)*, the DAE* (4.25) *has at most three real roots $\bar{\zeta}_i(x)$, $i = 1, 2, 3$, ordered according to* (4.35)

$$\bar{\zeta}_1(x) \geq -\mu \geq \bar{\zeta}_2(x) \geq \bar{\zeta}_3(x) \geq -\tfrac{1}{2}\nu\alpha^2.$$

For each of these roots, the function defined by

$$\bar{u}_i(x) = \int_0^x \frac{\sigma(s) + \alpha\bar{\zeta}_i(s)}{\bar{\zeta}_i(s) + \mu}\, ds \tag{4.47}$$

is a solution to (BVP1)*, provided that $\bar{\zeta}_2(x)$ and $\bar{\zeta}_3(x)$ are replaced by the real solution $\bar{\zeta}_1(x)$ when they are complex.*

For a given t such that σ_1 is determined by the cubic equation in (4.41)*, one of the possible three $\bar{u}_i(x)$, $i = 1, 2, 3$ solves solves (BVP2).*

Furthermore,

$$P_s(\bar{u}_i) = P_s^d(\bar{\zeta}_i),\ i = 1, 2, 3. \tag{4.48}$$

Proof. This theorem is a special application of the general analytic solution obtained in [28, 31]. We briefly stretch its proof below.

The relationship among the canonical dual solutions $\bar{\zeta}_i(x), i = 1, 2, 3$ is expressed in inequality (4.35), which has been proved in Theorem 4.1. For each $\bar{\zeta}_i(x)$, by rewriting (4.20) as $u_x = (\sigma(s) + \alpha\bar{\zeta}_i(s)/(\bar{\zeta}_i(s) + \mu)$ and integrating on [0,x), we can obtain the corresponding $\bar{u}_i(x)$, which solves (BVP1). For a given t, the axial load σ_1 is uniquely determined by the boundary condition of (BVP1), i.e., $t(\frac{1}{2}\nu t^2 - \frac{3}{2}\nu\alpha t + \mu + \nu\alpha^2) = \sigma(1)$, of which the left-hand side is a third-order polynomial in t, and at most three solutions for t can be determined analytically. Since one of the three solutions for t naturally satisfies the boundary condition (4.46) of (BVP2), there is one of the three distinct $\bar{u}_i(x)$ that is a solution of (BVP2).

The equality (4.48) can be obtained in two steps: First, from $\mathcal{P}(s)$, we obtain the Gao-Strang total complementary energy (4.18); second, by using $u_x = (\sigma(s) + \alpha\bar{\zeta}_i(s))(\bar{\zeta}_i(s) + \mu)$ or its integral form (4.47), the Gao-Strang total complementary energy becomes the pure complementary energy functional (4.22). Thus, the equality (4.48) holds. □

Theorem 4.4 (Global Minimizer and Local Extrema - Theorem 3 in [47]). *Given a body force f and an axial dead load σ_1, such that $\sigma(x)$ is defined by (4.21), the following hold true:*

If $\beta^2 > \eta > 0$, the DAE (4.25) has a unique root $\bar{\zeta}(x) > -\mu$, which is a global maximizer of P_s^d over $\mathcal{S}_a$, and the corresponding solution $\bar{u}$, given by (4.47) is a global minimizer of $P_s(u)$ over $\mathcal{U}_s$, i.e.,

$$P_s(\bar{u}) = \min_{u\in\mathcal{U}_a} P_s(u) = \max_{\zeta\in\mathcal{S}} P_s^d(\zeta) = P_s^d(\bar{\zeta}). \tag{4.49}$$

If $\beta^2 \leq \eta$, then the DAE (4.25) has three real roots ordered as in (4.35). For $\bar{\zeta}_1$, the corresponding solution $\bar{u}_1$ is a global minimizer of $P_s(u)$ and (4.49) holds. For $\bar{\zeta}_2$ and $\bar{\zeta}_3$, the corresponding solutions $\bar{u}_2$ and $\bar{u}_3$ are, respectively, a local minimizer and a local maximizer of $P_s(u)$, i.e.,

$$P_s(\bar{u}_2) = \min_{u\in\mathcal{U}_2} P_s(u) = \min_{\bar{\zeta}_3<\zeta<-\mu} P_s^d(\zeta) = P_s^d(\bar{\zeta}_2) \tag{4.50}$$

and

$$P_s(\bar{u}_3) = \max_{u\in\mathcal{U}_3} P_s(u) = \max_{-\frac{1}{2}\nu\alpha^2<\zeta<\bar{\zeta}_2} P_s^d(\zeta) = P_s^d(\bar{\zeta}_3), \tag{4.51}$$

where $\mathcal{U}_j$ is a neighborhood of $\bar{u}_j$, for $j = 2, 3$.

Proof. This theorem is a special application of the general analytic solution obtained in [28, 31]. □

For $\sigma(x)$ determined by (4.21), and $\beta(x) = \sigma(x) - \mu\alpha$, the DAE (4.25) can be written as

$$h^2(\zeta) = (\sigma - \mu\alpha)^2 = (\mu + \zeta)^2(2\nu^{-1}\zeta + \alpha^2) = \beta(x)^2. \tag{4.52}$$

The number of real solutions and their values $\zeta_i(x)$, $i = 1, 2, 3$ depend on the relative position of $\beta(x)$ and $h(\zeta)$. More interestingly, while the existence and multiple solution criteria are not straightforward for $(\mathcal{P}_s)$, they are clear from a dual perspective, which can be summarized in the following theorem.

Theorem 4.5 (Multiple Solution Criteria for (BVP1) - Theorem 4 in [47]). *Suppose that the body force f and dead load σ_1 are given and that $\sigma(x)$ is defined by (4.21).*
If $\eta < 0$, i.e., $\nu\alpha^2 \leq 2\mu$, then (BVP1) has a unique solution $\bar{u}_1(x)$, which also solves the variational problem $(\mathcal{P}_s)$.
If $\eta \geq 0$, then (BVP1) can have multiple solutions. In this case, if there exists a subdomain $I_0 \subset (0, 1)$ such that $\beta^2(x) > \eta, \forall x \in I_0$, then (BVP1) has a solution $\bar{u_1}(x)$ that is unique on I_0. On the other hand, if $\beta^2(x) < \eta, \forall x \in I_0$, then (BVP1) has three solutions $\bar{u_i}(x), i = 1, 2, 3$ given by (4.47), which are distinct on I_0.

Proof. We know that if $\eta \leq 0$, the strain energy $W(\gamma)$ is convex. Intuitively, from Fig. 4.2(a), the associated DAE (4.25) has only one real solution $\bar{\zeta}_1(x)$. Therefore, the corresponding $\bar{u}_1(x)$ solves uniquely both the variational problem $(\mathcal{P}_s)$ and (BVP1).

If $\eta > 0$, the strain energy $W(\gamma)$ is non-convex. From Fig. 4.2, we can see that the DAE (4.25) can have multiple real solutions. Specifically, if $\beta^2(x) > \eta, \forall x \in I_0$, then the DAE (4.25) has only one real root $\bar{\zeta}_1(x)$ on I_0. Therefore, the corresponding $\bar{u}_1(x)$ is the unique solution of (BVP1); if $\beta^2(x) \leq \eta, \forall x \in I_0$, then the DAE (4.25) has three real roots, ordered as in (4.35), and the corresponding $\bar{\zeta}_1(x), i = 1, 2, 3$, are the solutions of (BVP1) and are distinct on the subdomain I_0. □

Now, we can extend the idea of Theorem 4.5 to (BVP2).

Theorem 4.6 (Multiple Solution Criteria for (BVP2) - Theorem 5 in [47]). *Suppose that the boundary value t is given such that σ_1 is determined by*

$$\sigma_1 = t(\tfrac{1}{2}\nu t^2 - \tfrac{3}{2}\nu\alpha t + \mu + \nu\alpha^2). \tag{4.53}$$

Then, if $\eta < 0$, (BVP2) has a solution $\bar{u_1}(x)$ that is unique in the whole domain $(0, 1)$.

If $\eta > 0$, then (BVP2) can have multiple solutions in $(0, 1)$. In particular, if there exists a point $x_0 \in (0, 1]$ such that $\beta^2(x_0) > \eta$, while $\beta^2(x) < \eta$ for some $x \in (0, x_0)$, then (BVP2) has at least three solutions, which differ at least in a subdomain of $(0, x_0)$.

Proof. If $\eta < 0$, then the strain energy W is convex and the relation between σ_1 and t is one-to-one. In this case, the DAE (4.25) has only one real root $\bar{\zeta}_1(x)$ in the whole domain $(0, 1)$ and the corresponding $\bar{u}_1(x)$ is the unique solution of (BVP2).
If $\eta \geq 0$, then the total potential energy $\mathcal{P}_s(u)$ is non-convex and the DAE (4.25) may have more than one real solution. In particular, if there is a point $x_0 \in (0, 1]$ such that $\beta^2(x) > \eta$, then the DAE (4.25) has at least one real root $\bar{\zeta}(x)$ for $x \in [x_0, 1]$. It turns out that the total potential $\mathcal{P}_s(u)$ has at least one critical point $\bar{u}(x)$ in the subdomain $[x_0, 1]$, but only one of them satisfies the boundary condition $\bar{u}(1) = t$. Since $\beta^2(x) < \eta$ for some $x \in (0, x_0)$, the DAE (4.25) has three real roots $\bar{\zeta}_i(x)$ at all points in $(0, x_0)$ and the corresponding solutions $\bar{u}_i(x)$ satisfy the boundary condition $\bar{u}_i(0) = 0$. Therefore, any of these solutions combined with the solution $\bar{u}(x)$ in the domain $[x_0, 1]$ solves (BVP2). □

Generally speaking, the study of the existence and uniqueness of smooth solutions of (BVP1) and (BVP2) is difficult. However, these issues become clear from the canonical dual perspective. Theorem 4.7 below summarizes the existence criteria for smooth and nonsmooth solutions for both (BVP1) and (BVP2).

Theorem 4.7 (Existence Criteria for Smooth and Nonsmooth Solutions - Theorem 6 in [47]). *Suppose that the body force f and the dead load σ_1 are given, $\sigma(x)$ is defined by* (4.21)*, and $\beta(x) = \sigma(x) - \mu\alpha$.*

(i) If $\beta(x)$ doesn't change sign on $(0,1)$, then the canonical dual solution $\bar{\zeta}_1$, defined by (4.31) *is a smooth real function on $(0,1)$, and therefore, by Theorem 4.3,* (BVP1) *has at least one smooth solution $\bar{u}_1(x)$, which is the minimizing solution of $(\mathcal{P}_s)$.*

(ii) If $\beta(x)$ changes sign on $(0,1)$, then there is no such smooth minimizing solution.

(iii) If $\beta(x)^2 < \eta, \forall x \in (0,1)$ and β doesn't changes sign on $(0,1)$, then the canonical dual solutions $\bar{\zeta}_i$, $i = 1,2,3$ in (4.31), (4.32) *and* (4.33) *are smooth real functions on $(0,1)$ and the variational problem $(\mathcal{P}_s)$ has three smooth extrema solutions, with $\bar{u}_1(x)$ the global minimizer, $\bar{u}_2(x)$ the local minimizer and $\bar{u}_3(x)$ the local maximizer.*

(iv) If $\beta^2 < \eta, \forall x \in (0,1)$ and β changes sign on $(0,1)$, then the canonical dual solutions $\bar{\zeta}_i$, $i = 1,2$, in (4.31) and (4.32) are nonsmooth real functions on $(0,1)$. (BVP1) *has three smooth solutions $\bar{u}_{si}$, and among them, $\bar{u}_3$ is a smooth maximizing solution for the variational problem $(\mathcal{P}_s)$.*

(v) If $\beta^2 - \eta$ changes sign at either $\beta = \pm\sqrt{|\eta|}$, but not both, on $[0,1]$, then there exists a unique smooth solution for (BVP1).

(vi) If $\beta^2 - \eta$ changes sign at both $\beta = \pm\sqrt{|\eta|}$ on $[0,1]$, then there exists no smooth solution for (BVP1).

(vii) Of the smooth solutions that exist, the one satisfying (4.45) *is a smooth solution of* (BVP2).

Proof. This theorem is intuitively straightforward from the dual algebraic curve in Fig. 4.2, which qualitatively covers all possible combinations of parameters μ, ν and α.

(i) If β doesn't change sign on $(0,1)$, then there is at least one real dual solution $\bar{\zeta}_1 > -\mu$, which is clearly smooth. It follows from (4.47) that the corresponding primal solution $\bar{u}_1$ is smooth.

(ii) The fact that β changes sign at some material point, say x_0, implies the nonsmoothness of $\bar{\zeta}_1$ and $\bar{\zeta}_2$ at x_0, and therefore nonsmoothness of $\bar{u}_1$ and $\bar{u}_2$ at x_0, respectively the global minimizer and local minimizer of $\mathcal{P}_s(u)$. Thus, there exists no smooth minimizing solution.

(iii) If $\beta(x)^2 < \eta, \forall x \in (0,1)$ and β doesn't change sign on $(0,1)$, then there exist three dual solutions, ζ_i, $i = 1,2,3$, ordered as in (4.35). From Fig. 4.2(b), it is clear that they are smooth. By Theorem 4.3, there exist, correspondingly, three smooth primal solutions $\bar{u}_i$. By Theorem 4.4, $\bar{u}_1$ is the global minimizer, $\bar{u}_2$ the local minimizer and $\bar{u}_3$ the local maximizer.

(iv) If $\beta(x)^2 < \eta$, $\forall x \in (0,1)$ and β changes sign on $(0,1)$, then the canonical dual solutions $\bar{\zeta}_i$, $i = 1, 2$, in (4.31) and (4.32) are nonsmooth real functions on $(0,1)$. As stated in (ii), there exist no such smooth minimizing solutions. However, (BVP1) still has three smooth solutions $\bar{u}_{si}$. This is true because, by Theorem 4.1, the DAE (4.25) has three real solutions. Since σ is smooth on $(0,1)$, we know from Fig. 4.2(b) that these solutions are smooth. We denote them by $\bar{\zeta}_{si}, i = 1, 2$, $\bar{\zeta}_{s3} = \bar{\zeta}_3$. Suppose β changes sign at a certain $x_0 \in (0,1)$. Then, we have $\bar{\zeta}_{si}(x_0)|_{i=1,2} = -\mu$. By Theorem 4.1, there exist, correspondingly, three smooth primal solutions $\bar{u}_{si}, i = 1, 2, 3$, and $\bar{u}_{s3} = \bar{u}_3$. Therefore, (BVP1) has a smooth solution $\bar{u}_3$, which is a local maximizer of the variational problem $(\mathcal{P}_s)$. Note that when $\beta(x) = 0$, the two roots $\bar{\zeta}_1$ and $\bar{\zeta}_2$ coincide at $\zeta = -\mu$, and this is the transitional point at which the two local minima are equal. Thus, when β changes sign, the DAE (4.25) may still have smooth solutions - but they may not be ordered as in (4.35).

(v) In the transitional cases for which $\beta(x) = \sigma(x) - \alpha\mu = \pm\sqrt{\eta}$, the two roots $\bar{\zeta}_2$ and $\bar{\zeta}_3$ coincide and the local extrema described by (4.50) and (4.51) merge. If $\beta^2 - \eta$ changes sign at either $\beta = \pm\sqrt{|\eta|}$, but not both, on $[0,1]$, there is always a smooth path for $\bar{\zeta}_1$. Therefore, there exists a unique smooth dual solution $\bar{u}_1$ for (BVP1).

(vi) If $\beta(x)^2 - \eta$ changes sign at both $\beta = \pm\sqrt{|\eta|}$, then there are some parts of $[0,1]$ on which the DAE (4.25) has a unique solution $\bar{\zeta}_1$. This implies that the only possible smooth primal solution is $\bar{u}_1$, as defined in Theorem 4.3, which is not smooth at $\beta = 0$. Therefore, there exist no smooth primal solutions.

(vii) This is self-evident, since the value of σ_1 has been calculated by setting the value of t in (4.42). □

4.3.2 Numerical Examples

In this section, the author will apply the theoretical results presented in this chapter, which are based on the canonical duality theory, to five numerical examples. The body force f and parameters μ, ν, α are purposely chosen to demonstrate the diversity of results in Theorems 4.1-4.7. For convenience, we rewrite (4.44) in the form

$$(BVP2) := \begin{cases} (\frac{1}{2}\nu u_x^2 - 3\nu\alpha u_x + \mu + \nu\alpha^2)u_{xx} + f = 0, \\ u(0) = 0, \quad u_x(1) = t. \end{cases}$$

To solve (BVP2) numerically, two choices need to be made. First, the nonlinear ODE needs to be linearized. Second, the spatial derivatives need to be discretized. For the linearization, we use two approaches: a fixed point (Picard) iteration (see section 3.3.2) and Newton's method (see Section 3.3.1). For the spatial discretization, we use the FDM (see Section 3.2.1). Thus, two numerical methods will be used in our investigation: (i) a fixed point iteration and a finite difference

discretization (FPI-FDM); and (ii) Newton's method and a finite difference method (NM-FDM). We briefly describe both approaches below.

Fixed Point Iteration and Finite Difference Method (FPI-FDM) is used to solve (BVP2) to check its possible smooth solutions. These smooth solutions are then compared with those obtained by using the *canonical duality theory*.

We first linearize (BVP2) by lagging all the lower-order derivatives. This yields the following iterations, where k is the iteration number:

$$(\tfrac{3}{2}\nu u_x^2 - 3\nu\alpha u_x + \mu + \nu\alpha^2)^k u_{xx}^{k+1} + f = 0. \tag{4.54}$$

Then, the high-order derivatives are discretized using the FDM. Let u_j^k be the kth iterate in the numerical approximation of $u(jh)$, where h is the spatial mesh size, $0 \le j \le N$ and $Nh = 1$. We then obtain

$$u_{j+1}^{k+1} - 2u_j^{k+1} + u_{j-1}^{k+1} = \frac{-f_j\ h^2}{(\frac{3}{2}\nu u_x^2 - 3\nu\alpha u_x + \mu + \nu\alpha^2)_j^k}, \tag{4.55}$$

for $1 \le j \le N-1$. This forms a tridiagonal system

$$\mathbf{A}_s \cdot \mathbf{u}^{k+1} = \mathbf{g}^k, \tag{4.56}$$

where the matrix

$$\mathbf{A}_s = \begin{pmatrix} -2 & 1 & & & \\ 1 & -2 & 1 & & \\ & \ddots & \ddots & \ddots & \\ & & 1 & -2 & 1 \\ & & & 1 & -1 \end{pmatrix}$$

is modified to include boundary conditions, $\mathbf{u}^k = (u_1^k, u_2^k, \ldots, u_{N-1}^k)$, $\mathbf{g}^k = (g_1^k, g_2^k, \ldots, g_{N-1}^k)$ and g_j^k is defined as the right-hand side of (4.55). Finally, starting with an initial guess, $\mathbf{u}^0$, the iterations $\mathbf{u}^k, k = 1, 2, 3, ...$ are computed until the convergence criterion $\|\mathbf{u}^k - \mathbf{u}^{k+1}\|_2 \le 10^{-6}$ is satisfied.

Newton's Method and Finite Difference Method (NM-FDM) is used to solve (BVP2) numerically and then compare the results with those obtained by using the FPI-FDM.

The nonlinear ODE in (BVP2) is first discretized by using the FDM, outlined in Section 3.2.1. The first-order and second-order derivatives are approximated using central finite differences. Let u_j^k denote the kth iterate in the numerical approximation of $u(jh)$, where h is the spatial mesh size, $0 \le j \le N-1$, and $Nh = 1$. We then obtain

$$\left(\frac{u_{j+1} - 2u_j + u_{j-1}}{h^2}\right)\left[\tfrac{3}{2}\nu\left(\frac{u_{j+1} - u_{j-1}}{2h}\right)^2 - 3\nu\alpha\left(\frac{u_{j+1} - u_{j-1}}{2h}\right) + \mu + \nu\alpha^2\right] + f_j = 0, \tag{4.57}$$

for $1 \leq j \leq N-1$. These $N-1$ equations, together with the corresponding boundary conditions, can be written as

$$\mathbf{F}(\mathbf{u}) + \mathbf{f} = \mathbf{0}, \tag{4.58}$$

where $\mathbf{F} : \mathbb{R}^{N-1} \to \mathbb{R}^{N-1}$is a nonlinear function, $\mathbf{u} := (u_1, u_2, ..., u_{N-1}) \in \mathbb{R}^{N-1}$ is the solution vector, and $\mathbf{f} := (f_1, f_2, ..., f_{N-1}) \in \mathbb{R}^{N-1}$ is the forcing vector. To solve (4.58) numerically, we use Newton's method, described in Section 3.3.2.

Now we start investigating both theoretically and numerically (BVP2) for five test problems (corresponding to five different parameter settings). To ensure that the numerical results are indeed representative of the physical behavior of (BVP2) and not due to numerical artifacts, we use in Example 4.1A both FPI-FDM and NM-FDM to check whether the two numerical methods yield the same results.

Example 4.1 In (BVP1), we set $\mu = 0.5, \nu = 1$, and $\alpha = 3$, so that $\nu\alpha^2 > 8\mu$ and $\eta = (8/3)^3 \approx 19$. In this case, W has a double-well structure, as shown in Fig. 4.1(c). We choose $f(x) = -3\sin(0.2x)$. It is convenient to fix $\sigma(1)$ by selecting the value of t in (4.42). Here we take the values $t = 0.1$, $t = 1$ and $t = 2$, for Examples 1A, 1B and 1C, respectively. The purpose of taking different values of t is to show the relevance of (BVP1) and (BVP2).

Example 4.1A Let $t = 0.1$. Before we proceed to apply the canonical duality theory, let us first check the consistency of the FPI-FDM for (BVP1) and (BVP2) by using meshes of different sizes. Fig. 4.4 shows that the FPI-FDM with different mesh sizes converges to the same solution consistently.

Next, we apply NM-FDM to solve (BVP2). As pointed out in Section 3.3.2, Newton's method is very sensitive to the initial guess $\mathbf{u}^0$. In our numerical experiments, when $\mathbf{u}^0$ is given by a random generator, most of the time, NM-FDM either doesn't converge, or converges only to a bizarre solution with random nonsmoothness. However, given a $\mathbf{u}^0$ that is close to the exact solution, NM-FDM is able to produce the same results as the FPI-FDM within the prescribed tolerance, as shown in Fig. 4.5.

In conclusion, for this numerical example, the FPI-FDM and NM-FDM produced similar numerical results. NM-FDM, however, displayed a high sensitivity with respect to the initial guess. Thus, we will use only the FPI-FDM in all the other numerical examples in this chapter.

Now we solve $(\mathcal{P}_s)$ by applying the theoretical results in Section 4.3.1, which are based on the canonical duality theory. For $x \in [0, 1]$, the graph of f is approximately a straight line as shown in Fig. 4.6(a). The dual algebraic curves are shown in Fig. 4.6(b) with $h(\zeta)$ plotted against ζ. For comparison, the corresponding function $\beta = \mu\alpha - \sigma$, calculated from (4.30) is superimposed as a function of $x \in [0, 1]$ in the same figure. Since $\beta(x)^2 < \eta$ for all $x \in [0, 1]$, by Theorem 4.1

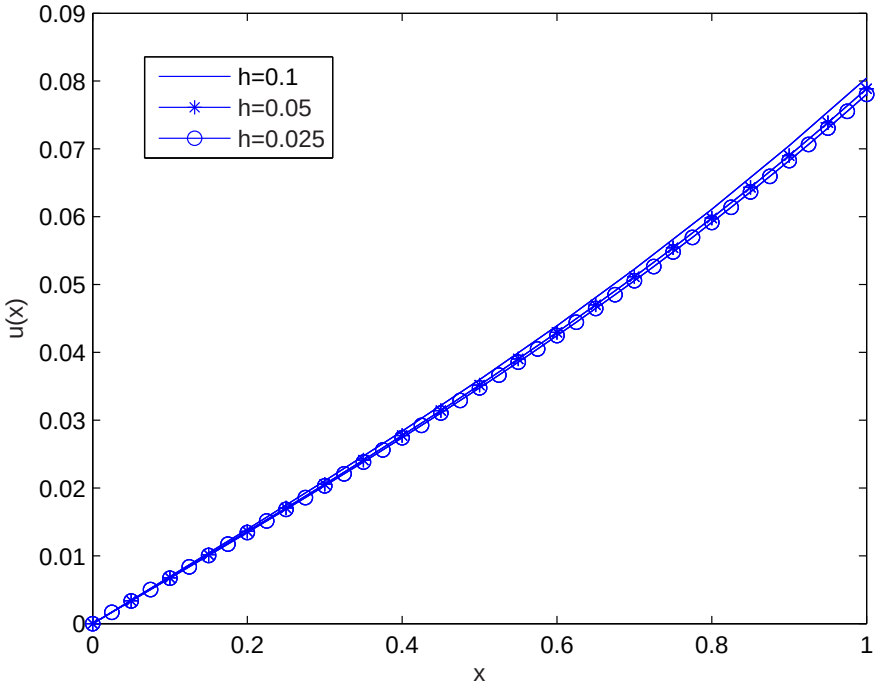

Figure 4.4: Example 4.1A - Solutions by the FPI-FDM using various mesh sizes: $h = 0.1,\ 0.05$, and 0.025.

(ii)(b), the DAE (4.25) has multiple solutions over the whole domain $[0, 1]$. Then, by Theorem 4.5, (BVP1) has three solutions given by (4.47) over the whole domain $[0, 1]$.

The dual extremal solutions $\bar{\zeta}_i$, $i = 1, 2, 3$, for $P_s^d(\zeta)$, and their associated primal extremal solutions $\bar{u}_i$, $i = 1, 2, 3$, defined in Theorem 4.3 are shown in Fig. 4.7. Note that while $\bar{\zeta}_1 > \bar{\zeta}_2 > \bar{\zeta}_3$, we have $\bar{u}_2 \geq \bar{u}_3 \geq \bar{u}_1$. By Theorem 4.4, $\bar{u}_1$ is the global minimizing solution, $\bar{u}_2$ the local minimizing solution, and $\bar{u}_3$ the maximizing solution of $(\mathcal{P}_s)$.

It is also clear from Fig. 4.6(b) that $\beta = \mu\alpha - \sigma$ is negative and does not change sign. Thus, according to Theorem 4.7 (iii), $\bar{u}_i, i = 1, 2, 3$ are three smooth solutions of (BVP1), and this is illustrated in Fig. 4.7(b). Among the three solutions, by Theorem 4.7 (vii), $\bar{u}_1$ is a smooth solution of (BVP2), because $\bar{u}_1$ satisfies the Neumann boundary condition, i.e., $u_x(1) = t = 0.1$.

The graph of $\bar{u}_1$ in Fig. 4.7(b) is overlaid with and indistinguishable from the FPI-FDM solution u_0. Thus, in this example, the FPI-FDM solution converges to the global minimizing smooth solution $\bar{u}_1$.

Example 4.1B This is similar to Example 4.1A, but differs in the boundary condition at $x = 1$,

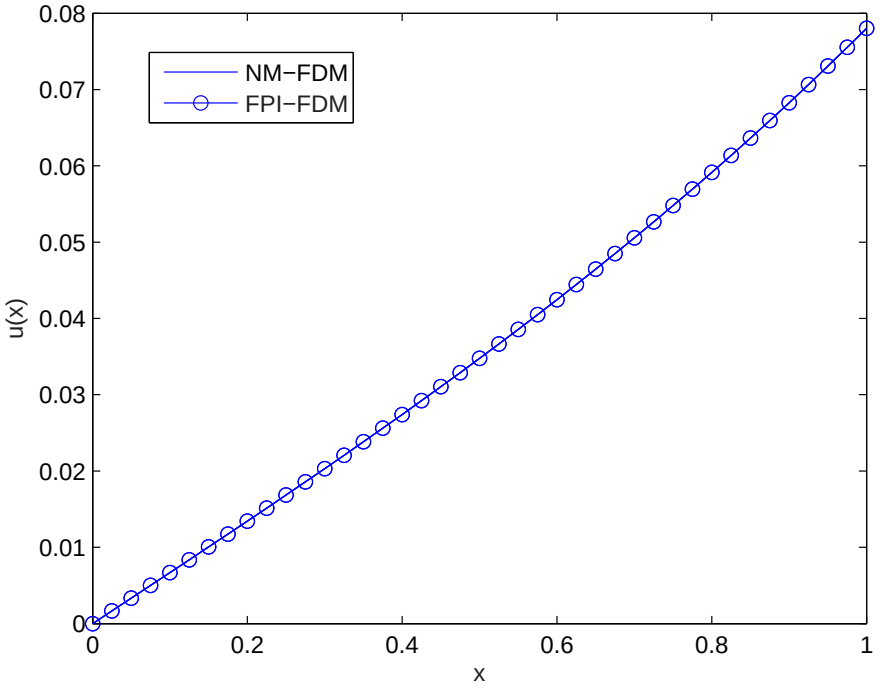

Figure 4.5: Example 4.1A - NM-FDM vs the FPI-FDM.

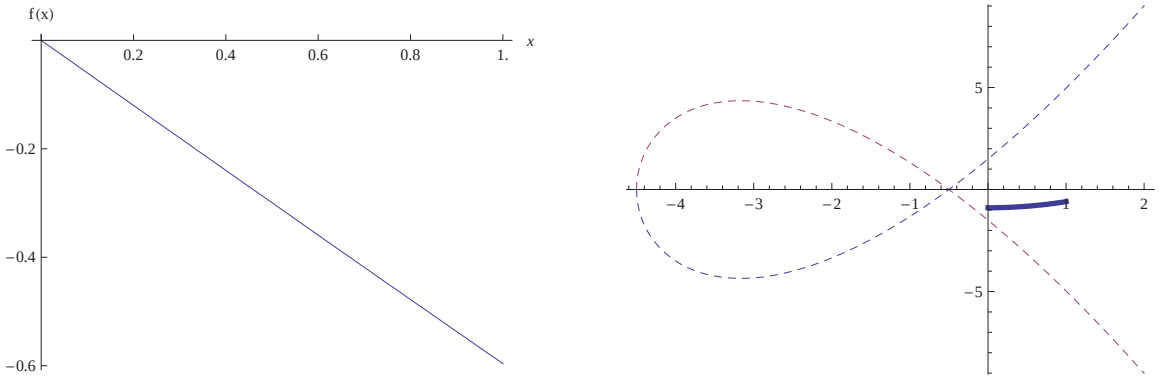

(a) Axial loading force f.

(b) Plots of the dual algebraic curve from (4.25) with $\sigma - \mu\alpha$ vs ζ (dashed curve) and $\sigma - \mu\alpha$ vs $x \in [0, 1]$ from (4.21) (solid curve).

Figure 4.6: Example 4.1A - Forces in the modified version of Ericksen's bar.

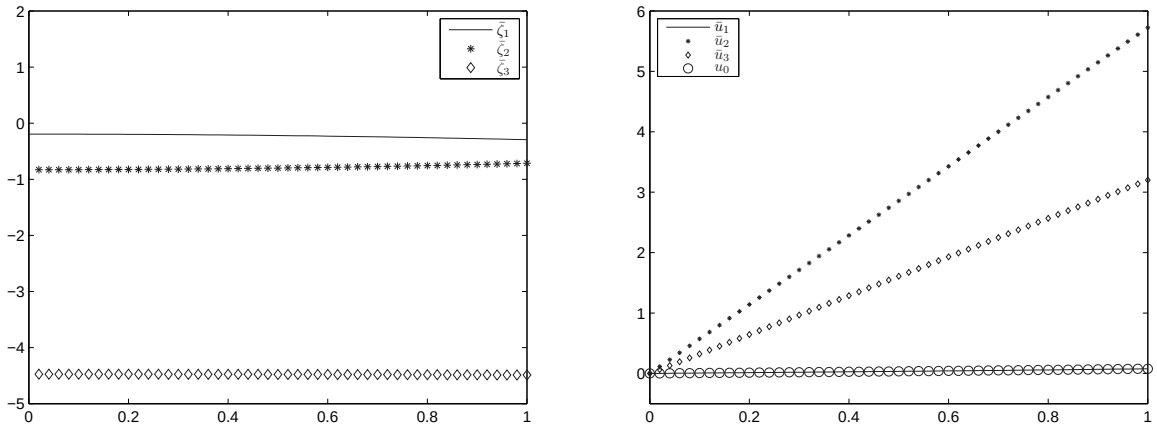

(a) Dual solutions $\bar{\zeta}_i$, $i = 1, 2, 3$.

(b) Primal solutions $\bar{u}_i$, $i = 1, 2, 3$.

Figure 4.7: Example 4.1A - Dual (4.25) and primal solutions (4.47) with $t = 0.1$. Also shown in (b) is the FPI-FDM solution u_0. The horizontal axis is the x-axis for both plots. The vertical axis is (a) the ζ-axis and (b) the u-axis.

for which $u_x(1) = t = 1$ is chosen. For $x \in [0, 1]$, $f(x)$ is shown in Fig. 4.8(a). The dual algebraic curves are shown in Fig. 4.8(b) with $h(\zeta)$ plotted against ζ. Again, since $\beta(x)^2 < \eta$ for all $x \in [0, 1]$, by Theorems 4.1 4.1 and 4.5, the DAE (4.25) and (BVP1) have multiple solutions over the whole domain $[0, 1]$.

The dual extremal solutions $\bar{\zeta}_i$, $i = 1, 2, 3$, for $P_s^d(\zeta)$, and their associated primal extremal solutions $\bar{u}_i$, $i = 1, 2, 3$, defined in Theorem 4.3 are shown in Fig. 4.9. Note that while $\bar{\zeta}_1 > \bar{\zeta}_2 > \bar{\zeta}_3$ we have $\bar{u}_1 \geq \bar{u}_3 \geq \bar{u}_2$ for $t = 1$. By Theorem 4.4, $\bar{u}_1$ is the global minimizing solution, $\bar{u}_2$ is the local minimizing solution, and $\bar{u}_3$ is the maximizing solution of $(\mathcal{P}_s)$.

It is also clear that β is positive and does not change sign. Thus, according to Theorem 4.7, (BVP1) has three smooth solutions, $\bar{u}_i, i = 1, 2, 3$, which is clearly illustrated in Fig. 4.9(b). Among them, by Theorem 4.7(vii), $\bar{u}_2$ is a smooth solution of (BVP2) for $t = 1$ since $\bar{u}_2$ satisfies the Neumann boundary condition, i.e., $u_x(1) = t = 1$.

The graph of $\bar{u}_1$ in Fig. 4.9(b) is overlaid with and indistinguishable from the FPI-FDM solution u_0. Note that $\bar{u}_2$ is such that $\bar{u}_{2,x}(1) = 1$, i.e., $\bar{u}_2$ is a smooth solution of (BVP2), but it is not a global minimizer of the associated variational problem. Instead, it is a smooth local minimizer.

Example 4.1C is similar to Examples 4.1A and 4.1B, but uses the boundary condition $u_x(1) =$

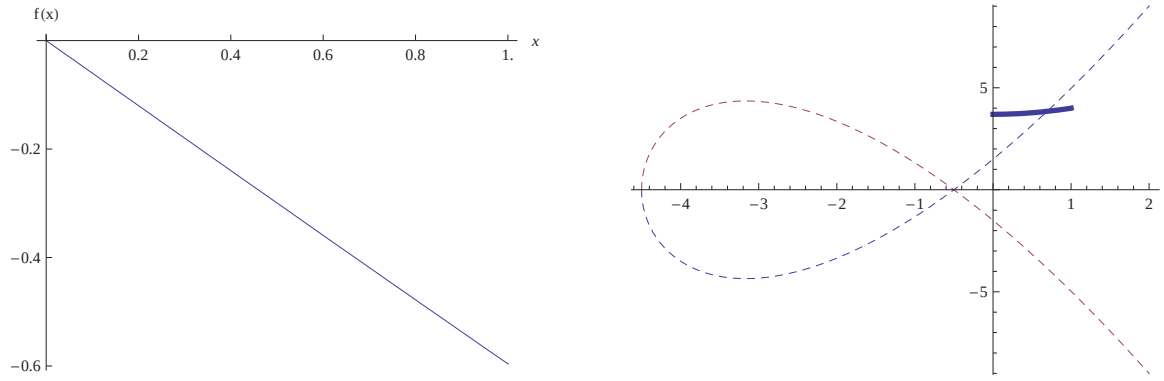

(a) Axial loading force f.

(b) Plots of the dual algebraic curve from (4.25) with $\sigma - \mu\alpha$ vs ζ (dashed curve) and $\sigma - \mu\alpha$ vs $x \in [0, 1]$ from (4.21) (solid curve).

Figure 4.8: Example 4.1B - Forces in the modified version of Ericksen's bar.

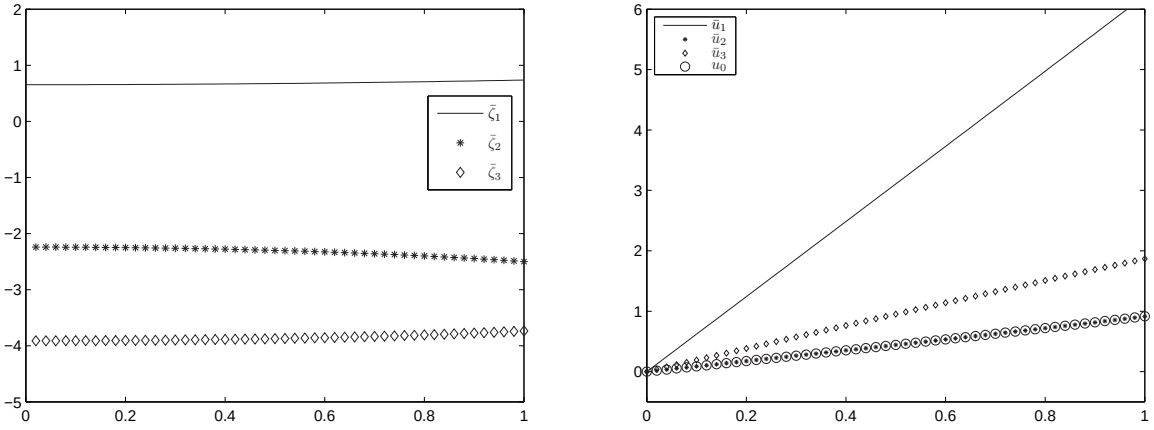

(a) Dual solutions ζ_i, $i = 1, 2, 3$.

(b) Primal solutions $\bar{u}_i$, $i = 1, 2, 3$.

Figure 4.9: Example 4.1B - Dual (4.25) and primal solutions (4.47) with $t = 1$. Also shown in (b) is the FPI-FDM solution u_0. The horizontal axis is the x-axis for both plots. The vertical axis is (a) the ζ-axis and (b) the u-axis.

$t = 2$. For $x \in [0, 1]$, $f(x)$ is shown in Fig. 4.10(a). The dual algebraic curves and β are shown in Fig. 4.10(b). Since $\beta(x)^2 < \eta$ for all $x \in [0, 1]$, by Theorems 4.1 and 4.3, the DAE (4.25) and

(BVP1) have multiple solutions over the whole domain $[0, 1]$.

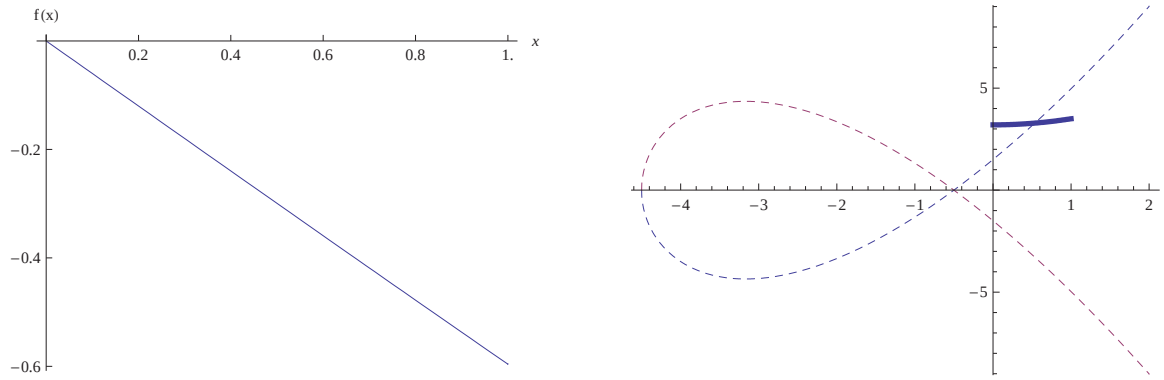

(a) Axial loading force f.

(b) Plots of the dual algebraic curve from (4.25) with $\sigma - \mu\alpha$ and ζ (dashed curve) and $\sigma - \mu\alpha$ vs $x \in [0, 1]$ from (4.21) (solid curve).

Figure 4.10: Example 4.1C - Forces in the modified version of Ericksen's bar.

Observe that β is positive and does not change sign. According to Theorem 4.7, (BVP1) has three smooth solutions, $\bar{u}_i, i = 1, 2, 3$. Fig. 4.11 shows that if $t = 2$ the numerical results are very similar to those for $t = 1$, including the ordering $\bar{u}_1 \geq \bar{u}_3 \geq \bar{u}_2$. However, it is interesting to note that in this case the FPI-FDM solution converges to $\bar{u}_3$, i.e., the local maximizing solution. Moreover, $\bar{u}_3$ is such that $\bar{u}_{3,x}(1) = 2$, i.e., $\bar{u}_3$ is a smooth solution of (BVP2), but certainly not a global minimizer of the associated variational problem.

In Examples 4.1A, 4.1B and 4.1C, we showed that, while we may have three smooth solution over the whole domain for (BVP1), only one of them satisfies the boundary condition (4.46) and thus solves (BVP2). This solution may be the global minimizer $\bar{u}_1$, the local minimizer $\bar{u}_2$ or the maximizer $\bar{u}_3$, as in Examples 4.1A, 4.1B and 4.1C, respectively.

Example 4.2 In this example, we set $\mu = 1.5, \nu = 3, \alpha = 1.5$, $f(x) = \sin(4x)$ and $t = 1.5$ in (BVP1). We then have $2\mu < \nu\alpha^2 < 8\mu$ and $\eta \approx 0.81$. The distributed force f is shown in Fig. 4.12(a) and $\sigma - \mu\alpha$ in Fig. 4.12(b), similarly to Fig. 4.6(b). By Theorem 4.1, the dual solutions $\bar{\zeta}_i$, $i = 1, 2, 3$ are obtained by solving the DAE (4.25) ; they are plotted in Fig. 4.13(a). The associated primal solutions $\bar{u}_i$ are calculated by using Theorem 4.3 and are plotted in Fig. 4.13(b).

With reference to Theorem 4.7 (iv), we note that $\beta^2 < \eta$ for all $x \in [0, 1]$ and that β changes sign on $[0, 1]$. Thus, there are three smooth solutions $\bar{\zeta}_i$, $i = 1, 2, 3$, as illustrated in Fig. 4.13(a). However, there is no smooth minimizing solution $\bar{u}_i$. The global minimizing solution $\bar{u}_1$ is nonsmooth, as

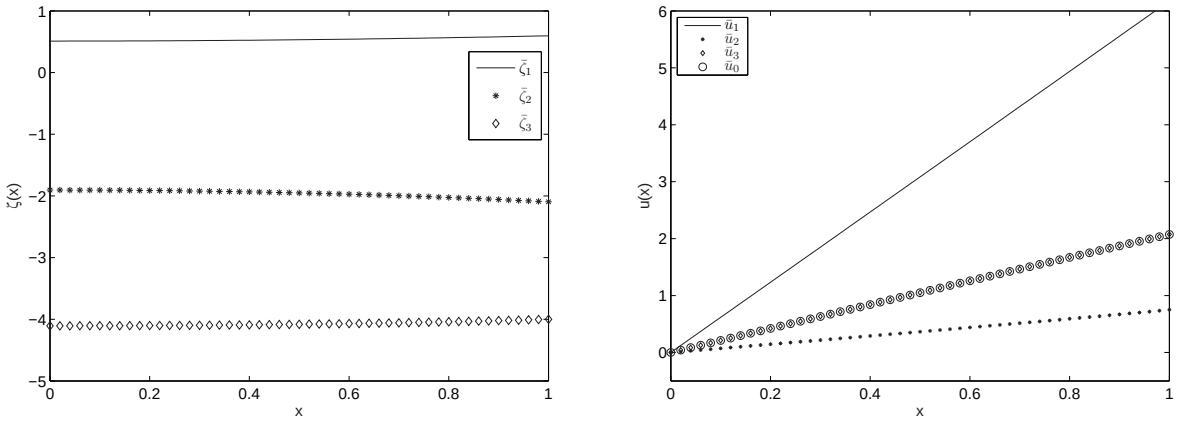

(a) Dual solutions ζ_i, $i = 1, 2, 3$.

(b) Primal solutions $\bar{u}_i$, $i = 1, 2, 3$.

Figure 4.11: Example 4.1C - Dual (4.25) and primal solutions (4.47) with $t = 2$. Also shown in (b) is the FPI-FDM solution u_0. The horizontal axis is the x-axis for both plots. The vertical axis is (a) the ζ-axis and (b) the u-axis.

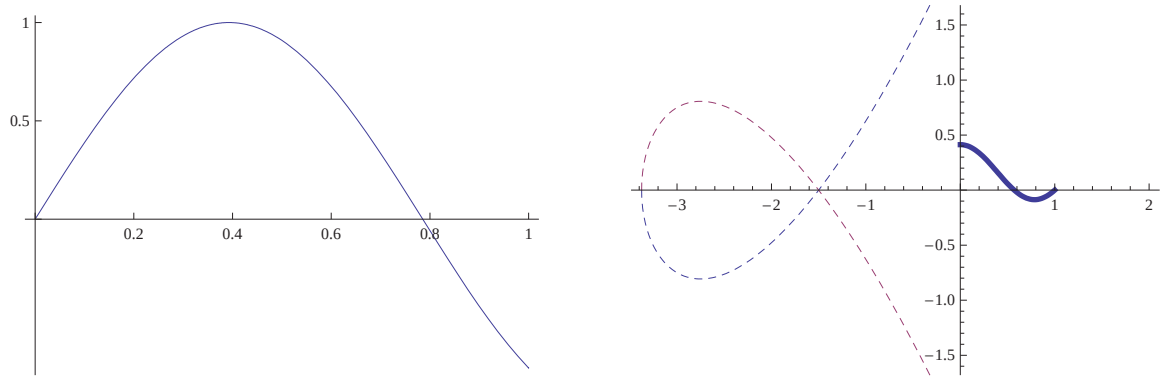

(a) Axial loading force f.

(b) Plots of the dual algebraic curve from (4.25) with $\sigma - \mu\alpha$ vs ζ (dashed curve) and $\sigma - \mu\alpha$ vs $x \in [0, 1]$ from (4.21) (solid curve).

Figure 4.12: Example 4.2 - Forces in the modified version of Ericksen's bar.

also is the local minimizer $\bar{u}_2$. This is associated with the switch between $\bar{\zeta}_1$ and $\bar{\zeta}_2$ at the value of x where β changes sign. The local maximizer $\bar{u}_3$ is smooth. The FPI-FDM solution converges to $u\bar{_3}$ and is not capable of capturing the nonsmooth minimizer. Note that $\bar{u}_{3,x}(1) = 1.5$, so that by

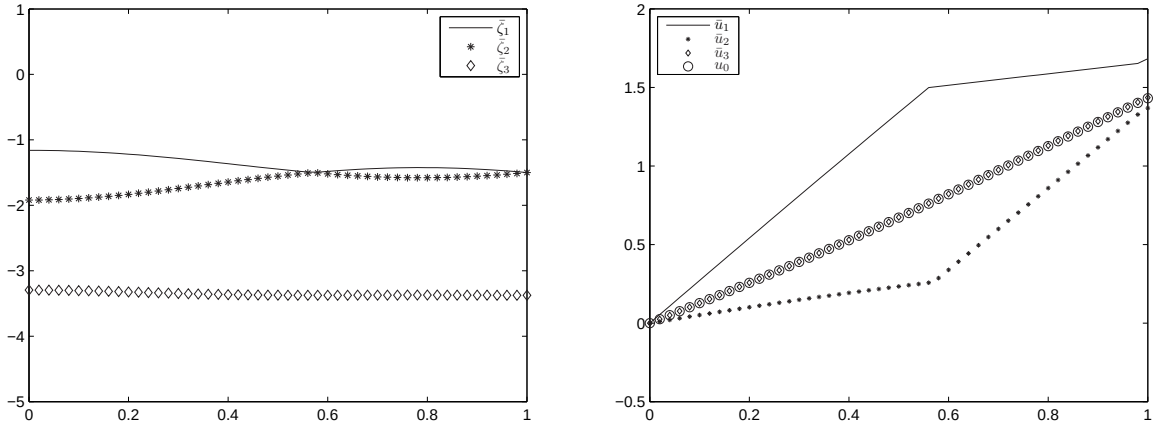

(a) Dual solutions $\bar{\zeta}_i$, $i = 1, 2, 3$.

(b) Primal solutions $\bar{u}_i$, $i = 1, 2, 3$.

Figure 4.13: Example 4.2 - Dual (4.25) and primal solutions (4.47). Also shown in (b) is the FPI-FDM solution u_0. The horizontal axis is the x-axis for both plots. The vertical axis is (a) the ζ-axis and (b) the u-axis.

Theorem 4.7 (vii) $\bar{u}_3$ is a smooth solution of (BVP2).

Example 4.3 We set $\mu = 1.5, \nu = 4, \alpha = 1.5$, $f(x) = 5\sin(3x)\mathrm{e}^x$ and $t = 1.5$ in (BVP1). As in Example 4.2, we have $2\mu < \nu\alpha^2 < 8\mu$, but in this case $\eta = 2$. The distributed force f is shown in Fig. 4.14(a). The functions β and $h(\zeta)$ are shown in Fig. 4.14(b).

The dual solutions $\bar{\zeta}_i$, $i = 1, 2, 3$ are obtained by solving the DAE (4.25) and are plotted in Fig. 4.15(a). The associated primal solutions $\bar{u}_i$ are calculated by using formula (4.47) in Theorem 4.3 and are plotted in Fig. 4.15(b).

Since β changes sign on $[0, 1]$, by Theorem 4.7(ii), there is no smooth minimizing solution of $(\mathcal{P}_s)$. However, by Theorem 4.7(v), there is a unique smooth dual solution, which we denote by ζ_s. From the dual perspective, smooth solution(s) can be constructed. The idea is straightforward: Indeed, from Fig. 4.15(a), we can obviously see that there is a (unique) smooth dual solution denoted by ζ_s, consisting of $\bar{\zeta}_1$ for $x \in [0, x_0]$ and $\bar{\zeta}_2$ for $x \in [x_0, 1]$, where x_0 is the value of x at which $\beta = 0$. A smooth primal solution u_s of (BVP1) can therefore be constructed, and this is shown in Fig. 4.16. In fact, u_s is such that $u_{s,x}(1) = t = 1.5$, and hence, by Theorem 4.4, u_s is also a smooth solution to (BVP2). The FPI-FDM for (BVP2) converges to u_0 after 6 iterations.

From Fig. 4.16, it is observed that the smooth primal solution u_s matches the solution u_0. As

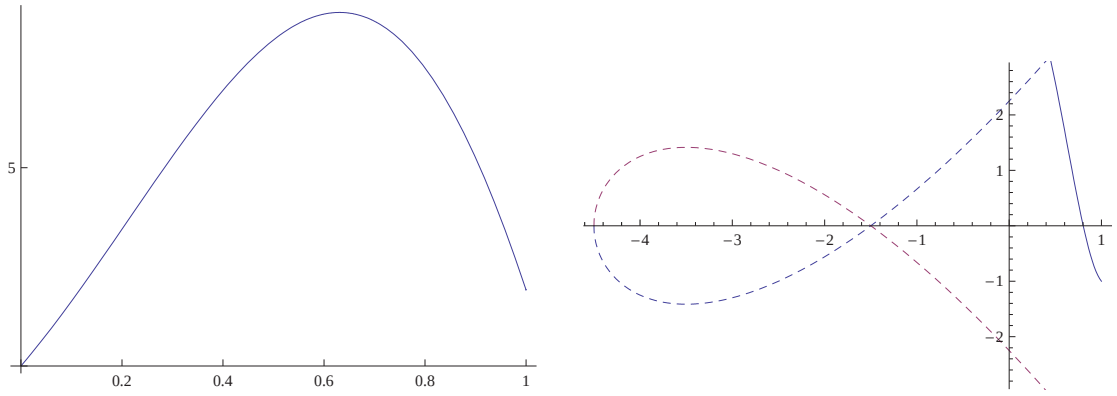

(a) Axial loading force f.

(b) Plots of the dual algebraic curve from (4.25) with $\sigma - \mu\alpha$ vs ζ (dashed curve) and $\sigma - \mu\alpha$ vs $x \in [0, 1]$ from (4.21) (solid curve).

Figure 4.14: Example 4.3 - Forces in the modified version of Ericksen's bar.

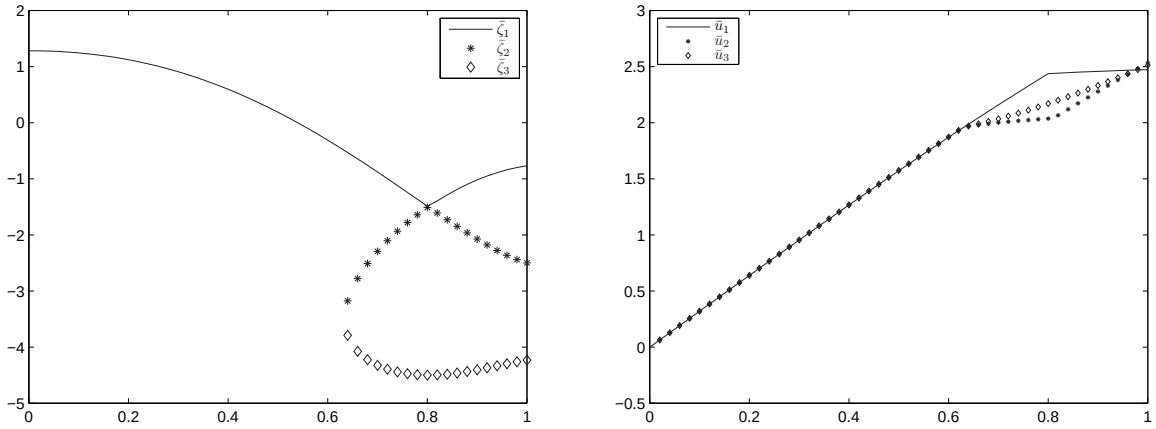

(a) Dual solutions ζ_i, $i = 1, 2, 3$.

(b) Primal solutions $\bar{u}_i$, $i = 1, 2, 3$.

Figure 4.15: Example 4.3 - Dual (4.25) and primal solutions (4.47). The horizontal axis is the x-axis for both plots. The vertical axis is (a) the ζ-axis and (b) the u-axis.

stated above, u_s is not a minimizing solution. Therefore, it is of interest to explore the reason why it is the case from an energy perspective. In order to demonstrate the triality theory, which is embodied in Theorem 4.4, and how the nonsmooth global minimizer arises, we rewrite the total

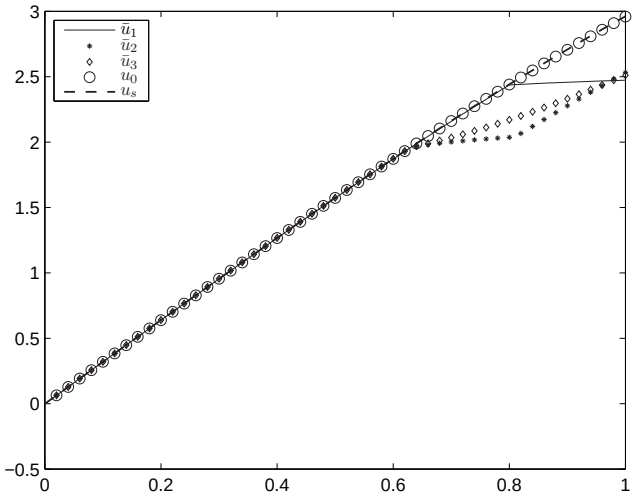

Figure 4.16: Example 4.3 - Plot of the primal solutions $\bar{u}_i$, $i = 1, 2, 3$, and the smooth solution u_s, together with the FPI-FDM solution u_0. The horizontal axis is the x-axis; the vertical axis is the u-axis.

energy functional P_s in (4.39) as

$$P_s(u) = \int_0^1 \left[\tfrac{1}{2}\mu {u_x}^2 + \tfrac{1}{2}\nu(\tfrac{1}{2}{u_x}^2 - \alpha u_x)^2 dx - \sigma u_x\right] dx. \tag{4.59}$$

The energy density curve $E(u_x)$ is the integrand function of $P_s(u)$, which can be viewed as a function of u_x:

$$E(u_x) = W(u_x) - \sigma u_x = \tfrac{1}{2}\mu {u_x}^2 + \tfrac{1}{2}\nu\left(\tfrac{1}{2}{u_x}^2 - \alpha u_x\right)^2 dx - \sigma u_x. \tag{4.60}$$

Fig. 4.17 presents the relationship between the FPI-FDM solutions and the energy curves. The first column of Fig. 4.17 shows the FPI-FDM iterations $(u_x)^k$, $k = 4, 5, 6$. The three solutions are converging, with $\| u^6 - u^5 \| \leq 10^{-6}$. In the second and third columns of Fig. 4.17, corresponding to the points $x = 0.5$ and 0.9, the numerical behavior of the FPI-FDM from an energy perspective is shown at the three consecutive iterations. At the two points, the energy density curves, calculated from $W(u_x) - \sigma u_x$, tilt in different directions, which reveals the switch of the global minimizer from right to left. The dots in the second and third columns show the corresponding FPI-FDM solution for $\bar{u}(x)$ at $x = 0.5$ and 0.9. Interestingly, at each iteration, $\bar{u}_x(0.5)$ and $\bar{u}_x(0.9)$ stay in a fixed potential well on the right until convergence is achieved. At different material points, the convergent sequence $\{\bar{u}_x^k\}$ may not converge to the global minimizer of the energy density. These results illustrate the important fact that smooth solutions of nonlinear mixed boundary value problems might not be minimizing solutions of the corresponding potential variational problems.

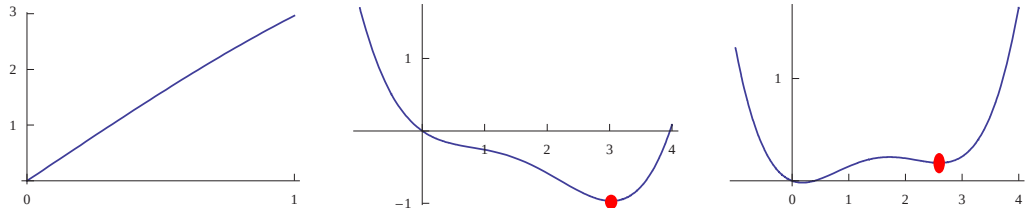

(a) The 4th FPI-FDM iteration.

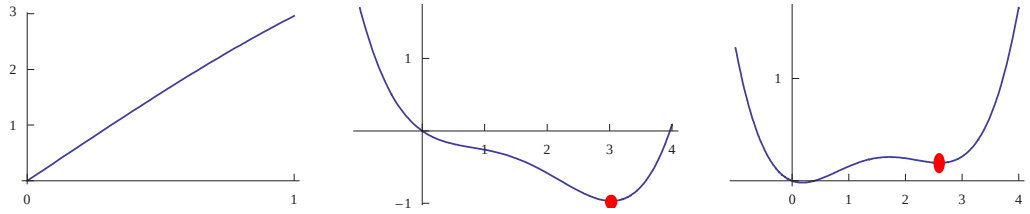

(b) The 5th FPI-FDM iteration.

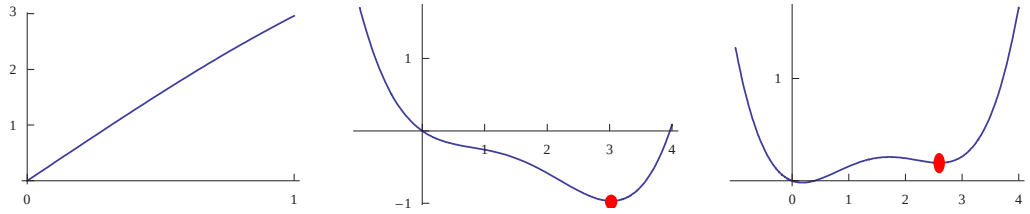

(c) The 6th FPI-FDM iteration.

Figure 4.17: Example 4.3 - Intermediate FPI-FDM iterative solutions for the fourth, fifth and sixth iterations (second and third columns for $x = 0.5, 0.9$, respectively), and $(u_x)^k(x)$ (indicated by the dots), along with the energy density curve $E(u_x)$. The left-hand column shows the corresponding solutions for $x \in [0, 1]$.

To illustrate how the nature of the non-convexity of the integrand of P_s varies with the point x, we plot the integrand E as a function of u_x at a number of fixed values of x in Fig. 4.18 superimposed on the plots in Fig. 4.15(a). Each plot is centered on the point to which it refers and shifted up for clarity. The scales of these plots and those of the background figures from Fig. 4.15(a) are, of course, entirely different. Note, in particular, that as x increases from 0, there is initially a single local minimum, then two local minima appear, and the global minimum switches from the

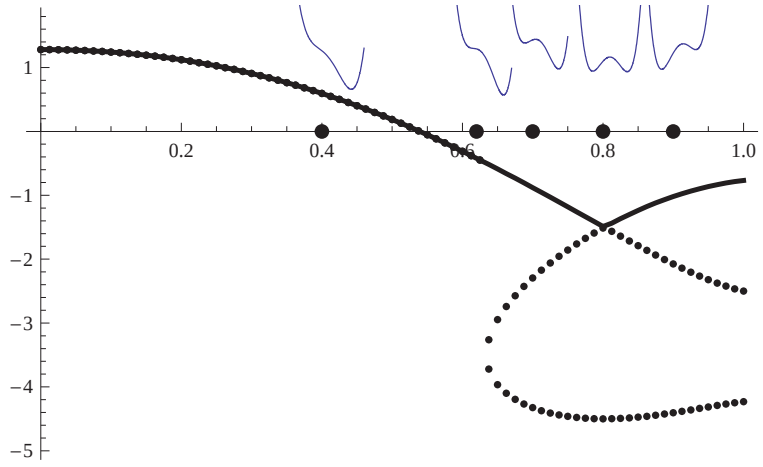

Figure 4.18: Example 4.3 - Dual solutions ζ_i, $i = 1, 2, 3$ from Fig. 4.15(a), with integrand functions $E(u_x)$ against u_x at $x = 0.4, 0.62, 0.7, 0.8, 0.9$.

right-hand side minimum to the left-hand side minimum as the value $x = 0.8$ (corresponding to the Maxwell stress) is passed, this being the point at which the minimizer $\bar{u}_1$ is nonsmooth.

At this point, we recall from (4.22) that the dual energy functional may be written as

$$P_s^d(\zeta) = -\frac{1}{2}\int_0^1 \left(\frac{(\sigma + \alpha\zeta)^2}{\mu + \zeta} + \nu^{-1}\zeta^2 \right) \mathrm{d}x.$$

In Fig. 4.19, we use this to show that the integrand functions P_s and P_s^d coincide for each solution pair (u, ζ). For four separate values of x (0.62, 0.7, 0.8 and 0.9), the integrands of P_s (for u_x from -2 to $+4$) and P_s^d (for ζ from -6 to $+4$) are plotted together in Fig. 4.19. The primal plots, which follow the pattern shown in Fig. 4.18, exemplify the general results stated in Theorem 4.4. In particular, the global minimum of the primal integrand is equal to the global maximum of the dual integrand for values of $\zeta > -\mu$ (to the right of the singularity in the dual integrand), while the local extrema of the primal and dual integrands coincide in accordance with Theorem 4.4. At $x = 0.62$, the dual solutions $\bar{\zeta}_2$ and $\bar{\zeta}_3$ coincide and the energy density has only two critical points, there being a horizontal point of inflection where $\bar{\zeta}_2$ and $\bar{\zeta}_3$ coincide. At $x = 0.8$, we have $\bar{\zeta}_1 = \bar{\zeta}_2 = -\mu$ (and $\sigma = \mu\alpha$), the two minima of the primal integrand are equal, the maximum is equal to the maximum of the dual integrand and the singularity in the integrand disappears.

Example 4.4 Let $\mu = 1.5, \nu = 4, \alpha = 1$, $f(x) = \sin(4x)$ and $t = 0.9$ in (BVP1). Then, we have $2\mu < \nu\alpha^2 < 8\mu$ and $\eta \approx 0.01$. The distributed force f is shown in Fig. 4.20(a) and $\sigma - \mu\alpha$ in Fig. 4.20(b).

The dual solutions $\bar{\zeta}_i$, $i = 1, 2, 3$, and the associated primal solutions $\bar{u}_i$ of (BVP1) are shown in Fig. 4.21. There is again a unique smooth solution ζ_s, comprising $\bar{\zeta}_1$ for $x \in [0, x_0] \cup [x_1, 1]$ and $\bar{\zeta}_2$

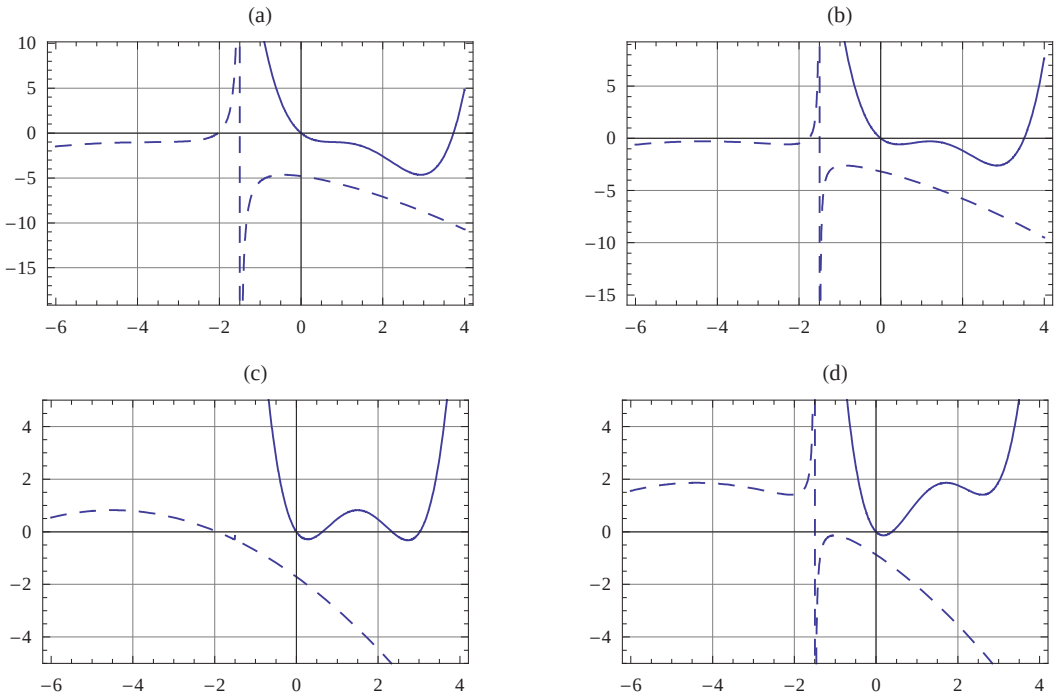

Figure 4.19: Example 4.3 - The integrand function of P_s vs u_x (solid curve) and the integrand function of P_s^d vs ζ (dashed curve) at different locations: (a) $x = 0.62$; (b) $x = 0.7$; (c) $x = 0.8$; (d) $x = 0.9$.

for $x \in [x_0, x_1]$, where x_0 and $x_1 > x_0$ are the two points where $\beta = 0$. From ζ_s, a smooth solution u_s of (BVP1) can be constructed. However, in this case, it does not satisfy the boundary condition for (BVP2). This is possibly the reason why the FPI-FDM does not converge to any solution after 500 iterations.

Following the idea of Example 4.3, the numerical behavior from an energy perspective is presented in Fig. 4.22. The first column of Fig. 4.22 suggests FPI-FDM method fails to converge to a solution. In the second and third columns of Fig. 4.22, the energy density curves near the two points $x = 0.2, 0.8$, for which the tilts of the curves are different, are shown. Located on these curves are the intermediate iterative points u_x^k (shown by red vertical bars) for three consecutive iterations ($k = 98, 99, 100$) in each case. Close to the free end of the bar, at $x \approx 0.9$, $\{u_x^k\}$ tends to converge to the local maximizer $\bar{u}_3$, since the Neumann boundary condition $u_x(1) = t = 0.9$ is satisfied only by $\bar{\zeta}_3$; at $x \approx 0.45$, $\{u_x^k\}$ tends to diverge from the stationary point, the bottom of the unique well; most dramatically, at $x \approx 0.1$, $\{u_x^k\}$ jumps around between the two potential wells, which implies the divergence of the FPI-FDM. Note that for the FPI-FDM solutions in the left-hand side column, the boundary condition $u_x(1) = 0.9$ for (BVP2) is satisfied at each iteration.

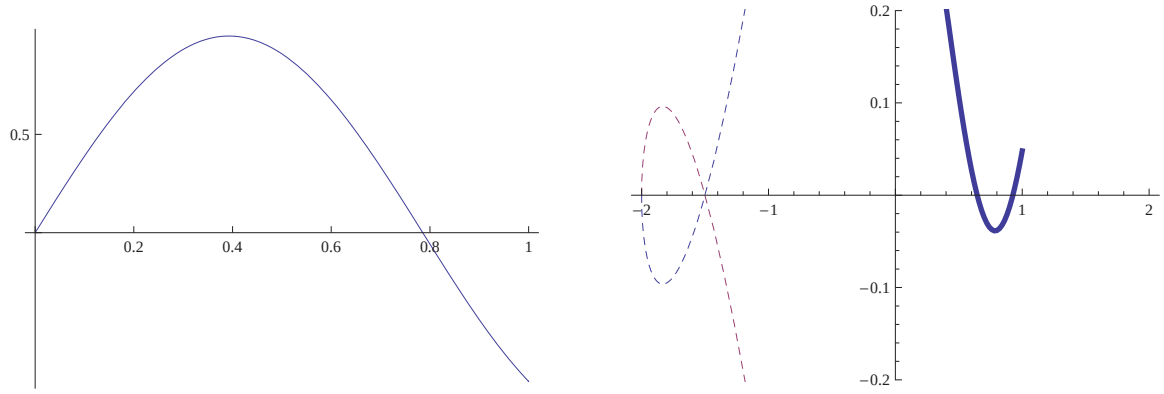

(a) Axial loading force f.

(b) Plots of the dual algebraic curve from (4.25) with $\sigma - \mu\alpha$ vs ζ (dashed curve) and $\sigma - \mu\alpha$ vs $x \in [0, 1]$ from (4.21) (solid curve).

Figure 4.20: Example 4.4 - Forces in the modified version of Ericksen's bar.

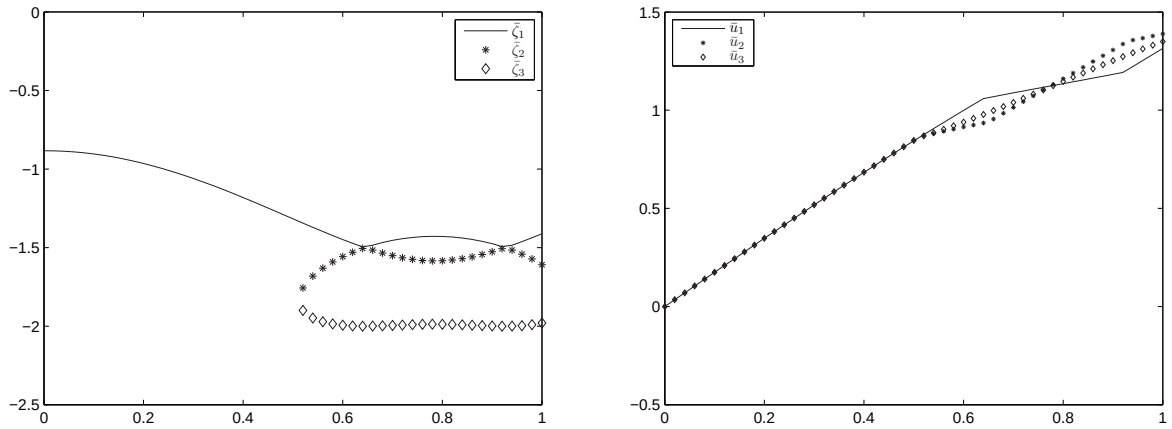

(a) Dual solutions ζ_i, $i = 1, 2, 3$.

(b) Primal solutions $\bar{u}_i$, $i = 1, 2, 3$.

Figure 4.21: Example 4.4 - Dual (4.25) and primal solutions (4.47). The horizontal axis is the x-axis for both plots. The vertical axis is (a) the ζ-axis and (b) the u-axis.

Example 4.5 Let $\mu = 1.5, \nu = 4, \alpha = 1.5$, $f(x) = 18\sin(4x)$ and $t = 2.5$ in (BVP1). Then, as in Example 4.3, we have $2\mu < \nu\alpha^2 < 8\mu$ and $\eta = 2$. The distributed force f is shown in Fig. 4.23(a) and $\sigma - \mu\alpha$ in Fig. 4.23(b). Clearly in Fig. 4.23(b), not only β changes sign, but also $\beta^2 - \eta$

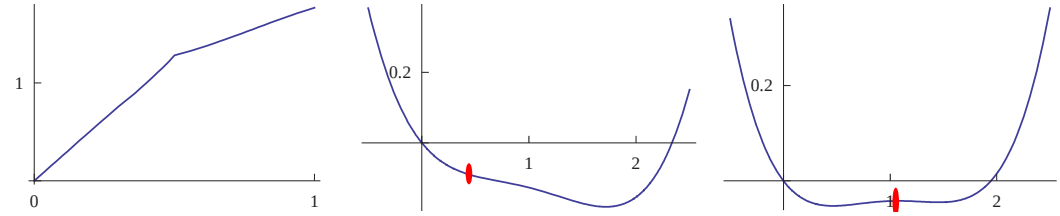

(a) The 98th FPI-FDM iteration.

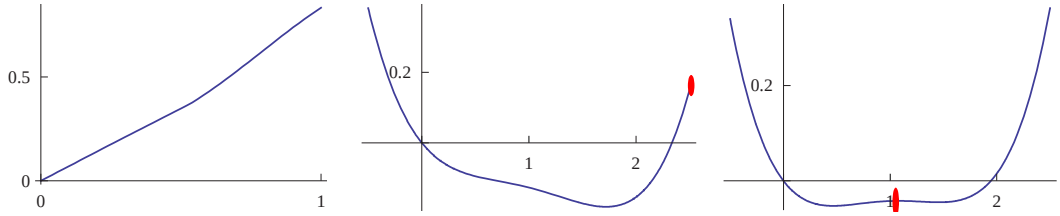

(b) The 99th FPI-FDM iteration.

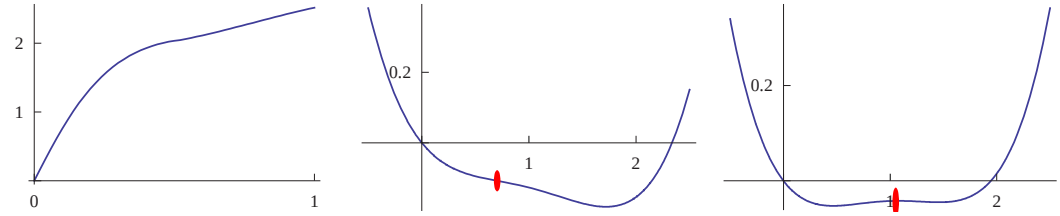

(c) The 100th FPI-FDM iteration.

Figure 4.22: Example 4.4 - Intermediate FPI-FDM iterative solutions (second and third columns for $x = 0.2, 0.8$, respectively), and $(u_x)^k(x)$ (indicated by the short vertical red lines), along with the energy density curve $E(u_x)$. The left-hand side column shows the corresponding solutions for $x \in [0, 1]$.

changes sign at both $\beta = \pm\sqrt{|\eta|}$ for some $x \in (0, 1)$. Thus, by Theorem 4.7(vi), there exists no smooth solution for (BVP1). The dual solutions $\bar{\zeta}_i$, $i = 1, 2, 3$, and the associated primal solutions $\bar{u}_i$ are shown in Fig. 4.24. In this case there is no smooth solution ζ and hence there are no smooth solutions to either (BVP1) or (BVP2). This may explain why the FPI-FDM cannot converge to any solution.

To end the investigation for the soft device, a seemingly "bizarre" scenario is presented in Fig. 4.25.

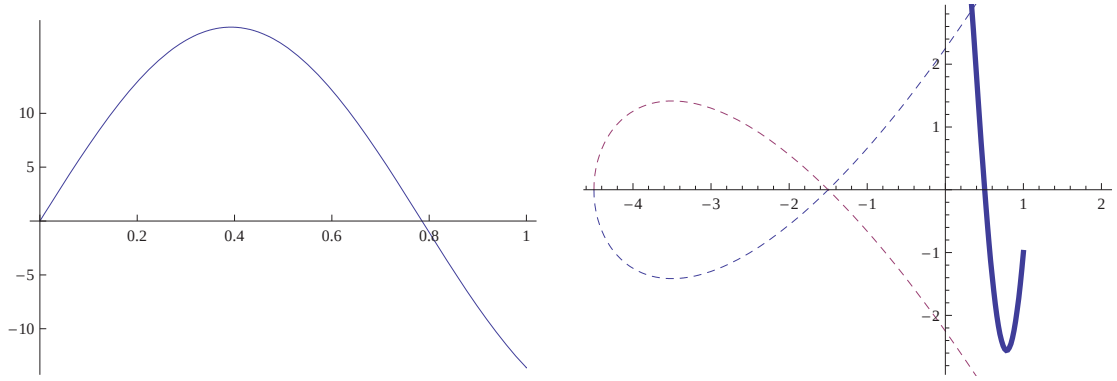

(a) Axial loading force f.

(b) Plots of the dual algebraic curve from (4.25) with $\sigma - \mu\alpha$ vs ζ (dashed curve) and $\sigma - \mu\alpha$ vs $x \in [0, 1]$ from (4.21) (solid curve).

Figure 4.23: Example 4.5 - Forces in the modified version of Ericksen's bar.

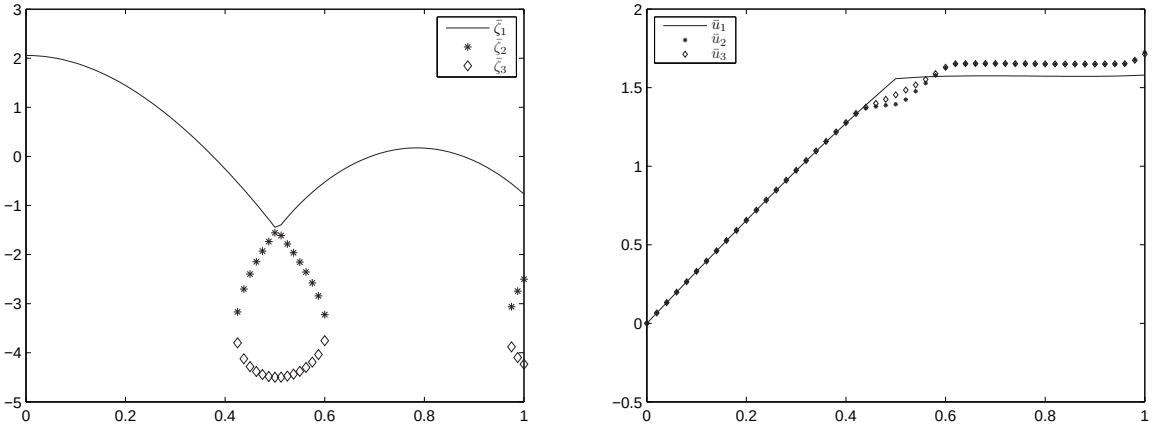

(a) Dual solutions $\bar{\zeta}_i, i = 1, 2, 3$.

(b) Primal solutions $\bar{u}_i$, $i = 1, 2, 3$.

Figure 4.24: Example 4.5 - Dual (4.25) and primal solutions (4.47). The horizontal axis is the x-axis for both plots. The vertical axis is (a) the ζ-axis and (b) the u-axis.

Note that in Fig. 4.24(a), for x in a certain interval $I_0 \subset (0.4, 0.6)$, there are three real dual solutions. Thus, at least theoretically, there are infinitely many possible solutions, as within I_0 solutions may randomly switch among the three states. Fig. 4.25 is obtained by a random sampling among the

three states at different material points in I_0. While this theoretical phenomenon is unconventional,

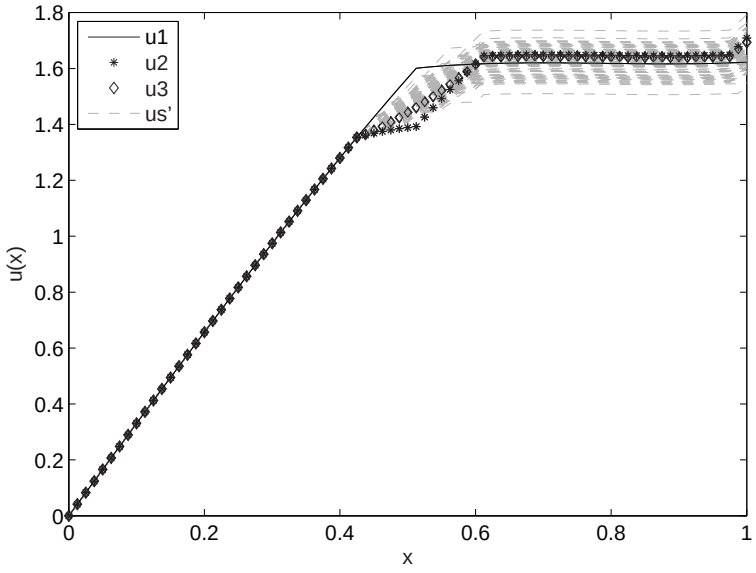

Figure 4.25: Example 4.5 - Multiple solutions.

it may help understanding the experimental observations of phase transitions and twinning in solids, which reveal fine layered micro-structures, as in Fig. 1.1 in Chapter 1.

Summary of Numerical Examples for The Soft Device In this section, the author applied the canonical duality theory to solve a modified version of Ericksen's bar for soft device. Based on the canonical duality theory, the criteria for the existence, uniqueness, smoothness and multiplicity of solutions were presented and discussed. The application of the FPI-FDM method illustrates the difficulty of capturing nonsmooth solutions and identifying extrema with standard numerical methods discussed in Chapter 3. These results illustrated the important fact that smooth analytic or numerical solutions of a nonlinear mixed boundary-value problem might not be minimizers of the associated potential variational problem.

Five numerical examples and numerous graphs were presented to support the theoretical results in Theorems 4.1-4.7. Next, for clarity of exposition, we summarize these numerical results in the Table 4.1. The second column lists smooth solutions for (BVP1). Symbols $\bar{u}_i, i = 1, 2, 3$ are consistent with the notations in Theorems 4.1-4.3. The symbols that contain the subscript 's' followed by numbers mean that, while a smooth $\bar{u}_1$ or $\bar{u}_2$ may not exist, a smooth solution can be constructed by combing different portions of $\bar{u}_1$ and $\bar{u}_2$. For example, $\bar{u}_{s121}$ is a smooth solution that consists of three portions, with the middle portion being from $\bar{u}_2$ and the rest from $\bar{u}_1$, as shown in Fig. 4.21(a). The '-' symbol means that there exists no smooth solution whatsoever. The third column

Examples	(BVP1) Sols.	(BVP2) Sols.	FPI-FDM Sols.	Theorems
Example 4.1A	$\bar{u}_1, \bar{u}_2, \bar{u}_3$	$\bar{u}_1$	$u_0 \approx \bar{u}_1$	4.7(i,iii,vii)
Example 4.1B	$\bar{u}_1, \bar{u}_2, \bar{u}_3$	$\bar{u}_2$	$u_0 \approx \bar{u}_2$	4.7(i,iii,vii)
Example 4.1C	$\bar{u}_1, \bar{u}_2, \bar{u}_3$	$\bar{u}_3$	$u_0 \approx \bar{u}_3$	4.7(i,iii,vii)
Example 4.2	$\bar{u}_{s12}, \bar{u}_{s21}, \bar{u}_3$	$\bar{u}_3$	$u_0 \approx \bar{u}_3$	4.7(ii,iv,vii)
Example 4.3	$\bar{u}_{s12}$	$\bar{u}_{s12}$	$u_0 \approx \bar{u}_{s12}$	4.7(ii,v,vii)
Example 4.4	$\bar{u}_{s121}$	-	-	4.7(ii,v,vii)
Example 4.5	-	-	-	4.7(vi,vii)

Table 4.1: Summary of the numerical examples for the soft device.

of Table 4.1 lists the smooth solutions for (BVP2). Note that these solutions always belong to the solution set of (BVP1). This is true because, for solutions of (BVP1), only those which satisfies the boundary conditions of (BVP2) solve (BVP2). In the fourth column, u_0 is the convergent solution yielded by the FPI-FDM. Symbol '$\approx$' means that the solutions are approximately the same, with the prescribed difference within the numerical tolerance. The last column lists the relevant theorems.

4.4 The Hard Device

For the modified version of Ericksen's bar of hard device, the feasible space is defined as

$$\mathcal{U}_h = \{u \in \mathcal{W}^{1,4}(0,1) \mid u(0) = 0,\ u(1) = d\}. \tag{4.61}$$

The primal variational problem (4.8) has the form

$$(\mathcal{P}_h): \quad \min_{u \in \mathcal{U}_h} \left\{ P_h(u) = \int_0^1 W(u_x)\mathrm{d}x - \int_0^1 fu\mathrm{d}x \right\}.$$

The criticality condition $\delta P_h(u) = 0$ leads to the Dirichlet boundary-value problem

$$(BVP3): \quad (\tfrac{1}{2}\nu u_x^2 - 3\nu\alpha u_x + \mu + \nu\alpha^2)u_{xx} + f = 0,$$

with boundary conditions

$$u(0) = 0 \tag{4.62}$$

and

$$u(1) = d. \tag{4.63}$$

4.4.1 Theoretical Results

For the soft device problem $(\mathcal{P}_s)$, once $\sigma(1)$ is given, closed form solutions are given by Theorem 4.3. Problem $(\mathcal{P}_h)$ can be solved by taking advantage of results from the soft device problem. To this end, we need to solve for $\sigma(1)$, which is initially unknown for the hard device. However, $\sigma(1)$ can be determined from the boundary condition $u(1) = d$ by using (4.47), in which

$$\bar{u_i}(1) = \int_0^1 \frac{\sigma(s) + \alpha\bar{\zeta_i}(s)}{\bar{\zeta_i}(s) + \mu} \mathrm{d}s. \tag{4.64}$$

Once we obtain $\sigma(1)$, the minimizing solution of (BVP3) is given by Theorem 4.3.

Theoretically, we are able to solve (4.64) with $i = 1, 2$ or 3. Practically, however, it is difficult to solve it if $i = 2$ or 3 is used for the following two reasons: First, since $\sigma(1)$ has not been determined, it is not clear whether there exist three real solutions of the cubic DAE (4.25) for any x in $(0, 1)$; second, while $\bar{\zeta_1}$ in (4.27) is real, $\bar{\zeta_2}$ and $\bar{\zeta_3}$ are not. This causes computational difficulty for standard numerical solvers employing Mathematica or Matlab. Therefore, in this thesis, we only solve for $\sigma(1)$ based on (4.47) with $i = 1$. The cases corresponding to $i = 2$ and 3 are left for future investigation. In the next subsection, we will present one numerical example to illustrate the application of the canonical duality theory on the hard device.

4.4.2 Numerical Example

To investigate the smooth solution (BVP3), we solve it using the FPI-FDM and we compare the resulting numerical approximation with the exact solution obtained by the canonical duality theory. Discretizing (BVP3), we form a tridiagonal system similar to that in (4.56), but with a different matrix:

$$\mathbf{A}_h = \begin{pmatrix} -2 & 1 & & & \\ 1 & -2 & 1 & & \\ & \ddots & \ddots & \ddots & \\ & & 1 & -2 & 1 \\ & & & 1 & -2 \end{pmatrix}.$$

Example 4.6 We choose $\mu = 1.5, \nu = 3, \alpha = 1.5$, $f(x) = 0.5\sin(x)$ and $u(1) = 1.2$ in (BVP3). First, we solve (4.64) with $i = 1$ and $\bar{u}(1) = 1.2$ to obtain $\sigma(1) = 2.0549$. Then, the dual solutions $\bar{\zeta_i}, i = 1, 2, 3$, given by Theorem 4.1 are plotted in Fig. 4.26(a). By Theorem 4.7 (ii), this figure suggests that there is no smooth minimizing solution. However, there are three smooth solutions for (BVP1). Theorem 4.3 then enables us to find the nonsmooth solution of $(\mathcal{P}_h)$ as

$$\bar{u}_1(x) = \int_0^x \frac{\sigma(s) + \alpha\bar{\zeta_1}(s)}{\bar{\zeta_1}(s) + \mu} \mathrm{d}s.$$

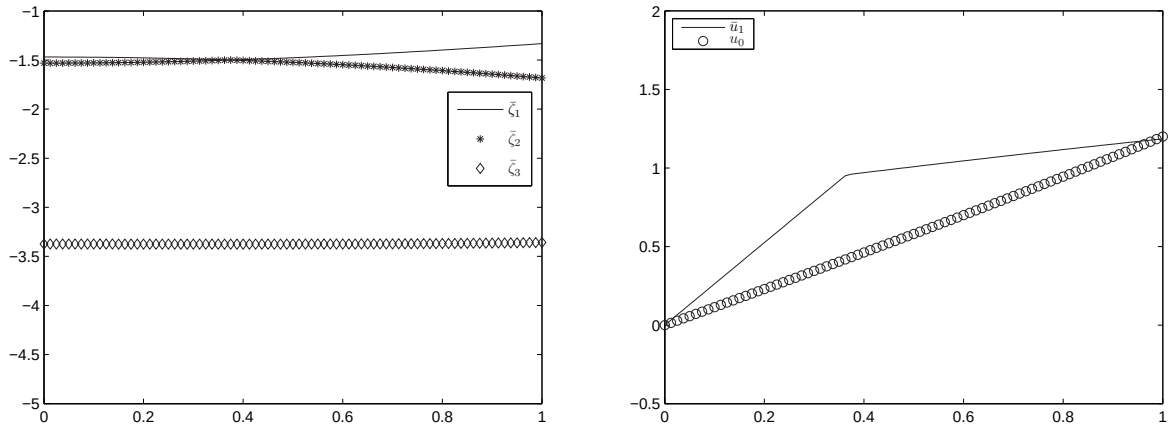

(a) Dual solutions $\bar{\zeta}_i, i = 1, 2, 3$.

(b) Primal solutions $\bar{u}_i$, $i = 1, 2, 3$.

Figure 4.26: Example 4.6 - Dual (4.25) and primal solutions (4.47) : (a) dual solutions ζ_i, $i = 1, 2, 3$, for $\sigma(1) = 2.0549$; (b) primal solutions $\bar{u}_1$, and the FPI-FDM solution u_0. The horizontal axis is the x-axis for both plots. The vertical axis is (a) the ζ-axis and (b) the u-axis.

Using the FPI-FDM, we obtain a smooth solution u_0 to (BVP3), as shown in Fig. 4.26(b), which clearly does not match $\bar{u}_1$. This is to say, the smooth solution u_0 obtained by FPI-FDM may not be the global minimizer.

4.5 Summary

In this chapter, the canonical duality theory is applied to a general non-convex variational problem, which is a modified version of Ericksen's bar. On the basis of the canonical duality theory, the nonlinear differential equation for the non-convex, non-homogeneous variational problem, here with either mixed or Dirichlet boundary conditions, is converted into an algebraic equation, which can be solved to obtain a complete set of solutions. The application of the theory also facilitates the identification and characterization of the local energy extrema and the global energy minimizer. From a dual perspective, the convergence (or non-convergence) of the FPI-FDM is explained and numerical examples are provided.

For the soft device, a complete set of closed-form solutions are provided, with the global minimizer and other extremal solutions identified by using the triality theory [28, 31]. The criteria for the existence, uniqueness, smoothness and multiplicity of solutions are developed and discussed. For

the hard loading device, the canonical duality theory is applied directly to obtain the minimizing solution. The results illustrate the important fact that smooth analytic or numerical solutions of a nonlinear mixed boundary-value problem might not be minimizers of the associated potential variational problem.

The numerical examples in this chapter illustrate the difficulty of capturing nonsmooth solutions and identifying extrema with standard numerical methods like the FPI-FDM. Generally speaking, linearizing the ODE by lagging all the lower-order terms essentially convexifies the original non-convex problem. At each iteration, the intermediate iterative solution is actually the minimizer of the convexified variational problem. However, this convexification might not be consistent in approximating the minimizer of the potential well. As a result, the intermediate solutions jump between the potential wells. A possible way to resolve this issue is to design the linearization such that the intermediate solution will follow the same potential well consistently. How to identify these intermediate solutions is a task that is difficult for the primal problem. However, by applying the canonical duality theory, the dual solutions are ordered in the inequality (4.35), and so are the primal solutions, which are identified by Theorem 4.4.

Another application of the canonical duality theory will be presented in the next chapter, in which the finite-element method is used to solve phase transition problems for solids governed by equations of Landau-Ginzburg type [51]. We note that the canonical duality theory can also be used for solving general non-convex variational problems for which the strain energy $W(\gamma)$ may be, for example, an exponential function [47] or a polynomial of degree higher than four [49, 33, 31]. Thus, the combination of triality theory and the results in this chapter could have more general implications in phase transitions, non-convex analysis and numerical computations.

Chapter 5

A Numerical Investigation of a Non-Convex Problem of Landau-Ginzburg Type

In Chapter 4, the canonical duality theory was applied to a modified version of Ericksen's bar. Both non-convex variational and the associated boundary-value problems were studied using Ericksen's soft and hard devices. We illustrated the difficulty of capturing non-smooth solutions and identifying extrema with standard numerical methods. The canonical duality theory provided a 'dual' perspective to investigate the behavior of standard numerical methods. In this chapter, we will work with a more complicated problem. For this problem, we will present a canonical dual finite element method, which is based on the canonical duality theory presented in Chapter 2, to solve a non-convex problem of Landau-Ginzburg type.

Recall that at the beginning of the thesis we introduced the non-convex problem:

$$(\mathcal{P}): \qquad P(u) = \frac{1}{2}\langle u, Au\rangle + W(u) - \langle u, f\rangle, \tag{5.1}$$

where the feasible space $\mathcal{U}_k$ is a convex subset of a normed space $\mathcal{U}$ with non-empty interior; $A : \mathcal{U} \to \mathcal{U}^*$ is a linear, self-adjoint operator ($A = A^*$), which maps each $u \in \mathcal{U}$ into its dual space $\mathcal{U}^*$; the bilinear form $\langle u, u\rangle : \mathcal{U} \times \mathcal{U}^* \to \mathbb{R}$ puts $\mathcal{U}$ and $\mathcal{U}^*$ in duality; $W : \mathcal{U} \to \mathbb{R}$ is a given function(al), either convex or non-convex; $f \in \mathcal{U}^*$ is a given input; and $P : \mathcal{U}_k \to \mathbb{R}$ represents the total cost (energy) function. In this chapter, we will work with a particular case of problem (5.1) - a problem of Landau-Ginzburg type.

The rest of the chapter is organized as follows. In Section 5.1, we briefly review the background and then specify the problem of Landau-Ginzburg type. In Section 5.2, a complementary extremum

principle is formulated, based on the canonical duality theory presented in Chapter 2. In Section 5.3, the canonical dual finite element method is formulated for the problem of Landau-Ginzburg type and a *triality theory* pertaining to the problem is given. In Sections 5.4 and 5.5, we apply the canonical dual finite element method and standard numerical methods to one-dimensional and two-dimensional examples. In section 5.6, the last section, we summarize the results.

5.1 A Non-Convex Problem of Landau-Ginzburg Type

In physics, the Landau-Ginzburg theory is a mathematical theory used to model superconductivity by examining the macroscopic properties of a superconductor with the aid of general thermodynamic theory [24]. In this section, we will set up a model based on the original Landau-Ginzburg problem [90, 40]. Specifically, we set the region $\Omega \subset \mathbb{R}^3$ occupied by the solid material to be a smooth, bounded, simply-connected domain with boundary $\Gamma = \partial\Omega$. The spontaneous polarization (i.e., dielectric displacement) $u(x)$ is a vector-valued function (the so-called order-parameter). Physically, $u(x)$ denotes a field whose values describe the phase of the system under consideration (cf. [80]). Then, the total potential P for the solid can be written as

$$P(u) = \int_\Omega [W_L(u) + W_G(\nabla u) - fu]\, \mathrm{d}\Omega, \tag{5.2}$$

where $W_L(u)$ is Landau's "coarse-grain" free energy [80], $W_G(\nabla u)$ is the micro-scale effect (or the generalized Ginzburg energy), and the third term is the macro-scale effect, where the force field $\mathbf{f}$ could model the distributed defects, or random field (see Gao *et al.* [40, 39]).

In the traditional Landau-Ginzburg theory of second-order ferroelectric transformations, the Landau potential $W_L(u)$ is a *double-well* function

$$W_L(u) = \frac{1}{2}\alpha \left(\frac{1}{2}|u|^2 - \lambda\right)^2, \tag{5.3}$$

where $\alpha,\ \lambda > 0$ are material constants. The Ginzburg energy is simply a convex function of $\boldsymbol{\epsilon} = \nabla u$,

$$W_G(\boldsymbol{\epsilon}) = \frac{1}{2}|\boldsymbol{\epsilon}|^2, \tag{5.4}$$

where $|\cdot|$ denotes the Euclidean norm. For example, if $\boldsymbol{\epsilon} = \{\epsilon_i\} \in \mathbb{R}^3$ is a vector, then $|\boldsymbol{\epsilon}| = \sqrt{\sum_{i,j=1}^3 \epsilon_i \epsilon_i}$. If $\boldsymbol{\epsilon} = \{\epsilon_{ij}\} \in \mathbb{R}^{3\times 3}$ is a second-order tensor, then $|\boldsymbol{\epsilon}| = \sqrt{\mathrm{tr}(\boldsymbol{\epsilon}\cdot\boldsymbol{\epsilon})} = \sqrt{\sum_{i,j=1}^3 \epsilon_{ij}\epsilon_{ij}}$. For a given material parameter $\lambda > 0$, each potential well of $W_L(u(x))$ defines the phase of the material at the point $x \in \Omega$.

Let $\mathcal{U}_a$ denote the kinematically admissible space

$$\mathcal{U}_a = \{u \in \mathcal{W}^{m,p}(\Omega) |\ u(x) = 0\ \ \forall x \in \Gamma\}, \tag{5.5}$$

where $\mathcal{W}^{m,p}$ is the standard Sobolev space with $p \in (1, \infty)$. Then the application of the minimum potential principle to this multi-scale phase transition leads to a non-convex variational problem:

$$(\mathcal{P}_{LG}): \quad \min_{u \in \mathcal{U}_a} \int_\Omega [W_L(u) + W_G(\nabla u) - fu] \, \mathrm{d}\Omega. \tag{5.6}$$

The criticality condition of the total potential P leads to a second-order equation of Landau-Ginzburg type:

$$-\Delta u + \alpha \left(\frac{1}{2}|u|^2 - \lambda \right) u = f. \tag{5.7}$$

It is known that, for a given force field f, the corresponding nonlinear partial differential equation may have multiple solutions at each material point $x \in \Omega$, which could be either local minimizers or local maximizers of P [39]. For example, in phase transitions of shape memory alloys, each local minimizer of P corresponds to a certain phase state of the material; in unilateral post-bifurcation analysis, the solution of the post-buckling state is usually a local minimizer (see [40]). From the point view of convex analysis, we know that, due to the non-convexity of the Landau potential W_L, very small perturbations of the Ginzburg energy term W_G and the force field may lead the system to different critical points with significantly different phase states [45, 51, 44]. To see the influence of the Ginzburg term on the double-well potential energy surface, the total potential as a functional of u was determined using Gauss-Green integral transformation

$$P(u) = \int_\Omega \left[\frac{1}{2}\alpha \left(\frac{1}{2}|u|^2 - \lambda \right)^2 - u f_u \right] \mathrm{d}\Omega + \int_\Gamma u \cdot \sigma(u) \cdot \mathbf{n} \, \mathrm{d}\Gamma, \tag{5.8}$$

where $f_u = \nabla \cdot \sigma(u) + f$ is the force field, and $\sigma(u) = \nabla u$ is the Ginzburg stress tensor field. In the case that the ordered parameter u is a scalar-valued function $u(x)$ that vanishes on the boundary, the graph of the stored energy density

$$J(u) = \frac{1}{2}\alpha \left(\frac{1}{2}|u|^2 - \lambda \right)^2 - uf \tag{5.9}$$

is shown in Fig. 5.1, where f_c is a critical force measure to be determined. Increasing f_u results in changes in the elative depths of the two minimizers and in the height of the local maximizer. The value u at which the minimizer(s) is (are) occurring shifts slightly with f_u. For $f_u > f_c$, the results demonstrate that the potential energy surface has a single potential well (tilts to the right) that is a global minimizer, whereas for $f_u = f_c$ it has a double potential well that has two equal local minimizers with a local maximizer in-between. When $f_u < 0$, there a single potential well (tilts to the left) that is a global minimizer. Since the vector field $f(u) = \nabla \cdot \sigma + f$ depends on the ordered parameters, the equation of Landau-Ginzburg type (5.7) may have multiple solutions $u_i(x),\ i = 1, 2, 3$ at each material point $x \in \Omega$, and all these solutions are the critical points of the non-convex energy P in (5.8). Thus, in order to find the global minimizer of P, a mathematical

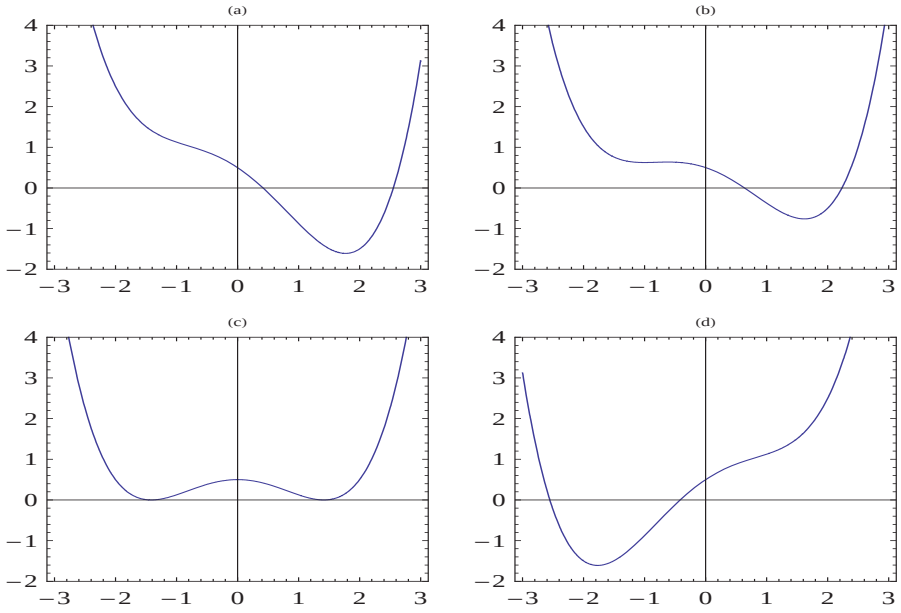

(a) $f_u > f_c$ (b) $f_u = f_c$ (c) $f_u = 0$ (d) $f_u < 0$

Figure 5.1: Effect of driving force f_u on potential diagrams $J(u)$ given by (5.9). The horizontal axis is the u-axis. The vertical axis is the J-axis.

theory is needed to identify the extremality conditions of the critical points at each material point. From a computational perspective, a numerical discretization of the total potential will lead to a global optimization problem in a finite dimensional space. Actually, many such non-convex global optimization problems are NP-hard [58, 59]. To find the global minimizer for the discretized form of P, criteria are needed to identify the extremality conditions of the critical points at each discretization point. Lack of such criteria may contribute to the fact that results vary with the numerical methods used. This is one of the main reasons why many times traditional perturbation analysis and direct approaches cannot successfully be applied to non-convex mechanics.

We also note that, in phase transitions of imperfect ferroelectric materials, the free energy W_G depends on high order deformations of the order parameters. Thus, it is appropriate to consider a multi-scale modeling for the Landau-Ginzburg model [51]. Such a model was proposed in [51] by assuming that the generalized Ginzburg energy can be written in the following form:

$$W_G(\Lambda u) = \frac{1}{2}D_1|\nabla u|^2 + \frac{1}{2}D_2|\nabla^2 u|^2 + \cdots + \frac{1}{2}D_m|\nabla^m u|^2, \tag{5.10}$$

where $D_i > 0 \ \ (i = 1, 2, \ldots, m)$ are material constants. Clearly, W_G is the traditional Ginzburg energy if $m = 1$. Due to its computational complexity, the multi-scale model is not considered any further in this thesis.

5.2 Canonical Dual Variational Principle

Following the standard procedure of the canonical dual transformation introduced in Chapter 2, we introduce a geometrical nonlinear operator $\xi(u) = \frac{1}{2}|u|^2$ and a convex function

$$V(\xi) = \frac{1}{2}\alpha\,(\xi - \lambda)^2$$

such that the second-order Landau energy $W_L(u)$ can be written in canonical form:

$$W_L(u) = V(\xi(u)) = \frac{1}{2}\alpha\,(\xi(u) - \lambda)^2\,.$$

Then, the canonical dual variable ς is uniquely defined as

$$\varsigma = \frac{\partial V}{\partial \xi} = \alpha(\xi - \lambda).$$

The complementary energy V^* can be obtained by the Legendre transformation:

$$V^*(\varsigma) = \{\xi\varsigma - V(\xi)\ :\ \xi = \varsigma/\alpha + \lambda\} = \frac{1}{2\alpha}\varsigma^2 + \lambda\varsigma. \tag{5.11}$$

The function $V^*(\varsigma)$ is also convex, and the following equivalent relations hold:

$$\varsigma = \frac{\partial V}{\partial \xi} \ \Leftrightarrow\ \xi = \frac{\partial V^*}{\partial \varsigma} \ \Leftrightarrow\ V(\xi) + V^*(\varsigma) = \xi\varsigma.$$

According to the definition introduced in [33], $(\xi,\ \varsigma)$ is called a *canonical dual pair*. By using the Fenchel-Young equality $V(\xi) = \xi\varsigma - V^*(\varsigma)$, the Landau energy can be written as

$$W_L(u) = \xi(u)\varsigma - \frac{1}{2\alpha}\varsigma^2 - \lambda\varsigma.$$

Thus, in terms of u and ς, the total potential energy of the multi-scale phase transition of solids can be written in the canonical mixed variational form, which yields the so-called *total complementary energy* [33]

$$\Xi(u,\varsigma) = \int_\Omega \left[\left(\frac{1}{2}|u|^2 - \lambda\right)\varsigma - \frac{1}{2\alpha}\varsigma^2 + W_G(u) - f\cdot u\right]\,\mathrm{d}\Omega. \tag{5.12}$$

It is easy to see that for each given u, $\Xi(u,\varsigma)$ is a strictly concave functional of the canonical dual variable ς. The criticality condition $\delta\Xi(u,\varsigma) = 0$ leads to the *canonical Lagrangian equations*

$$Au + \varsigma u = f, \tag{5.13}$$

$$\varsigma = \alpha\left(\frac{1}{2}|u|^2 - \lambda\right). \tag{5.14}$$

Clearly, for each given ς, the order parameter u can be determined through the equation (5.13) in terms of ς. Thus, the canonical dual functional P^d can be well-defined by the following canonical dual transformation

$$P^d(\varsigma) = \{\Xi(u,\varsigma)\ |\ \ \delta_u\Xi(u,\varsigma) = 0\}, \tag{5.15}$$

where $\delta_u \Xi$ stands for the Gâteaux derivative of Ξ with respect to u. The explicit form of the canonical dual functional $P^d(\varsigma)$ depends on the linear operator A and the force field f, which has a simple form in finite dimensional space. Let $\mathcal{S}_a$ be a statically admissible space, on which the canonical dual functional $P^d(\varsigma)$ is well-defined. Then, the canonical dual problem can be written as follows:

$$(\mathcal{P}^d): \quad \max_{\varsigma \in \mathcal{S}_a} P^d(\varsigma). \tag{5.16}$$

Since A is a linear operator defined on $\mathcal{U}_a$, its smallest eigenvalue $\lambda_1 > 0$ can be defined by

$$\lambda_1 = \min_{u \in \mathcal{U}_a} \lambda(u), \tag{5.17}$$

where

$$\lambda(u) = \frac{\langle u, Au \rangle}{\langle u, u \rangle} = \frac{\int_\Omega \sum_{i=1}^p D_i |\nabla^i u|^2}{\int_\Omega |u|^2 \, \mathrm{d}\Omega}. \tag{5.18}$$

Based on the triality theory developed in [33], the canonical duality theorem for the generalized Landau-Ginzburg equation can be written as follows:

Theorem 5.1 (Canonical Duality - Theorem 1 in [51]). *The problem $(\mathcal{P}^d)$ is canonically dual to $(\mathcal{P})$ in the sense that if $(\bar{u}, \bar{\varsigma})$ is a critical point of Ξ, then $\bar{u}$ is a critical point of P, $\bar{\varsigma}$ is a critical point of P^d, and the following strong duality relation holds*

$$P(\bar{u}) = \Xi(\bar{u}, \bar{\varsigma}) = P^d(\bar{\varsigma}). \tag{5.19}$$

Moreover, if $\bar{\varsigma}(u) + \lambda_1 > 0 \ \ \forall u \in \Omega$, then $\bar{u}$ is a global minimizer of P over $\mathcal{U}_a$, and $\bar{\varsigma}$ is a global maximizer of P^d for all $\varsigma > -\lambda_1$, i.e.,

$$P(\bar{u}) = \min_{u \in \mathcal{U}_a} P(u) = \max_{\varsigma > -\lambda_1} P^d(\varsigma) = P^d(\bar{\varsigma}). \tag{5.20}$$

Proof. The proof of statement (5.19) follows from the canonical duality theory. By using the Gauss-Green integration theorem, the total complementary energy $\Xi(u, \varsigma)$ can be written as

$$\Xi(u, \varsigma) = \frac{1}{2} \langle u, (A + \varsigma) u \rangle + \int_\Omega (V^*(\varsigma) - f \cdot u) \, \mathrm{d}\Omega, \tag{5.21}$$

in which the quadratic function

$$G(u, \varsigma) = \frac{1}{2} \langle u, (A + \bar{\varsigma}) u \rangle \tag{5.22}$$

is the so-called complementary gap function defined by Gao and Strang in [50]. Clearly, if $\bar{\varsigma}(x) + \lambda_1 \geq 0 \ \ \forall x \in \Omega$, the gap function $G(u, \bar{\varsigma})$ is convex in $u \in \mathcal{U}_a$. Thus, the total complementary energy $\Xi(u, \bar{\varsigma})$ is a saddle functional on $\mathcal{U}_a \times (-\lambda_1, \infty)$. By the general result proved in [50], the critical point $\bar{\varsigma} > -\lambda_1$ is a global maximizer of $P^d(\varsigma)$ on the open domain $(-\lambda_1, \infty)$, and $\bar{u}$ is a global minimizer of P on $\mathcal{U}_a$. □

This theorem shows that the global minimizer of the total potential energy depends on the canonical dual measure ς and the first eigenvalue of the linear operator A.

Since the generalized Ginzburg energy W_G is convex, the phase transition is due to the non-convexity of the Landau energy W_L. From equation (5.7), we can see that the effect of the micro-multi-scale stress Au and the macro-effect f are identical, i.e., both contributions act as a driving force in the equation. The following theorem reveals an essential property of phase transitions.

Theorem 5.2 (Multi-Scale Effects on Phase Transitions - Theorem 2 in [51]). *For the given distributed parameter $\lambda > 0$ and the force field f, let $(\bar{u}, \bar{\varsigma})$ be a critical point of Ξ, and $f(x) = |f(x) - A\bar{u}(x)|$. If $f(x) > f_c = \sqrt{8\alpha^2\lambda^3/27}$ $\forall x \in \Omega$, then the critical point $(\bar{u}, \bar{\varsigma})$ is the only solution of the generalized Landau-Ginzburg equation on Ω, and the $\bar{u}$ is a global minimizer of P.*

Otherwise, if there exists a subdomain $\Omega_r \subset \Omega$ such that $f(x) < f_c$ $\forall x \in \Omega_r$, then the generalized Landau-Ginzburg equation may have three sets of solutions $(\bar{u}_i, \bar{\varsigma}_i)$ (i=1,2,3) in Ω_r satisfying $\bar{\varsigma}_3 < \bar{\varsigma}_2 < 0 < \bar{\varsigma}_1$. In this case, $\bar{u}_1$ is a global minimizer of P, $\bar{u}_2$ is a local minimizer of P and $\bar{u}_3$ is local maximizer of P.

Proof. From the canonical Lagrange forms (5.13) and (5.14), the multi-scale effects on the canonical dual variable ς can be written as

$$2\bar{\varsigma}^2(\bar{\varsigma}/\alpha + \lambda) = f^2 = |f(x) - A\bar{u}(x)|^2. \tag{5.23}$$

This is the so-called canonical dual algebraic equation in non-convex mechanics (see [33] p.133). Let $\psi(\varsigma) = \pm\varsigma\sqrt{2(\varsigma/\alpha + \lambda)}$. The graph $\psi(\varsigma)$ is the so-called singular elliptic curve (see Fig. 5.2). The singularity means that the curve passes through the origin. For fixed parameters $\lambda > 0$, there exists a critical load $f_c = \sqrt{8\alpha^2\lambda^3/27}$ such that if $f > f_c$, the level set $\psi(\varsigma) = f$ has only one cross point (see Fig. 5.2). In this case, the algebraic equation (5.23) has one real root $\varsigma_1 > 0$, which leads to a global minimizer $\bar{u}$ of the total potential P (see Fig. 5.1(a)). However, when $f < f_c$, the level set $\psi(\varsigma) = f$ has three cross points (see Fig. 5.1 (d)). Thus, the algebraic equation (5.23) has three real roots ς_i $(i = 1, 2, 3)$, satisfying $\bar{\varsigma}_3 < \bar{\varsigma}_2 < 0 < \bar{\varsigma}_1$. In this case, P has a double potential well (see Fig. 5.1(c)). The triality theory developed in [33] indicates that $\bar{\varsigma}_1$ corresponds to the global minimizer $\bar{u}_1$ of P, $\bar{\varsigma}_2$ and $\bar{\varsigma}_3$ are corresponding to the local minimizer $\bar{u}_2$ and local maximizer $\bar{u}_3$, respectively. □

5.3 Canonical Dual Finite Element Method

In this section, we will use the canonical duality theorem (Theorem 5.1) to develop an approach based on the finite element method outlined in Chapter 3. This approach, called the *Canonical*

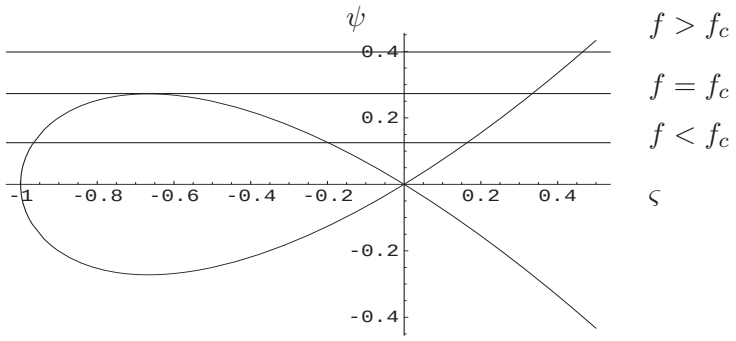

Figure 5.2: The singular elliptic curve of dual solutions for equation (5.23).

Dual Finite Element Method, can be used to solve the modified Landau-Ginzburg equation (5.7) in finite dimensional spaces.

Suppose that the domain Ω can be discretized by non-overlapping finite elements such that $\Omega = \bigcup_h \Omega^h$. In each element Ω^h, we choose suitable independent interpolations for u and ς:

$$u(x) = \mathbf{N_u}(x) \cdot \boldsymbol{u}^h, \quad \varsigma(x) = \mathbf{N}_\varsigma(x) \cdot \boldsymbol{\varsigma}^h, \;\; x \in \Omega^h, \tag{5.24}$$

where $\mathbf{N_u}$ and $\mathbf{N}_\varsigma$ are interpolation matrices expressing the local values of $u(x)$ and $\varsigma(x)$ in terms of element parameters $\boldsymbol{u}^h$ and $\boldsymbol{\varsigma}^h$, respectively. Thus, for this numerical discretization, the total complementary energy Ξ in (5.21) can be written in the following general form:

$$\begin{aligned}
\Xi(u^h, \boldsymbol{\varsigma}^h) &= \int_\Omega \left[\left(W_G(u) + \frac{1}{2}|u|^2 \varsigma \right) - \left(\frac{1}{2\alpha}\varsigma^2 + \lambda\varsigma \right) - f \cdot u \right] \mathrm{d}\Omega \\
&= \sum_{\Omega^h} \int_{\Omega^h} \left[\left(W_G(u) + \frac{1}{2}|u|^2 \varsigma \right) - \left(\frac{1}{2\alpha}\varsigma^2 + \lambda\varsigma \right) - f \cdot u \right] \mathrm{d}\Omega^h \\
&\approx \frac{1}{2}\boldsymbol{u}^h \cdot (\mathbf{A} + \mathbf{C}(\boldsymbol{\varsigma}^h)) \cdot \boldsymbol{u}^h - \bar{V}^*(\boldsymbol{\varsigma}^h) - \mathbf{f} \cdot \boldsymbol{u}^h,
\end{aligned} \tag{5.25}$$

where $\boldsymbol{u}^h \in \mathbb{R}^n$ is a vector, its components represent the order parameters at discretized material points in the domain Ω , $\boldsymbol{\varsigma}^h \in \mathbb{R}^m$ is the discretized canonical dual vector, $\mathbf{A} \in \mathbb{R}^{n\times n}$ is a symmetric matrix assembled from the discretized term $W_G(u)$ in each element, $\mathbf{C} : \mathbb{R}^m \to \mathbb{R}^{n\times n}$ is a symmetric linear matrix assembled from the discretized term $\frac{1}{2}|u|^2\varsigma$ in each element, $\mathbf{f} \in \mathbb{R}^n$ is the force vector, and $\bar{V}^*(\boldsymbol{\varsigma}^h)$ is a quadratic function of $\boldsymbol{\varsigma}^h$:

$$\bar{V}^*(\boldsymbol{\varsigma}^h) = \frac{1}{2}\boldsymbol{\varsigma}^h \cdot \mathbf{D} \cdot \boldsymbol{\varsigma}^h + \mathbf{b}(\lambda) \cdot \boldsymbol{\varsigma}^h,$$

where $\mathbf{D} = \mathbf{D}^T \in \mathbb{R}^{m\times m}$ is a positive definite matrix, and $\mathbf{b} \in \mathbb{R}^m$ is a vector that depends on the parameter λ.

Let $\mathcal{U}_a^h \subset \mathbb{R}^n$ be a discretized admissible space. The criticality condition of the discretized total complementary energy $\Xi : \mathcal{U}_a^h \times \mathbb{R}^m \to \mathbb{R}$ leads to the discretized canonical Lagrangian equations

$$(\mathbf{A} + \mathbf{C}(\boldsymbol{\varsigma}^h))\boldsymbol{u}^h = \mathbf{f}, \tag{5.26}$$

$$\frac{1}{2}\boldsymbol{u}^h\mathbf{C}'\boldsymbol{u}^h - \mathbf{D}\boldsymbol{\varsigma}^h = \mathbf{b}(\lambda), \tag{5.27}$$

where $\mathbf{C}' \in \mathbb{R}^{n\times m\times n}$ is a third-order tensor.

Since the matrix $\mathbf{D} \in \mathbb{R}^{m\times m}$ is positive definite, the discretized constitutive equation (5.27) can be written as

$$\boldsymbol{\varsigma}^h = \mathbf{D}^{-1}\left(\frac{1}{2}\boldsymbol{u}^h\mathbf{C}'\boldsymbol{u}^h - \mathbf{b}(\lambda)\right). \tag{5.28}$$

Substituting (5.28) into $\Xi(\boldsymbol{u}^h, \boldsymbol{\varsigma}^h)$ leads to the so-called mixed finite element (see, e.g., [10, 11]) model of the total potential:

$$P_h(\boldsymbol{u}^h) = \Xi(\boldsymbol{u}^h, \boldsymbol{\varsigma}^h(\boldsymbol{u}^h)),$$

where $\boldsymbol{\varsigma}^h : \mathcal{U}_a^h \to \mathbb{R}$. It is known that using direct methods for solving the discretized primal problem

$$(\mathcal{P}_h): \quad \min_{\boldsymbol{u}^h\in\mathcal{U}_a^h} P_h(\boldsymbol{u}^h) \tag{5.29}$$

is difficult due to the non-convexity of P_h. This motivates us to look for solutions from the canonical dual perspective.

For a given $\mathbf{f} \in \mathbb{R}^n$, the linear balance equation (5.26) has a unique solution

$$\boldsymbol{u}^h = (\mathbf{A} + \mathbf{C}(\boldsymbol{\varsigma}^h))^{-1}\mathbf{f}$$

if and only if $(\mathbf{A} + \mathbf{C}(\boldsymbol{\varsigma}^h))$ is invertible. Hence, the canonical dual feasible set $\mathcal{S}_a^h$ in this discretized problem should be written as

$$\mathcal{S}_a^h = \{\boldsymbol{\varsigma}^h \in \mathbb{R}^m |\ \ \mathbf{A} + \mathbf{C}(\boldsymbol{\varsigma}^h) \text{ is invertible}\}.$$

Thus, over $\mathcal{S}_a^h$, the canonical dual function P_h^d can be defined by

$$\begin{aligned} P_h^d(\boldsymbol{\varsigma}^h) &= \{\Xi(\boldsymbol{u}^h, \boldsymbol{\varsigma}^h) : \ \ \boldsymbol{u}^h = (\mathbf{A} + \mathbf{C}(\boldsymbol{\varsigma}^h))^{-1}\mathbf{f}\} \\ &= \frac{1}{2}\mathbf{f}^T(\mathbf{A} + \mathbf{C}(\boldsymbol{\varsigma}^h))^{-1}\mathbf{f} - \bar{V}^*(\boldsymbol{\varsigma}^h) - \mathbf{f}\cdot(\mathbf{A} + \mathbf{C}(\boldsymbol{\varsigma}^h))^{-1}\mathbf{f} \qquad (5.30) \\ &= -\frac{1}{2}\mathbf{f}^T(\mathbf{A} + \mathbf{C}(\boldsymbol{\varsigma}^h))^{-1}\mathbf{f} - \bar{V}^*(\boldsymbol{\varsigma}^h). \qquad (5.31) \end{aligned}$$

Generally speaking, this canonical dual function is non-convex on the dual feasible space $\mathcal{S}_a^h$ and it might have multiple critical points over $\mathcal{S}_a^h$. In order to determine the global minimizer and local extrema, we introduce the following subsets:

$$\mathcal{S}_+^h = \{\varsigma \in \mathbb{R}^m |\ \ (\mathbf{A} + C(\boldsymbol{\varsigma})) \text{ is positive definite}\}, \tag{5.32}$$

$$\mathcal{S}_-^h = \{\varsigma \in \mathbb{R}^m |\ \ (\mathbf{A} + C(\boldsymbol{\varsigma})) \text{ is negative definite}\}. \tag{5.33}$$

By the triality theory proposed in [43, 33, 36], extremality conditions of the non-convex variational problem can be described by Theorem 5.3. This theorem is analogous to Theorem 2.3, which is a more general case.

Theorem 5.3 (Triality Theorem - Theorem 3 in [51]). *If $\bar{\boldsymbol{\varsigma}}^h$ is a critical point of the discretized canonical dual function P_h^d, then the vector*

$$\bar{\boldsymbol{u}}^h = (\mathbf{A} + \mathbf{C}(\bar{\boldsymbol{\varsigma}}^h))^{-1}\mathbf{f} \tag{5.34}$$

is a critical point of P_h and

$$P_h(\bar{\boldsymbol{u}}^h) = P_h^d(\bar{\boldsymbol{\varsigma}}^h). \tag{5.35}$$

If $\bar{\boldsymbol{\varsigma}}^h \in \mathcal{S}_+^h$, then $\bar{\boldsymbol{\varsigma}}^h$ is a global maximizer of P_h^d on $\mathcal{S}_+^h$, while $\bar{\boldsymbol{u}}^h$ is a global minimizer of P_h on $\mathcal{U}_a^h$, and

$$P_h(\bar{\boldsymbol{u}}^h) = \min_{\boldsymbol{u}\in\mathcal{U}_a^h} P_h(\boldsymbol{u}^h) = \max_{\boldsymbol{\varsigma}^h\in\mathcal{S}_+^h} P_h^d(\boldsymbol{\varsigma}^h) = P_h^d(\bar{\boldsymbol{\varsigma}}^h). \tag{5.36}$$

If $\bar{\boldsymbol{\varsigma}}^h \in \mathcal{S}_-^h$, then $\bar{\boldsymbol{\varsigma}}^h$ and the associated $\bar{\boldsymbol{u}}^h$ are local critical points of P_h^d and P_h, respectively. In this case, on the neighborhood [1] *$\mathcal{U}_r^h \times \mathcal{S}_r^h \subset \mathcal{U}_a^h \times \mathcal{S}_-^h$ of $(\bar{\boldsymbol{u}}^h, \bar{\boldsymbol{\varsigma}}^h)$, we have that either*

$$P_h(\bar{\boldsymbol{u}}^h) = \min_{\boldsymbol{u}^h\in\mathcal{U}_r^h} P_h(\boldsymbol{u}^h) = \min_{\boldsymbol{\varsigma}^h\in\mathcal{S}_r^h} P_h^d(\boldsymbol{\varsigma}^h) = P_h^d(\bar{\boldsymbol{\varsigma}}^h), \tag{5.37}$$

or

$$P_h(\bar{\boldsymbol{u}}^h) = \max_{\boldsymbol{u}^h\in\mathcal{U}_r^h} P_h(\boldsymbol{u}^h) = \max_{\boldsymbol{\varsigma}^h\in\mathcal{S}_r^h} P_h^d(\boldsymbol{\varsigma}^h) = P_h^d(\bar{\boldsymbol{\varsigma}}^h) \tag{5.38}$$

holds.

Proof. By the general triality theory developed in [33], we know that if $\bar{\boldsymbol{\varsigma}}^h \in \mathcal{S}_+^h$, then the complementary gap function is

$$G(u^h, \bar{\boldsymbol{\varsigma}}^h) = u^h \cdot (\mathbf{A} + \mathbf{C}(\bar{\boldsymbol{\varsigma}}^h)) \cdot u^h \geq 0 \ \ \forall u^h \in \mathcal{U}_a^h.$$

Thus, by the general result given by Gao and Strang in [49], we know that the critical point $(\bar{\boldsymbol{u}}^h, \bar{\boldsymbol{\varsigma}}^h)$ is a saddle point of the discretized total complementary energy (5.25), the vector $\bar{\boldsymbol{u}}^h$ is a global minimizer of P_h on $\mathcal{U}_a^h$, and $\bar{\boldsymbol{\varsigma}}^h$ is a global maximizer of P_h^d on $\mathcal{S}_+^h$.

However, if $\bar{\boldsymbol{\varsigma}}^h \in \mathcal{S}_-^h$, then the critical point $(\bar{\boldsymbol{u}}^h, \bar{\boldsymbol{\varsigma}}^h)$ is a so-called *super critical point* of the discretized total complementary energy (5.25). In this case, the bi-duality theory developed in [33] shows that $\bar{\boldsymbol{u}}^h$ and $\bar{\boldsymbol{\varsigma}}^h$ are either local minimizers or local maximizers of P_h and P_h^d in their neighborhoods $\mathcal{U}_r^h$ and $\mathcal{S}_r^h$. □

The triality theorem (Theorem 5.3) describes unequivocally the critical points of the discretized non-convex problem. Since the canonical dual function $P_h^d(\boldsymbol{\varsigma}^h)$ is strictly concave on $\mathcal{S}_+^h$, the canonical dual problem

$$(\mathcal{P}_h^d): \quad \max_{\boldsymbol{\varsigma}^h\in\mathcal{S}_+^h} P_h^d(\boldsymbol{\varsigma}^h) \tag{5.39}$$

[1] The sub-product space $\mathcal{U}_r^h \times \mathcal{S}_r^h \subset \mathcal{U}_a^h \times \mathcal{S}_-^h$ is said to be a neighborhood of the critical point pair $(\bar{\boldsymbol{u}}^h, \bar{\boldsymbol{\varsigma}}^h)$ if $\bar{\boldsymbol{u}}^h$ is the only critical point of P_h on $\mathcal{U}_r^h$ and $\bar{\boldsymbol{\varsigma}}^h$ is the only critical point of P_h^d on $\mathcal{S}_r^h$.

can be solved by standard optimization methods. Let

$$\partial\mathcal{S}_+^h = \{\boldsymbol{\varsigma}^h \in \mathbb{R}^m | \ \det(\mathbf{A} + \mathbf{C}(\boldsymbol{\varsigma}^h)) = 0\} \tag{5.40}$$

denote the boundary of the dual feasible space $\mathcal{S}_+^h$. The existence and uniqueness of the global solution of the canonical dual problem (5.39) are provided in the following theorem.

Theorem 5.4 (Existence and Uniqueness Criteria - Theorem 4 in [51]). *Suppose that for certain mixed finite element interpolations (5.24), the matrix $\mathbf{C} : \mathbb{R}^m \to \mathbb{R}^{n\times n}$ is a linear matrix-valued function, $\bar{V}^* : \mathbb{R}^m \to \mathbb{R}$ is strictly convex, and for the given matrix $\mathbf{A} \in \mathbb{R}^{n\times n}$ and force vector $\mathbf{f} \in \mathbb{R}^m$ are given. If there exists at least one $\boldsymbol{\varsigma}_0^h \in \mathcal{S}_+^h$ such that $P_h^d(\boldsymbol{\varsigma}_0^h) > -\infty$ and the conditions*

$$\lim_{\boldsymbol{\varsigma}^h \to \partial\mathcal{S}_+^h} P_h^d(\boldsymbol{\varsigma}^h) = -\infty \ \ \forall \boldsymbol{\varsigma}^h \in \mathcal{S}_+^h \tag{5.41}$$

and

$$\lim_{|\boldsymbol{\varsigma}^h| \to \infty} P_h^d(\boldsymbol{\varsigma}^h) = -\infty \ \ \forall \boldsymbol{\varsigma}^h \in \mathcal{S}_+^h \tag{5.42}$$

hold, then the canonical dual problem $(\mathcal{P}_h^d)$ has a unique global maximizer $\bar{\boldsymbol{\varsigma}}^h \in \mathcal{S}_+^h$ and $\bar{\boldsymbol{u}}^h = (\mathbf{A} + \mathbf{C}(\bar{\boldsymbol{\varsigma}}^h))^{-1}\mathbf{f}$ is a unique global minimizer of the discretized primal problem $(\mathcal{P}_h)$.

Proof. By definition, the canonical dual feasible space $\mathcal{S}_+^h$ is an open convex subset of $\mathbb{R}^m$ whose boundary $\partial\mathcal{S}_+^h$ is a singular hyper-surface in $\mathbb{R}^m$. Since the canonical dual function $P_h^d : \mathcal{S}_+^h \to \mathbb{R} \cup -\infty$ is strictly concave, if there exists at least one $\boldsymbol{\varsigma}_0^h \in \mathcal{S}_+^h$ such that $P_h^d(\boldsymbol{\varsigma}_0^h) > -\infty$ and the conditions (5.41) and (5.42) hold, then the canonical dual problem $(\mathcal{P}_h^d)$ has a unique critical point $\bar{\boldsymbol{\varsigma}}^h$ which is a maximizer of P_h^d over $\mathcal{S}_+^h$. Furthermore, the discretized total complementary energy $\Xi : \mathcal{U}_a^h \times \mathcal{S}_+^h \to \mathbb{R}$ is a saddle point function which is strictly convex in $\boldsymbol{u}^h \in \mathcal{U}_a^h$ and strictly concave in $\boldsymbol{\varsigma}^h \in \mathcal{S}_+^h$. Therefore, the saddle variational problem

$$\min_{\boldsymbol{u}^h \in \mathcal{U}_a^h} \max_{\boldsymbol{\varsigma}^h \in \mathcal{S}_+^h} \Xi(\boldsymbol{u}^h, \boldsymbol{\varsigma}^h) = \max_{\boldsymbol{\varsigma}^h \in \mathcal{S}_+^h} \min_{\boldsymbol{u}^h \in \mathcal{U}_a^h} \Xi(\boldsymbol{u}^h, \boldsymbol{\varsigma}^h)$$

has a unique saddle point $(\bar{\boldsymbol{u}}^h, \bar{\boldsymbol{\varsigma}}^h)$ which satisfies the discretized canonical Lagrangian equations (5.26) and (5.27). By the triality theorem, we know that $\bar{\boldsymbol{\varsigma}}^h$ is a global maximizer of $(\mathcal{P}_h^d)$, and $\bar{\boldsymbol{u}}^h = (\mathbf{A} + \mathbf{C}(\bar{\boldsymbol{\varsigma}}^h))^{-1}\mathbf{f}$ is a global minimizer of $(\mathcal{P}_h)$. □.

We are now ready to illustrate numerically the theoretical developments presented in Sections 4.1-4.3. To test the efficiency and robustness of the canonical dual finite element method proposed above, we start by considering a one-dimensional problem in Sections 4.4 and 4.5. Then, in Section 4.6 we consider a two-dimensional problem.

5.4 Application to One-Dimensional Problems

To specify the problem, we let $\Omega = [0, 1]$. Then, the order parameter is a scalar valued function $u : \Omega \to \mathbb{R}$. The total potential of Landau-Ginzburg type can be written as

$$P(u) = \int_0^1 \left[\frac{1}{2}(u'(x))^2 + \frac{1}{2}\alpha \left(\frac{1}{2}u^2 - \lambda \right)^2 - uf \right] \, \mathrm{d}x. \tag{5.43}$$

Its equilibrium equation is

$$-\Delta u + \alpha \left(\frac{1}{2}|u|^2 - \lambda \right) u = f. \tag{5.44}$$

The boundary conditions are prescribed as $u(0) = u(1) = 0$. It is convenient to rewrite (5.44) in the form

$$(BVP4) \quad \begin{cases} -\Delta u + \alpha \left(\frac{1}{2}|u|^2 - \lambda \right) u = f, \\ u(0) = 0, \ u(1) = 0. \end{cases} \tag{5.45}$$

In this section, the canonical dual finite element method proposed in Section 5.3, together with several standard numerical methods introduced in Chapter 3 are applied to a one-dimensional problem of Landau-Ginzburg type. We are interested not only in solving the problem numerically, but also in assessing the robustness of the various numerical methods employed. Thus, the sensitivity of (BVP4) with respect to parameters λ and α, and initial guess u_0, is investigated. The corresponding numerical experiments are organized in three parts, with focus on parameters λ, α and initial guess u_0, respectively.

5.4.1 Canonical Dual FEM Formulation

For simplicity, we choose linear finite elements, for both u and ς in each element $\Omega^i = (x_{i-1}, x_i)$, $i = 1, 2, \ldots, N$, where $x_0 = 0$, $x_i = ih$, $x_N = 1$ and $h = \frac{1}{N}$. The total complementary energy in discretized form in equation (5.25) is

$$\Xi(\boldsymbol{u}^h, \boldsymbol{\varsigma}^h) = \frac{1}{2}\boldsymbol{u}^h \cdot (\mathbf{A} + \mathbf{C}(\boldsymbol{\varsigma}^h)) \cdot \boldsymbol{u}^h - \bar{V}^*(\boldsymbol{\varsigma}^h) - \boldsymbol{u}^h \cdot \mathbf{f}, \tag{5.46}$$

where

$$\mathbb{R}^{n-1} \ni \boldsymbol{u}^h = (u_1, \ u_2, \ldots, u_{N-2}, \ u_{N-1})^T,$$

$$\mathbb{R}^{n-1} \ni \boldsymbol{\varsigma}^h = (\varsigma_1, \ \varsigma_2, \cdots, \ \varsigma_{N-2}, \ \varsigma_{N-1})^T,$$

$$\mathbf{A}_1 = \begin{pmatrix} 2 & -1 & & & \\ -1 & 2 & -1 & & \\ & \ddots & \ddots & \ddots & \\ & & -1 & 2 & -1 \\ & & & -1 & 2 \end{pmatrix} \in \mathbb{R}^{(n-1)\times(n-1)}$$

with the boundary conditions $u_0 = u(0) = 0$ and $u_N = u(1) = 0$ being incorporated into $\mathbf{A}_1$.

The matrix

$$\mathbf{C}_1(\boldsymbol{\varsigma}) = h \begin{pmatrix} \frac{\varsigma_1}{12} + \frac{\varsigma_2}{2} + \frac{\varsigma_3}{12} & \frac{\varsigma_2}{12} + \frac{\varsigma_3}{12} & & & \\ \frac{\varsigma_2}{12} + \frac{\varsigma_3}{12} & \frac{\varsigma_2}{12} + \frac{\varsigma_3}{2} + \frac{\varsigma_4}{12} & \frac{\varsigma_3}{12} + \frac{\varsigma_4}{12} & & \\ & \ddots & \ddots & \ddots & \\ & & \frac{\varsigma_{N-3}}{12} + \frac{\varsigma_{N-2}}{12} & \frac{\varsigma_{N-3}}{12} + \frac{\varsigma_{N-2}}{2} + \frac{\varsigma_{N-1}}{12} & \frac{\varsigma_{N-2}}{12} + \frac{\varsigma_{N-1}}{12} \\ & & & \frac{\varsigma_{N-2}}{12} + \frac{\varsigma_{N-1}}{12} & \frac{\varsigma_{N-2}}{12} + \frac{\varsigma_{N-1}}{2} + \frac{\varsigma_N}{12} \end{pmatrix}$$

with $\mathbf{C}_1(\boldsymbol{\varsigma}) \in \mathbb{R}^{(n-1)\times(n-1)}$, is obtained by assembling the local matrices $\mathbf{C}_{1,i}(\boldsymbol{\varsigma}^h)$, for the ith element. These local matrices have the following form:

$$\mathbf{C}_{1,i}(\boldsymbol{\varsigma}^h) = h \begin{pmatrix} \frac{\varsigma_{i-1}}{4} + \frac{\varsigma_i}{12} & \frac{\varsigma_{i-1}}{12} + \frac{\varsigma_i}{12} \\ \frac{\varsigma_{i-1}}{12} + \frac{\varsigma_i}{12} & \frac{\varsigma_{i-1}}{12} + \frac{\varsigma_i}{4} \end{pmatrix},$$

and correspond to the term $\frac{1}{2}|\boldsymbol{u}|^2\varsigma$ in (5.25). The function $\mathbf{b}$ is given by $\mathbf{b}(\lambda) = \lambda$ in this case and $\frac{1}{2}\boldsymbol{\varsigma}^h \cdot \mathbf{D} \cdot \boldsymbol{\varsigma}^h$ is obtained by assembling the terms corresponding to $\frac{1}{2\alpha}\varsigma^2$ in (5.25) for all elements, so that

$$\begin{aligned} \bar{V}_1^*(\boldsymbol{\varsigma}^h) &= \frac{1}{2}\boldsymbol{\varsigma}^h \cdot \mathbf{D} \cdot \boldsymbol{\varsigma}^h + \mathbf{b}(\lambda) \cdot \boldsymbol{\varsigma}^h \\ &= h \sum_{i=1}^{N-1} \left(\frac{{\varsigma_i}^2 + \varsigma_i\varsigma_{i+1} + {\varsigma_{i+1}}^2}{6} + \frac{(\varsigma_i + \varsigma_{i+1})\lambda}{2} \right). \end{aligned} \tag{5.47}$$

Thus, by Theorem 5.1, the one-dimensional canonical dual problem reads

$$\max_{\boldsymbol{\varsigma}^h \in \mathcal{S}_+^h} \left\{ P^d(\boldsymbol{\varsigma}^h) = -\frac{1}{2}\mathbf{f} \cdot (\mathbf{A} + \mathbf{C}(\boldsymbol{\varsigma})^{-1} \cdot \mathbf{f} - \bar{V}^*(\boldsymbol{\varsigma}^h) \right\}. \tag{5.48}$$

The dual problem (5.48) is a constrained convex optimization problem as we are seeking a maximizer in a convex set $\mathcal{S}_+^h$. To solve the problem numerically, we use the Broyden-Fletcher-Goldfarb-Shanno (BFGS) method described in Chapter 3. While we seek the maximizer numerically, we need to ensure that each intermediate solution during the seeking procedure is confined to $\mathcal{S}_+^h$. As a result, it is necessary to check the convexity of the dual function $P^d(\boldsymbol{\varsigma}^h)$ at each step. The BFGS method is an appropriate choice because it is computationally efficient - it is a quasi-Newton method, in which the Hessian matrix is updated by analyzing successive gradient vectors instead of directly computing the Hessian matrix [69]. More details about the BFGS algorithm are given in Chapter 3.

5.4.2 Standard Numerical Methods

As stated in the previous chapters, one of the main goals of this work is to investigate the accuracy and robustness of the canonical dual framework proposed. To this end, we compare its numerical

behavior with that of the standard methods discussed in Chapter 3. Specifically, to solve the problem (BVP4), we use the following numerical methods: (i) fixed point iteration and finite difference method (FPI-FDM); (ii) Newton's method and finite difference method (NM-FDM); and (iii) nonlinear shooting method and finite difference method (NS-FDM). Next, we briefly describe these three standard numerical methods.

Fixed Point Iteration and Finite Difference Method (FPI-FDM) is used to approximate the solution of (BVP4). We first linearize the nonlinear equation (5.44) by lagging all the lower-order derivatives. This yields the following iterations, where k is the iteration number:

$$u_{xx}^{k+1} - \alpha u^{k+1}\left(\frac{3}{2}(u^k)^2 - \lambda\right) = -f - \alpha(u^k)^3 \tag{5.49}$$

Then, the high-order derivatives are discretized using the FDM. Let u_j^k be the k-th iterate of the numerical approximation of $u(jh)$, where h is the spatial mesh size, $0 \le j \le N$ and $Nh = 1$. We then obtain

$$\frac{u_{j+1}^{k+1} - \left[2 + \frac{3}{2}\alpha\left((u_j^k)^2 - \lambda\right)h^2\right]u_j^{k+1} + u_{j-1}^{k+1}}{h^2} = -f_j - \alpha(u_j^k)^3, \quad 1 \le j \le N-1. \tag{5.50}$$

This forms a tridiagonal system

$$\mathbf{A}_{1f} \cdot \mathbf{u}^{k+1} = \mathbf{g}^k, \tag{5.51}$$

where

$$\mathbf{A}_{1f} = \begin{pmatrix} -2 & 1 & & & \\ 1 & -2 & 1 & & \\ & \ddots & \ddots & \ddots & \\ & & 1 & -2 & 1 \\ & & & 1 & -1 \end{pmatrix},$$

$\mathbf{u}^k = (u_1^k, u_2^k, \ldots, u_{N-1}^k)$, $\mathbf{g}^k = (g_1^k, g_2^k, \ldots, g_{N-1}^k)$ and g_j^k is defined as the right-hand side of (5.50). Finally, starting with an initial guess, $\mathbf{u}^0$, the iterations $\mathbf{u}^k, k = 1, 2, 3, ...$ are computed until the convergence criterion $\|\mathbf{u}^k - \mathbf{u}^{k+1}\|_2 \le 10^{-6}$ is satisfied.

Remark 2. *Note that there are more than one way of lagging different nonlinear terms. For example, one could employ the following scheme:*

$$\frac{u_{j+1}^{k+1} - 2u_j^{k+1} + u_{j-1}^{k+1}}{h^2} - \alpha u_j^{k+1}\left(\frac{1}{2}(u_j^k)^2 - \lambda\right) = -f_j, \quad 1 \le j \le N. \tag{5.52}$$

Newton's Method and Finite Difference Method (NM-FDM) is used to obtain approximations solution of the solution of (BVP4), which will be compared with the other methods discussed

in this section. The method was applied in Chapter 4 for solving a modified version of Ericksen's bar. We only briefly describe it next. The nonlinear ODE in (BVP4) is first discretized by using the FDM. Thus, the first-order and second-order derivatives are approximated using central finite differences. Let u_j^k be the k-th iteration in the numerical approximation of $u(jh)$, where h is the spatial mesh size, $0 \leq j \leq N$, and $Nh = 1$. We then obtain

$$\frac{u_{j+1} - 2u_j + u_{j-1}}{h^2} - \frac{1}{2}(u_j)^3 - \lambda u_j + f_j = 0, \quad 1 \leq j \leq N-1. \tag{5.53}$$

These $N-1$ equations can be written in in the following form,

$$\mathbf{F}(\mathbf{u}) = \mathbf{0}, \tag{5.54}$$

where $\mathbf{F}$ is modified appropriately to reflect the boundary conditions in (5.54). Newton's method, described in Section 3.3.2 is then used to approximate numerically the solution of (5.54).

Nonlinear Shooting Method and Finite Difference Method (NS-FDM) works with the differential equation (5.7) directly. As described in Section 3.1, this is a numerical method for solving a boundary value problem by reducing it to the solution of a sequence of initial-value problems, involving a parameter t. To apply the nonlinear shooting method to (BVP4), we first solve a series of problems of the following form:

$$\begin{cases} \Delta u = \alpha \left(\frac{1}{2}|u|^2 - \lambda\right) u - f, \\ u(0) = 0, \quad u'(1) = t. \end{cases} \tag{5.55}$$

We then choose the parameter $t = t_k$ in a manner to ensure that

$$\lim_{k \to \infty} u(1, t_k) = u(1) = 0, \tag{5.56}$$

where $u(x, t_k)$ denotes the solution of the initial-value problem with $t = t_k$, and $u(x)$ denotes the solution of the boundary-value problem (5.55). In this thesis, we use the nonlinear shooting algorithm provided in Section 3.2.

5.4.3 Numerical Results

As stated in the beginning of this chapter, due to the non-convexity of the Landau energy term W_L, the modified Landau-Ginzburg problem is sensitive to its parameters λ and α. Thus, we suspect that the corresponding numerical discretizations will also display a high sensitivity with respect to changes in λ and α. Furthermore, since iterative numerical methods require an initial guess $\mathbf{u}_0$, for a non-convex problem like the modified Landau-Ginzburg problem, the selection of initial guess may have a significant influence on the solutions obtained. Thus, it is of interest to find a numerical

method to solve ($\mathcal{P}_{LG}$), which leads to a minimizing solution, regardless of the parameters λ and α or the initial guess.

The numerical results presented in this section aim at gaining a better understanding of the proposed Landau-Ginzburg problem by studying its sensitivity with respect to the parameters λ and α, and initial guess $\mathbf{u}_0$ when both the canonical dual FEM formulation in Section 5.4.1 and the standard methods in Section 5.4.2 are used.

In Example 5.1, we check the consistency of both the canonical dual FEM formulation and the standard numerical methods by using different mesh sizes h. To this end, we choose the following example as a benchmark. Since it is convenient to have the exact solution(s), we assume that one exact solution, $u_0(x) = -10x^2(1-x)$, is given. Plugging this into (5.7), we can find the corresponding $f(x) = 20(1-x) - 40x - 10\alpha(1-x)x^2(50(1-x)^2x^4) - \alpha$. Then, we can assume that $f(x)$ is known and solve (BVP4).

Example 5.1 Set $\lambda = 9$ and $\alpha = 1$ in (BVP4). Then, given the exact solution, $u_0(x) = -10x^2(1-x)$, the field force is given by $f(x) = 20(1-x) - 40x - 10(1-x)x^2(50(1-x)^2x^4)$.

We first solve (BVP4) using the numerical methods reviewed in Subsection 5.4.2 and the canonical dual FEM with different mesh sizes $h = 0.1,\ 0.05$, and 0.025, respectively. The results are shown in Fig. 5.3. Observe that using the canonical dual FEM presented in Section 5.4.1, the numerical approximations consistently converge to a unique solution, regardless of the mesh size. Thus, we conclude that all the numerical methods display a relatively low sensitivity with respect to changes in the mesh size h.

All the numerical approximations as well as the exact solution u_0 are shown in Fig. 5.4. From this figure, it seems that all solutions are close to the exact solution. The profile of all the numerical methods is shown in Table 5.1. From this table, we can observe that among all numerical methods,

	h = 0.1			h = 0.05			h = 0.025		
Methods	Iter	Time(s)	Error	Iter	Time(s)	Error	Iter	Time(s)	Error
FPI-FDM	9	0.016	6.09×10^{-9}	7	< 0.001	1.91×10^{-8}	6	0.016	3.19×10^{-7}
NM-FDM	9	0.015	6.10×10^{-9}	7	0.016	9.21×10^{-8}	6	0.047	3.20×10^{-7}
NS-FDM	3	< 0.001	3.73×10^{-7}	2	< 0.001	9.27×10^{-7}	2	0.015	1.84×10^{-7}
Dual FEM	79	10.266	9.47×10^{-7}	81	32.874	9.14×10^{-7}	89	177.45	9.39×10^{-7}

Table 5.1: Example 5.1 - Profiles of the four numerical methods tested: FPI-FDM, NM-FDM, NS-FDM, and Dual FEM. For various mesh sizes h, the number of iterations, the total execution time and the error are listed.

the canonical dual FEM is the slowest to obtain an approximate solution and displays a relatively poor performance in terms of accuracy.

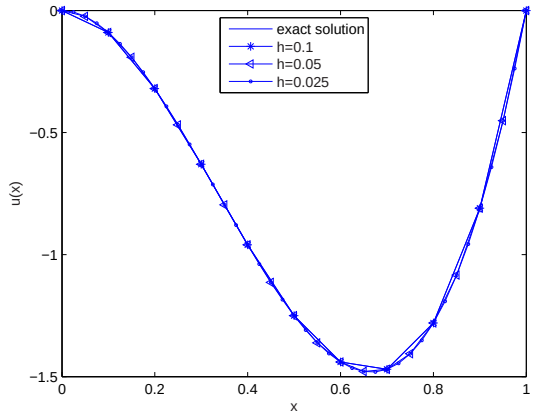

(a) $\bar{u}_1$ obtained by the FPI-FDM.

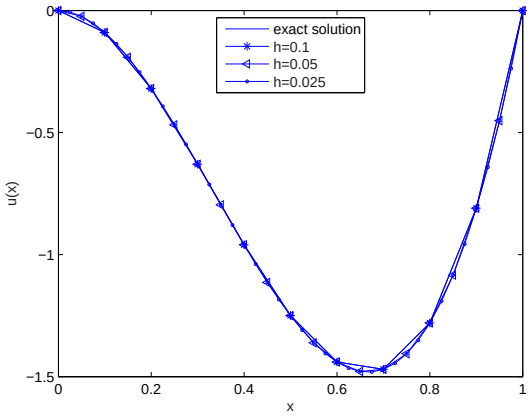

(b) $\bar{u}_2$ obtained by the NM-FDM.

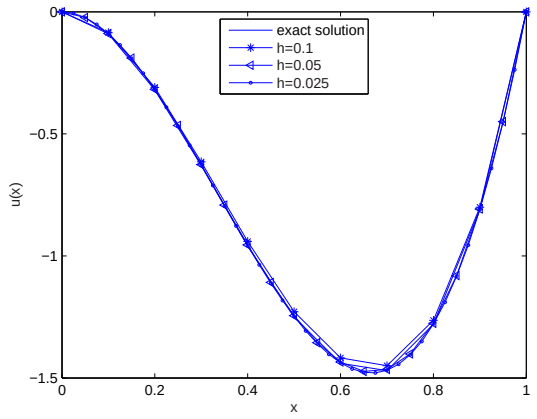

(c) $\bar{u}_3$ obtained by the NS-FDM.

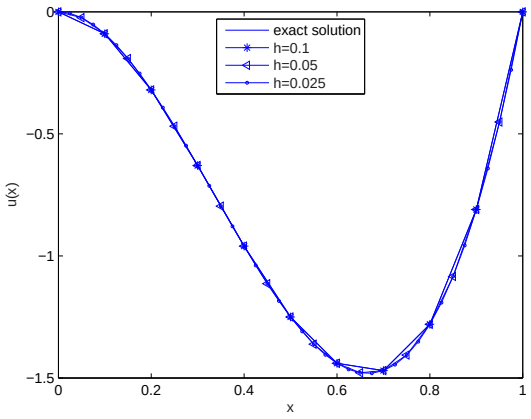

(d) $\bar{u}$ by the canonical dual FEM.

Figure 5.3: Example 5.1 - Solutions obtained by: (a) FPI-FDM; (b) NM-FDM; (c) NS-FDM; (d) canonical dual FEM using various mesh sizes, compared with the exact solution u_0.

Note that the existence of solutions is obvious, as we choose an external force f corresponding to a given solution u_0. However, the uniqueness of solutions is not clear without further analysis. Actually, our interest is to see multiple solutions, because sensitivity may become more dramatic if small perturbations lead the numerical methods to different solutions.

Sensitivity Analysis With Respect to λ

Example 5.2 To study the sensitivity of (BVP4) with respect to λ, we modify Example 5.1 by

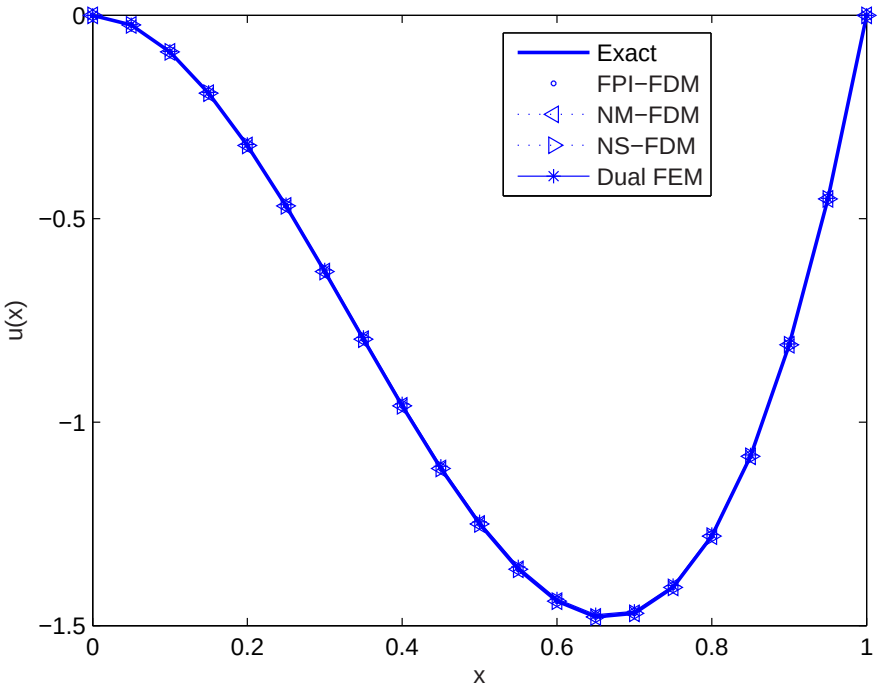

Figure 5.4: Example 5.1 - Exact solution and numerical approximations (FPI-FDM, NM-FDM, NS-FDM and Dual FEM).

changing λ from $\lambda = 9$ to $\lambda = 20$. Thus, we have $\lambda = 20$ and $\alpha = 1$ in (BVP4). We solve this problem using the numerical methods reviewed in Subsection 5.4.2 and the canonical dual FEM. All the numerical approximations as well as the exact solution u_0 are shown in Fig. 5.5. We notice that different numerical methods lead to different numerical approximations.

The profile of all the numerical methods is shown in Table 5.2. From this table, we can observe, as in Example 5.1, that among all numerical methods, the canonical dual FEM is the slowest to obtain an approximate solution and displays a relatively poor performance in terms of accuracy.

To check if we have obtained the global minimizer by the proposed the canonical dual FEM, we calculate the total energy of the functional (5.8), based on the numerical integration of the corresponding numerical approximations. Using the trapezoidal rule, we have $P(u_0) \approx P(u_{NM-FDM}) \approx P(u_{NS-FDM}) \approx 165.68$, and $P(u_{FPI-FDM}) = 189.40$. In contrast, $P(u_{Dual\ FEM}) = 124.25$. Obviously, the canonical dual FEM gives the solution of the lowest total energy.

Sensitivity Analysis With Respect to α

Example 5.3 To study the sensitivity of (BVP4) with respect to α, we modify example 5.1 by

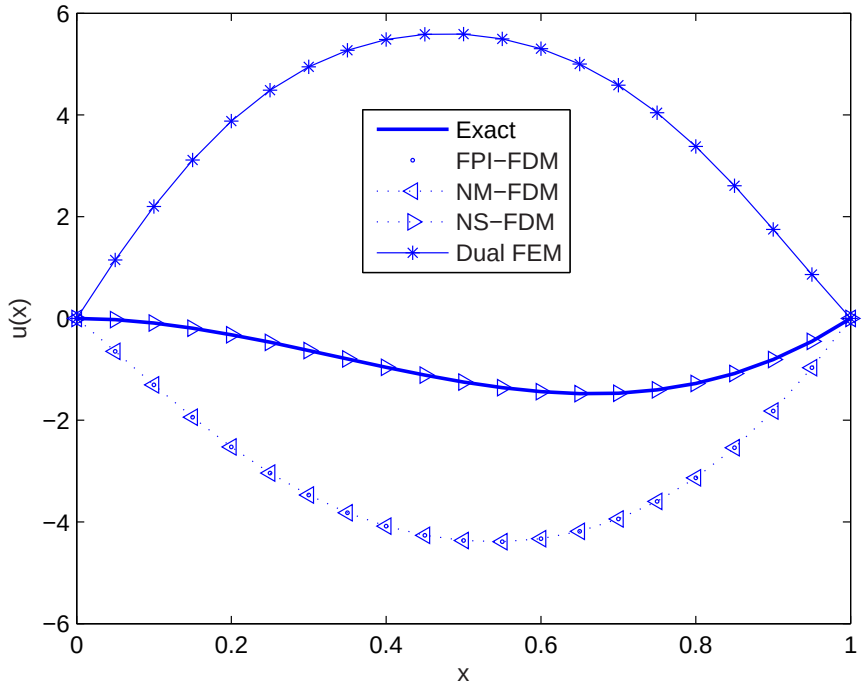

Figure 5.5: Example 5.2 - Exact solution and numerical approximations (FPI-FDM, NM-FDM, NS-FDM and Dual FEM).

changing λ from $\alpha = 1$ to $\alpha = 3$. Thus, we have $\alpha = 3$ and $\lambda = 9$ in (BVP4). The exact solution u_0 and the numerical approximations are shown in Fig. 5.6. From this figure, it seems that different numerical methods lead to different numerical approximations.

The profile of all the numerical methods is shown in Table 5.4.3. From this table, we can again observe that among all numerical methods, the canonical dual FEM is the slowest to obtain an approximate solution and displays a relatively poor performance in terms of accuracy.

To check if we obtained the global minimizer with the different numerical methods employed, we calculate the total energy of the functional (5.8), based on the numerical integration of the numerical approximations. Using the trapezoidal rule, we have $P(u_0) \approx P(u_{NS-FDM}) \approx 52.33$, and $P(u_{NM-FDM}) \approx P(u_{FPI-FDM}) = 58.86$. In contrast, $P(u_{DualFEM}) = 16.02$. Obviously, the canonical dual FEM gives the solution of the least total energy.

Sensitivity With Respect to Initial Guess $\mathbf{u}_0$

Example 5.4 Set $\alpha = 1,\ \lambda = 20$, and the force field $f(x) = 10cos(\pi x)e^x$ in (BVP4). We investigate whether different initial guesses $\mathbf{u}^0$ lead to different solutions. To this end, we first fix the mesh size

	h = 0.05		
Methods	Iter	Time(s)	Error
FPI-FDM	4	< 0.001	5.02×10^{-7}
NM-FDM	5	0.015	5.15×10^{-13}
NS-FDM	3	< 0.016	6.27×10^{-7}
Dual FEM	114	12.641	8.77×10^{-7}

Table 5.2: Example 5.2 - Profiles of the four numerical methods tested: FPI-FDM, NM-FDM, NS-FDM, and Dual FEM. The number of iterations, the total execution time and the error are listed.

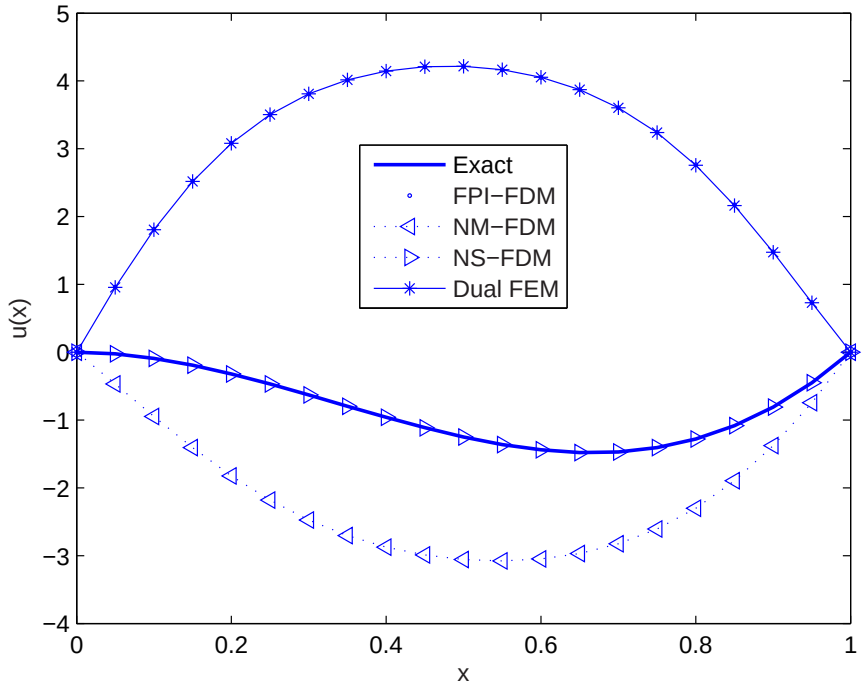

Figure 5.6: Example 5.3 - Exact solution and numerical approximations (FPI-FDM, NM-FDM, NS-FDM and Dual FEM).

$h = 0.025$ and then employ the FPI-FDM with different initial guesses. After using 50 different initial guesses $\mathbf{u}^0$, randomly generated by Mathematica, the FPI-FDM gives three different solutions u_1, u_2, u_3, which are shown in Fig. 5.7, with the solution u_{min} obtained by the canonical dual FEM overlaid. Thus, Example 5.4 clearly shows that by choosing different initial guesses, the FPI-FDM can lead to different solutions.

	h = 0.05		
Methods	Iter	Time(s)	Error
FPI-FDM	4	< 0.001	5.02×10^{-7}
NM-FDM	5	0.015	5.15×10^{-13}
NS-FDM	3	< 0.016	6.27×10^{-7}
Dual FEM	114	12.641	8.77×10^{-7}

Table 5.3: Example 5.3 - Profiles of the four numerical methods tested: FPI-FDM, NM-FDM, NS-FDM, and Dual FEM. The number of iterations, the total execution time and the error are listed.

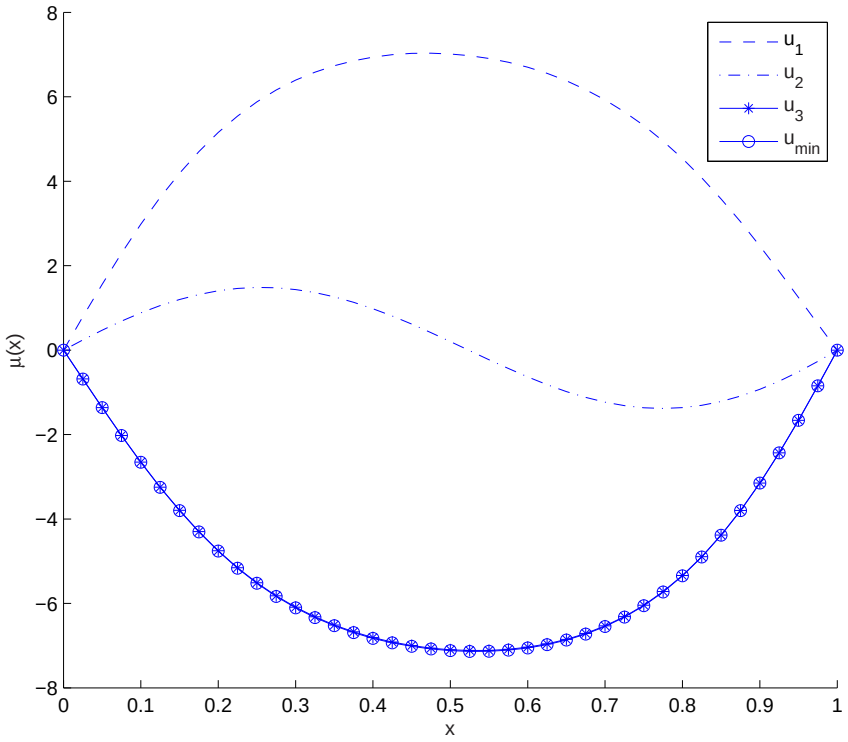

Figure 5.7: Example 5.4 - For different initial guesses, the FPI-FDM yields multiple solutions, u_1, u_2 and u_3. The canonical dual FEM yields a unique solution u_{min}, which is a global minimizer.

Recall that one of our main goals in this chapter is to locate the global minimizer solutions. By Theorems 5.3 and 5.4, the canonical dual FEM leads to the global minimizer solution, regardless of the initial guess. To check whether we obtained the global minimizer using the canonical dual FEM, we calculate the total energy of the functional (5.8) by using numerical integration for

the numerical approximations. Using the trapezoidal rule, we obtain $P(u_1) = 165.68$, $P(u_2) = 196.17$, and $P(u_3) = 149.06$. In contrast, $P(u_{DualFEM}) = P(u_{min}) = 149.42$. We note that $P(u_3)$ and $P(u_{DualFEM})$ are close, the difference being due to numerical errors in either the numerical integration or the finite difference approximation. Obviously, the canonical dual FEM gives the solution that has the lowest total energy.

Summary of The One-Dimensional Numerical Experiments

Example 5.2, 5.3 and 5.4 in this section show that, for different parameters λ and α, and various initial guesses $\mathbf{u}^0$, standard numerical methods, such as the FPI-FDM, can converge to multiple solutions. For these standard numerical methods, there is no way of choosing, among the various numerical approximations, one which minimizes the total energy. Theorem 5.3, however, guarantees that the canonical dual FEM will always yield the global minimizer. Examples 5.2, 5.3 and 5.4 clearly show that the numerical approximation obtained by using the canonical dual FEM always yields the lowest potential energy.

5.5 Application to Two-Dimensional Problems

We now apply the canonical dual FEM to two-dimensional cases. We simply let $\Omega = [0,1] \times [0,1]$. The ordered parameter is a scalar valued function $u : \Omega \to \mathbb{R}$ with $u(x,y) = 0$ on Γ, where Γ is the boundary of Ω. The Landau-Ginzburg type total potential can be written as

$$P(u) = \int_0^1 \int_0^1 \left[\frac{1}{2}[(u'(x))^2 + (u'(y))^2] + \frac{1}{2}\alpha \left(\frac{1}{2}u^2 - \lambda \right)^2 - uf \right] \, \mathrm{d}x \, \mathrm{d}y. \tag{5.57}$$

Its equilibrium equation is

$$-\Delta u + \alpha \left(\frac{1}{2}|u|^2 - \lambda \right) u = f. \tag{5.58}$$

The boundary conditions are prescribed as $u(0,y) = u(1,y) = u(x,0) = u(x,1) = 0$. It is convenient to rewrite the problem in the form

$$(BVP5) \quad \begin{cases} -\Delta u + \alpha \left(\frac{1}{2}|u|^2 - \lambda \right) u = f \\ \mathrm{u(x,y)} = 0 \quad \forall (x,y) \in \Gamma. \end{cases} \tag{5.59}$$

In this section, the canonical dual FEM and standard numerical methods are applied to the two-dimensional (BVP5). Similar to the one-dimensional case, we expect the solutions of (BVP5) to be sensitive with respect to the parameters λ and α, and the initial guess u_0. The numerical examples in Section 5.5.3 show that this is indeed the case.

5.5.1 Canonical Dual FEM Formulation

For simplicity, we choose linear triangular finite element basis functions to discretize both $\mathbf{u}$ and ζ. A sample two-dimensional finite element mesh is plotted in Fig. 5.8.

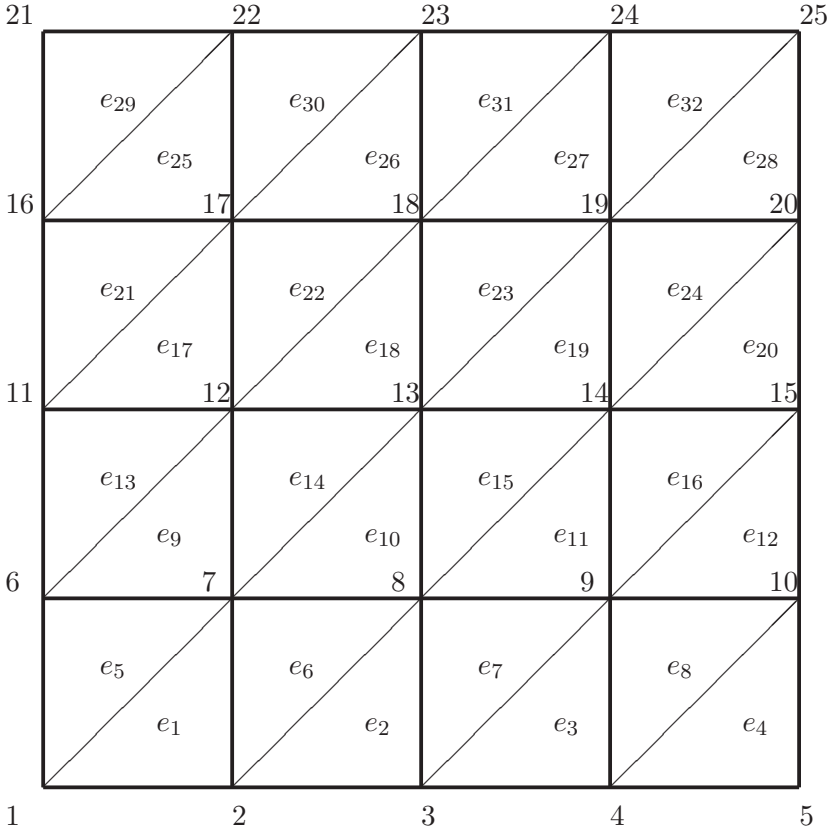

Figure 5.8: Sample two-dimensional mesh for the canonical dual FEM.

Similar to the one-dimensional case in Section 5.4, the total complementary energy in discretized form is

$$\Xi(\boldsymbol{u}^h, \boldsymbol{\varsigma}^h) = \frac{1}{2}\boldsymbol{u}^h \cdot (\mathbf{A}_2 + \mathbf{C}_2(\boldsymbol{\varsigma}^h)) \cdot \boldsymbol{u}^h - \bar{V}_2^*(\boldsymbol{\varsigma}^h) - \boldsymbol{u}^h \cdot \mathbf{f}, \tag{5.60}$$

where

$$\mathbb{R}^9 \ni \mathbf{u}^h = (u_7, u_8, u_9, u_{12}, u_{13}, u_{14}, u_{17}, u_{18}, u_{19})^T,$$

and

$$\mathbb{R}^9 \ni \boldsymbol{\varsigma}^h = (\varsigma_7, \varsigma_8, \varsigma_9, \varsigma_{12}, \varsigma_{13}, \varsigma_{14}, \varsigma_{17}, \varsigma_{18}, \varsigma_{19})^T.$$

The matrix $\mathbf{A}_2$ is given by the following formula:

$$\mathbf{A}_2 = \begin{pmatrix} 4. & -0.5 & 0 & -0.5 & -1. & 0 & 0 & 0 & 0 \\ -0.5 & 4. & -0.5 & 0 & -0.5 & -1. & 0 & 0 & 0 \\ 0 & -0.5 & 4. & 0 & 0 & -0.5 & 0 & 0 & 0 \\ -0.5 & 0 & 0 & 4. & -0.5 & 0 & -0.5 & -1. & 0 \\ -1. & -0.5 & 0 & -0.5 & 4. & -0.5 & 0 & -0.5 & -1. \\ 0 & -1. & -0.5 & 0 & -0.5 & 4. & 0 & 0 & -0.5 \\ 0 & 0 & 0 & -0.5 & 0 & 0 & 4. & -0.5 & 0 \\ 0 & 0 & 0 & -1. & -0.5 & 0 & -0.5 & 4. & -0.5 \\ 0 & 0 & 0 & 0 & -1. & -0.5 & 0 & -0.5 & 4. \end{pmatrix} \in \mathbb{R}^{9\times 9}, \tag{5.61}$$

which is obtained by assembling the local matrices $\mathbf{A}_{2,i}$,

$$\mathbf{A}_{2,i} = \begin{pmatrix} 0.5 & -0.5 & 0 \\ -0.5 & 1 & -0.5 \\ 0 & -0.5 & 0.5 \end{pmatrix},$$

and adjusted to include the homogeneous boundary conditions. The matrix $\mathbf{C}_2(\boldsymbol{\varsigma}) \in \mathbb{R}^{9\times 9}$ in (5.60) is obtained by assembling the local matrices $\mathbf{C}_{2,i}(\boldsymbol{\varsigma}^h)$ for each element i. These local matrices $\mathbf{C}_{2,i}(\boldsymbol{\varsigma}^h)$ correspond to the term $\frac{1}{2}|u|^2\varsigma$ in (5.25). For example, for node 7,

$$\mathbf{C}_{2,7}(\boldsymbol{\varsigma}^h) = h^2 \begin{pmatrix} \left(\frac{\varsigma_1}{20} + \frac{\varsigma_2}{60} + \frac{\varsigma_7}{60}\right) & \left(\frac{\varsigma_1}{60} + \frac{\varsigma_2}{60} + \frac{\varsigma_7}{120}\right) & \left(\frac{\varsigma_1}{60} + \frac{\varsigma_2}{120} + \frac{\varsigma_7}{60}\right) \\ \left(\frac{\varsigma_1}{60} + \frac{\varsigma_2}{60} + \frac{\varsigma_7}{120}\right) & \left(\frac{\varsigma_1}{60} + \frac{\varsigma_2}{20} + \frac{\varsigma_7}{60}\right) & \left(\frac{\varsigma_1}{120} + \frac{\varsigma_2}{60} + \frac{\varsigma_7}{60}\right) \\ \left(\frac{\varsigma_1}{60} + \frac{\varsigma_2}{120} + \frac{\varsigma_7}{60}\right) & \left(\frac{\varsigma_1}{120} + \frac{\varsigma_2}{60} + \frac{\varsigma_7}{60}\right) & \left(\frac{\varsigma_1}{60} + \frac{\varsigma_2}{60} + \frac{\varsigma_7}{20}\right) \end{pmatrix}. \tag{5.62}$$

The function $\mathbf{b}$ is given by $\mathbf{b}(\lambda) = \lambda$ in this case and $\frac{1}{2}\boldsymbol{\varsigma}^h \cdot \mathbf{D} \cdot \boldsymbol{\varsigma}^h$ is obtained by assembling terms corresponding to $\frac{1}{2\alpha}\varsigma^2$ in (5.25) for all elements, so that

$$\bar{V}_2^*(\boldsymbol{\varsigma}^h) = \frac{1}{2}\boldsymbol{\varsigma}^h \cdot \mathbf{D} \cdot \boldsymbol{\varsigma}^h + \mathbf{b}(\lambda) \cdot \boldsymbol{\varsigma}^h = h^2 \sum_{i=1}^{9} \bar{V}_{2,n_i}^*(\boldsymbol{\varsigma}^h).$$

For example, for node $n_1 = 7$,

$$\bar{V}_{2,7}^*(\boldsymbol{\varsigma}^h) = \left(\frac{{\varsigma_1}^2}{24\alpha} + \frac{\varsigma_1\varsigma_2}{24\alpha} + \frac{{\varsigma_2}^2}{24\alpha} + \frac{\varsigma_1\varsigma_7}{24\alpha} + \frac{\varsigma_2\varsigma_7}{24\alpha} + \frac{{\varsigma_7}^2}{24\alpha} + \frac{\varsigma_1\lambda}{6} + \frac{\varsigma_2\lambda}{6} + \frac{\varsigma_7\lambda}{6}\right). \tag{5.63}$$

Thus, by Theorem 5.1, the two-dimensional canonical dual problem can be written as

$$\max_{\boldsymbol{\varsigma}^h \in \mathcal{S}_+^h} \left\{ P^d(\boldsymbol{\varsigma}^h) = -\frac{1}{2}\mathbf{f} \cdot ((\mathbf{A} + \mathbf{C}(\boldsymbol{\varsigma}))^{-1}\mathbf{f} - \bar{V}^*(\boldsymbol{\varsigma}^h) \right\}. \tag{5.64}$$

The dual problem (5.64) is a constrained convex optimization problem as we are seeking a maximizer in a convex set $\mathcal{S}_+^h$. To solve the problem numerically, we use the Broyden-Fletcher-Goldfarb-Shanno (BFGS) method described in Section 3.4.

5.5.2 Standard Numerical Methods

As stated in the previous chapters, one of the main goals of this work is to investigate the accuracy and robustness of the proposed dual methodology. To this end, we compare its numerical behavior with that of the fixed point iteration with finite difference method (FPI-FDM). Next, we briefly describe this standard numerical method. We first linearize the nonlinear equation (5.58) by lagging all the low-order derivatives. This yields the following iterative scheme:

$$-u_{xx}^{k+1} - u_{yy}^{k+1} + \alpha u^{k+1}(\frac{1}{2}(u^k)^2 - \lambda) = -f, \tag{5.65}$$

where k is the iteration number. The high-order derivatives are discretized using the FDM. Let u_{ij}^k be the kth iterate of numerical approximation of $u(ih, jh)$, where h is the spatial mesh size and $Nh = 1$. We then obtain

$$\frac{u_{i,j+1}^{k+1} + u_{i+1,j}^{k+1} - \left[4 + \frac{1}{2}\alpha h^2((u_{i,j}^k)^2 - \lambda)\right] u_{i,j}^{k+1} + u_{i-1,j}^{k+1} + u_{i,j-1}^{k+1}}{h^2} = -f_{i,j}, \tag{5.66}$$

for $1 \le i, j \le N-1$. This forms a tridiagonal system

$$\mathbf{A}_{2f} \cdot \mathbf{u}^{k+1} = \mathbf{g}^k. \tag{5.67}$$

We choose a mesh size $h = 0.25$, so that $N = 4$. We will use the mesh in Fig. 5.9 to illustrate the FPI-FDM iterative scheme for simplicity.

Now, the matrix $\mathbf{A}_{2f}$ has the following form:

$$\mathbf{A}_{2f} = \begin{pmatrix} d_{1,1} & 1 & 0 & 1 & & & & & \\ 1 & d_{2,1} & 1 & 0 & 1 & & & & \\ 0 & 1 & d_{3,1} & 0 & 0 & 1 & & & \\ 1 & 0 & 0 & d_{1,2} & 1 & 0 & 1 & & \\ & 1 & 0 & 1 & d_{2,2} & 1 & 0 & 1 & \\ & & 1 & 0 & 1 & d_{3,2} & 0 & 0 & 1 \\ & & & 1 & 0 & 0 & d_{1,3} & 1 & 0 \\ & & & & 1 & 0 & 1 & d_{2,3} & 1 \\ & & & & & 1 & 0 & 1 & d_{3,3} \end{pmatrix},$$

where

$$d_{ij} = -4 - \alpha(\frac{1}{2}(u_{ij}^k)^2 - \lambda)h^2.$$

The vectors $\mathbf{u}^k$ and $\mathbf{g}^k$ in (5.67) are defined as:

$$\mathbf{u}^k = (u_{1,1}^k, u_{2,1}^k, u_{3,1}^k, u_{1,2}^k, u_{2,2}^k, u_{3,2}^k, u_{1,3}^k, u_{2,3}^k, u_{3,3}^k) \in \mathbb{R}^9,$$

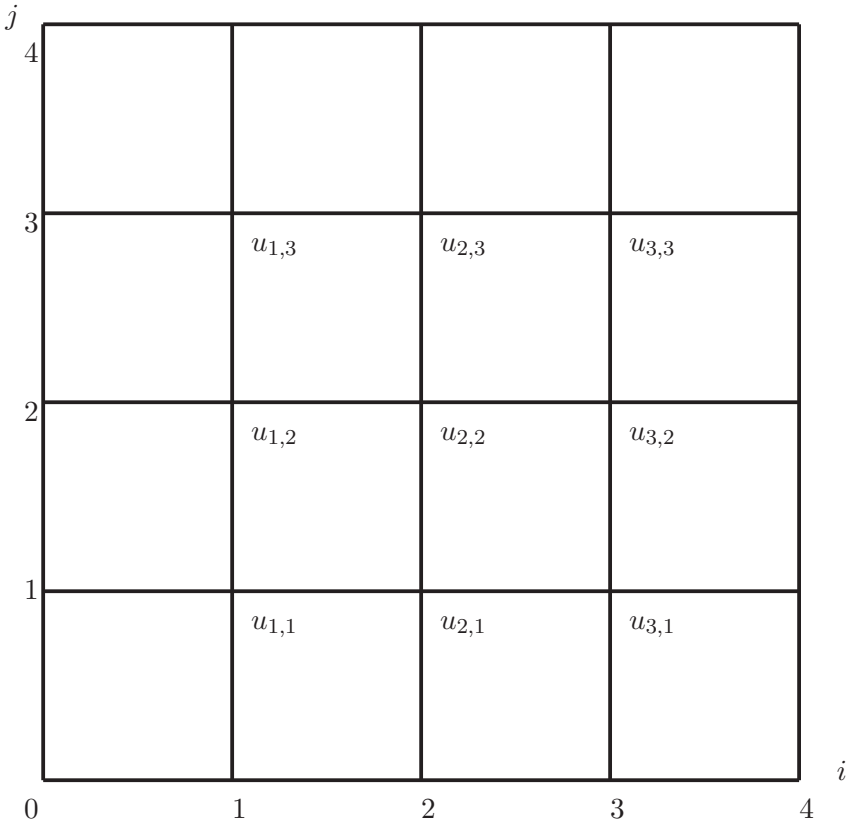

Figure 5.9: Sample two-dimensional mesh for the FPI-FDM.

and

$$\mathbf{g}^k = (g^k_{1,1}, g^k_{2,1}, g^k_{3,1}, g^k_{1,2}, g^k_{2,2}, g^k_{3,2}, g^k_{1,3}, g^k_{2,3}, g^k_{3,3}) \in \mathbb{R}^9,$$

where g^k_j is defined as the right-hand side of (5.66). Finally, starting with an initial guess, $\mathbf{u}^0$, the iterations $\mathbf{u}^k, k = 1, 2, 3, ...$ are computed until the convergence criterion $\|\mathbf{u}^k - \mathbf{u}^{k+1}\|_2 \leq 10^{-6}$ is satisfied.

5.5.3 Numerical Results

As in the one-dimensional case, the following two-dimensional examples aim at investigating numerically whether the dual FEM does indeed yield a numerical approximation that represents a global minimizer as predicted by the theory. For comparison purposes, numerical results with a standard numerical method, the FPI-FDM, are also included.

Example 5.5 In this example, we set $\alpha = 1, \lambda = 1$ in (BVP5). Since it is convenient to have the exact solution(s), we assume that one exact solution, $u(x, y) = 10x(1 - x)y(1 - y)$, is given. Plugging this exact solution into (5.58), we can find the corresponding forcing function $f(x, y) =$

$20(1-x)x+20(1-y)y+10(1-x)x(1-y)y\left(-1+50(1-x)^2x^2(1-y)^2y^2\right)$. Then, we can assume that $f(x,y)$ is known and solve (BVP5) using the numerical methods reviewed in Subsection 5.5.2 and the canonical dual FEM with different mesh sizes $h = h_x = h_y = 0.1$. The results are shown in Fig. 5.10.

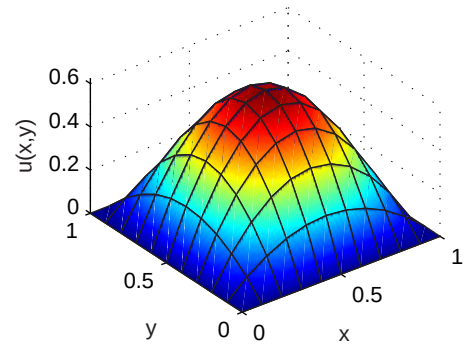

(a) Exact solution u with $P(u) = -0.2355$.

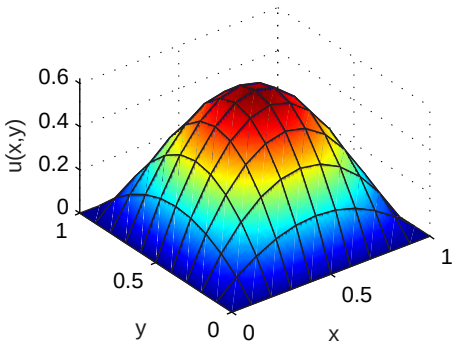

(b) $\bar{u}_1$ obtained by the FPI-FDM with $P(\bar{u}_1) = -0.2355$.

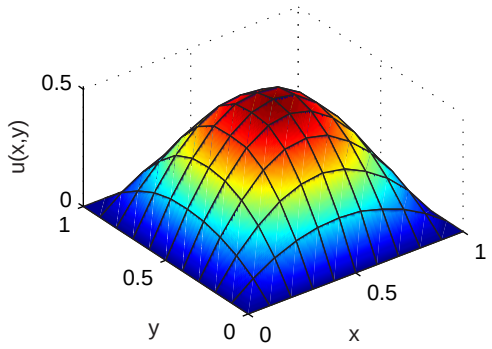

(c) $\bar{u}_2$ obtained by the FPI-FDM with $P(\bar{u}_2) = -0.2347$.

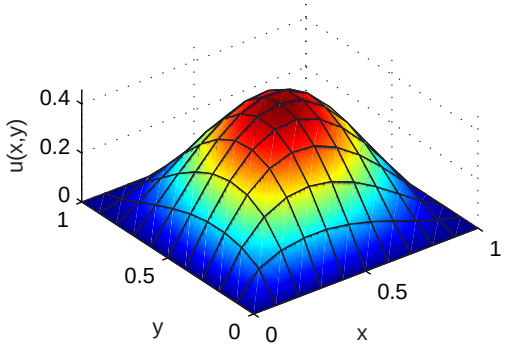

(d) $\bar{u}$ obtained by the dual FEM with $P(\bar{u}) = -0.2616$.

Figure 5.10: Example 5.5 - Exact solution u, multiple solutions $\bar{u}_1, \bar{u}_2$ by the FPI-FDM and global minimizer solution $\bar{u}$ by the canonical dual FEM.

To check if we have obtained the global minimizer by the proposed the canonical dual FEM, we calculate the total energy of the functional (5.57), based on the numerical integration of the obtained approximations. Obviously, from Fig. 5.10, we can see that the canonical dual FEM gives the solution of the lowest total energy, whereas the FPI-FDM does not.

Example 5.6 In this example, we set $\alpha = 3, \lambda = 3$ in (BVP5). Again, we assume that we have the exact solution $u(x,y) = 10x(1-x)y(1-y)$. Plugging this exact solution into (5.58), we obtain $f(x,y) = 20(1-x)x+20(1-y)y+30(1-x)x(1-y)y\left(-3+50(1-x)^2x^2(1-y)^2y^2\right)$. Then, we can

assume that $f(x, y)$ is known and solve (BVP5) using the numerical methods reviewed in Subsection 5.5.2 and the canonical dual FEM with different mesh sizes $h = h_x = h_y = 0.1$. The results are shown in Fig. 5.11.

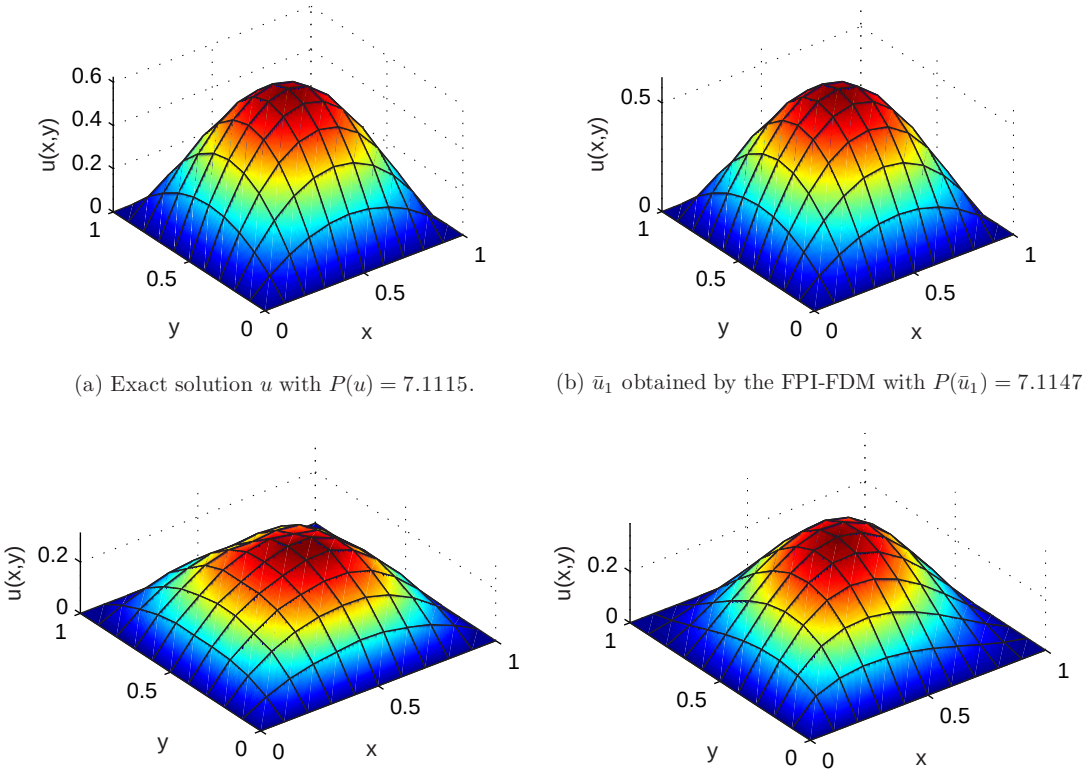

(a) Exact solution u with $P(u) = 7.1115$.

(b) $\bar{u}_1$ obtained by the FPI-FDM with $P(\bar{u}_1) = 7.1147$.

(c) $\bar{u}_2$ obtained by the FPI-FDM with $P(\bar{u}_2) = 7.1934$.

(d) $\bar{u}$ obtained by the dual FEM with $P(\bar{u}) = 7.0331$.

Figure 5.11: Example 5.6 - Exact solution u, multiple solutions $\bar{u}_1, \bar{u}_2$ by the FPI-FDM and global minimizer solution $\bar{u}$ by the canonical dual FEM.

To check if we have obtained the global minimizer by the proposed the canonical dual FEM, we calculate the total energy of the functional (5.57) by using the numerical integration of the obtained approximations. Obviously, from Fig. 5.11, we can see that the canonical dual FEM gives the solution of the lowest total energy, whereas the FPI-FDM does not.

Example 5.7 In this example, we set $f(x, y) = 100xy^2$ and will show how different initial guesses $\mathbf{u}^0$ lead to different solutions. To this end, we first solve (BVP5) using the proposed canonical dual FEM with a mesh size $h = h_x = h_y = 0.1$. The obtained solution is shown in Fig. 5.12. Then, we apply the FPI-FDM to solve (BVP5) with the same mesh size. After using 50 different initial guess

$\mathbf{u}^0$, which are randomly generated by Mathematica, the FPI-FDM gives three different solutions u_1, u_2, u_3, which are shown in Fig. 5.12 (b),(c), and (d), correspondingly.

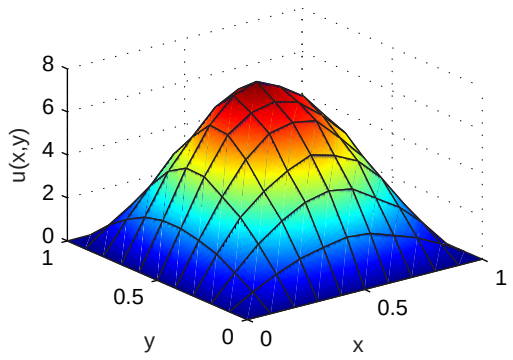

(b) $\bar{u}_1$ obtained by the FPI-FDM with $P(\bar{u}_1) = 58.7153$.

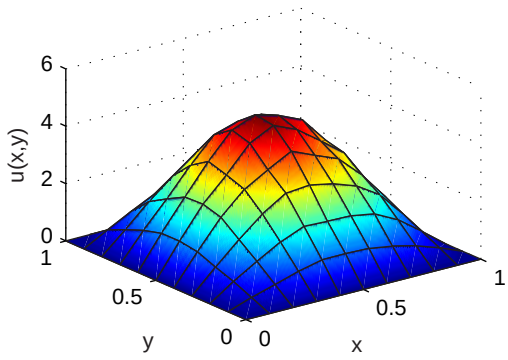

(b) $\bar{u}_2$ obtained by the FPI-FDM with $P(\bar{u}_2) = 46.959$.

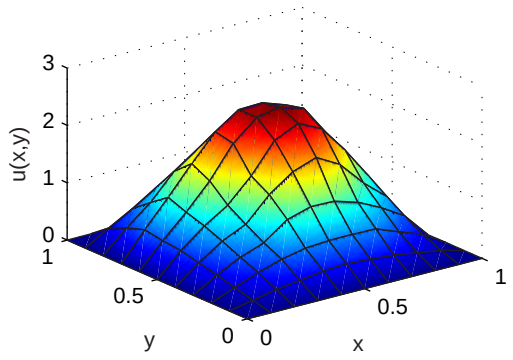

(c) $\bar{u}_3$ obtained by the FPI-FDM with $P(\bar{u}_3) = 40.0602$.

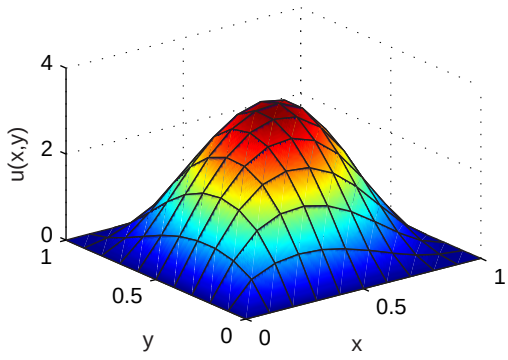

(d) $\bar{u}$ obtained by the dual FEM with $P(\bar{u}) = 37.2303$.

Figure 5.12: Example 5.7 - Multiple solutions $\bar{u}_1, \bar{u}_2$ and $\bar{u}_3$ by the FPI-FDM and global minimizer solution $\bar{u}$ by the canonical dual FEM.

Example 5.7 shows that by choosing different initial guesses, the FPI-FDM leads to different solutions. Recall that one of our main goals in this chapter is to locate the global minimizer solutions. By Theorems 5.3 and 5.4, the canonical dual FEM leads to the global minimizer solution, regardless of the initial guess. To check whether we obtained the global minimizer using the canonical dual FEM, we calculate the total energy of the functional (5.57) by preforming the numerical integration of the canonical dual FEM solution. Obviously, from Fig. 5.12, we can see that the canonical dual FEM gives the solution that has the lowest total energy, whereas the FPI-FDM does not.

Summary of the Two-Dimensional Numerical Experiments

As in the one-dimensional examples 5.2, 5.3 and 5.4, examples 5.5, 5.6 and 5.7 in this section show

that, for different parameters λ and α, and various initial guesses u^0, standard numerical methods, such as the FPI-FDM, can converge to multiple solutions. For these standard numerical methods, there is no way of choosing, among the various numerical approximations, one which minimizes the total energy. Theorem 5.3, however, guarantees that the canonical dual FEM will always yield the global minimizer. Examples 5.5, 5.6 and 5.7 clearly show that the numerical approximation obtained by using the canonical dual FEM always yields the lowest potential energy.

5.6 Summary

In this chapter, the canonical duality theory is applied to a general non-convex variational problem, which is a problem of Landau-Ginzburg type. The problem is governed by a semi-linear non-convex PDE which can be converted into a coupled quadratic mixed variational problem by the canonical dual transformation method. The extremality conditions of this variational problem are controlled by a triality theory. On the basis of the canonical duality theory, a canonical dual FEM is proposed.

Numerical examples show that for different parameters λ and α, and various initial guesses u^0, standard numerical methods, such as the FPI-FDM, can converge to multiple solutions, and there is no way of choosing among the various numerical approximations one which minimizes the total energy. However, the canonical dual FEM has one important advantage over these standard numerical methods: it always yields the lowest potential energy, regardless of the parameters λ and α, and initial guess u_0. On the other hand, the canonical dual FEM has two main disadvantages when compared with the standard numerical methods: it is the slowest to obtain an approximate solution and displays a relatively poor performance in terms of accuracy.

Chapter 6

Summary and Future Work

This thesis represents a theoretical and computational investigation of the canonical duality theory applied to two nonlinear/non-convex problems: a modified version of Ericksen's bar and a problem of Landau-Ginzburg type. For both applications, a critical assessment of the canonical duality theory is performed, both strengths and weaknesses being discussed.

In the first application, a one-dimensional non-convex variational problem is examined using a modified version of Ericksen's bar problem in the context of nonlinear elastic rod theory. Ericksen's bar provides an attractive setting for the study of, for example, phase transitions. For both soft and hard loading devices, Ericksen showed that the solutions obtained are meta-stable (neutrally stable) and may have an arbitrary number of discontinuities. On the basis of the canonical duality theory, the non-convex differential equation associated with the modified Ericksen's bar can be converted into an algebraic equation, which can be solved to obtain a complete set of solutions. The global minimizer and the local extrema can be identified. For the soft device, a complete set of closed-form solutions are provided, with the global minimizer and other extremal solutions identified by using the triality theory [47]. The criteria for the existence, uniqueness, smoothness and multiplicity of solutions are developed and discussed. For the hard loading device, the canonical duality theory is applied directly to obtain the minimizing solution. The numerical examples illustrate the difficulty of capturing non-smooth solutions and identifying extrema with standard numerical methods, such as the fixed point iteration with a finite difference discretization. Generally speaking, linearizing the ordinary differential equation by lagging all the lower-order terms essentially convexifies the original non-convex problem. At each iteration, the intermediate iterative solution is actually the minimizer of the convexified variational problem. However, this convexification might not be consistent in approximating the minimizer of the potential well. As a result, the intermediate solutions jump between the potential wells. A possible way to resolve this issue is to design the linearization such that the intermediate solution will follow the same potential well consistently. How to identify these

intermediate solutions is a task that is difficult for the primal problem. However, by applying the canonical duality theory, the dual solutions are ordered, and so are the primal solutions.

The second application of the canonical duality theory is a non-convex problem of Landau-Ginzburg type. The extremality conditions of this variational problem lead to a boundary value problem that can be approached through traditional techniques. The canonical duality theory, on the other hand, leads to a canonical dual finite element method for which sound theoretical support is provided. This new dual finite element method is compared with standard numerical methods in several one-dimensional and two-dimensional test problems. The dual finite element method always yields the numerical approximation that corresponds to minimum potential energy; the standard numerical methods are not capable of achieving this consistently. A particular emphasis is placed on the sensitivity of the two different numerical approaches with respect to changes in input parameters and initial guesses in the iterative processes. This sensitivity studies are important in assessing the robustness of the proposed numerical methods in practical situations. Based on the numerical results, the dual finite element method is robust to changes in parameters and initial guesses, whereas the standard numerical methods are not.

Based on the results obtained in the above two applications, several conclusions regarding the canonical duality theory emerge. The main strengths of the canonical duality theory are the following: First, for non-convex nonlinear variational problems, the canonical duality theory provides a means for identifying the solution (either analytical or numerical) that minimizes the total energy. In contrast, standard numerical methods based on traditional approaches for solving the variational problem cannot single out the energy minimizing solution among the multiple solutions of the corresponding boundary value problem. The second essential strength of the canonical duality theory is that the numerical methods that it provides are generally robust to changes in input parameters or initial guesses in the iterative processes. The standard numerical methods, however, display a sensitivity with respect to both parameters and initial guesses. The canonical duality theory, however, also displays a significant weakness. Indeed, compared with the standard numerical methods, the canonical dual finite element method is significantly slower.

There are several research avenues that the author plans to investigate in the future. First, the author would like to explore new numerical algorithms for decreasing the computational cost of the canonical dual finite element method. Second, in the modified Ericksen's bar problem, for the hard device, the author hopes to characterize a complete set of solutions. That is, the author aims at characterizing not only the global minimizer, but also the local minimizer and maximizer, as for the soft device. Third, in the modified problem of Landau-Ginzburg type, the author intends to extend the application of the canonical dual finite element method to higher dimensions. Fourth, the author would like to investigate the application of the canonical duality theory to global optimization. In particular, the box-constrained problem and the max-cut problem are closely related to the general

non-convex variational problem studied in this thesis and appear as natural candidates for the use of the canonical duality theory [37, 38, 41, 42]. Finally, the application of the canonical duality theory to fully nonlinear systems [28, 33, 32] will also be explored.

Bibliography

[1] R. A. Adams, *Sobolev spaces*, vol. 65, Academic press New York, 1975.

[2] A. Ambrosetti and A. Malchiodi, *Nonlinear analysis and semilinear elliptic problems*, Cambridge Studies in Advanced Mathematics, vol. 104, Cambridge University Press, Cambridge, 2007.

[3] A. M. Arthurs, *Complementary variational principles*, second ed., The Clarendon Press Oxford University Press, New York, 1980, Oxford Mathematical Monographs.

[4] A. A. Atai and D. J. Steigmann, *Coupled deformations of elastic curves and surfaces*, Internat. J. Solids Structures **35** (1998), no. 16, 1915–1952.

[5] J.-P. Aubin and I. Ekeland, *Applied nonlinear analysis*, Dover Publications Inc., Mineola, NY, 2006, Reprint of the 1984 original.

[6] G. Auchmuty, *Duality for non-convex variational principles*, J. Differential Equations **50** (1983), no. 1, 80–145.

[7] ———, *Variational principles for self-adjoint elliptic eigenproblems*, Non-smooth/non-convex mechanics (Blacksburg, VA, 1999), Non-convex Optim. Appl., vol. 50, Kluwer Acad. Publ., Dordrecht, 2001, pp. 15–42.

[8] O. Axelsson and V. A. Barker, *Finite element solution of boundary value problems: theory and computation*, vol. 35, Society for Industrial Mathematics, 2001.

[9] J. M. Ball and R. D. James, *Fine phase mixtures as minimizers of energy*, Arch. Rational Mech. Anal. **100** (1987), no. 1, 13–52.

[10] F. Brezzi, *A survey of mixed finite element methods*, Finite elements (Hampton, VA, 1986), ICASE/NASA LaRC Ser., Springer, New York, 1988, pp. 34–49.

[11] F. Brezzi and M. Fortin, *Mixed and hybrid finite element methods*, Springer Series in Computational Mathematics, vol. 15, Springer-Verlag, New York, 1991.

[12] R. L. Burden and J. D. Faires, *Numerical analysis*, Brooks/Cole Publishing Company, 2000.

[13] J. Carr, M. E. Gurtin, and M. Slemrod, *Structured phase transitions on a finite interval*, Arch. Rational Mech. Anal. **86** (1984), no. 4, 317–351.

[14] E. W. Cheney and D. R. Kincaid, *Numerical mathematics and computing*, Brooks/Cole Pub Co, 2007.

[15] F. H. Clarke, *The dual action, optimal control, and generalized gradients*, Mathematical control theory, Banach Center Publ., vol. 14, PWN, Warsaw, 1985, pp. 109–119.

[16] B. Dacorogna, *Direct methods in the calculus of variations*, Springer-Verlag, Berlin, 1989 (English).

[17] J. W. Demmel et al., *Applied numerical linear algebra*, vol. 150, Society for Industrial and Applied Mathematics Philadelphia, PA,, USA, 1997.

[18] I. Ekeland, *Legendre duality in non-convex optimization and calculus of variations*, SIAM J. Control Optimization **15** (1977), no. 6, 905–934.

[19] ———, *Convexity methods in Hamiltonian mechanics*, Ergebnisse der Mathematik und ihrer Grenzgebiete (3) [Results in Mathematics and Related Areas (3)], vol. 19, Springer-Verlag, Berlin, 1990.

[20] ———, *Non-convex duality*, Complementarity, duality and symmetry in nonlinear mechanics, Adv. Mech. Math., vol. 6, Kluwer Acad. Publ., Boston, MA, 2004, pp. 13–19.

[21] C. M. Elliott and S. Zheng, *On the Cahn-Hilliard equation*, Arch. Rational Mech. Anal. **96** (1986), no. 4, 339–357.

[22] J. L. Ericksen, *Equilibrium of bars*, J. Elasticity **5** (1975), no. 3–4, 191–201.

[23] ———, *Twinning of crystals. I*, Metastability and incompletely posed problems (Minneapolis, Minn., 1985), IMA Vol. Math. Appl., vol. 3, Springer, New York, 1987, pp. 77–93.

[24] ———, *Introduction to the thermodynamics of solids*, revised ed., Applied Mathematical Sciences, vol. 131, Springer-Verlag, New York, 1998.

[25] A. Ern and J.-L. Guermond, *Theory and practice of finite elements*, Applied Mathematical Sciences, vol. 159, Springer-Verlag, New York, 2004.

[26] I. Fonseca, *The lower quasiconvex envelope of the stored energy function for an elastic crystal*, J. Math. Pures Appl. (9) **67** (1988), no. 2, 175–195.

[27] E. Fried and M. E. Gurtin, *Dynamic solid-solid transitions with phase characterized by an order parameter*, Phys. D **72** (1994), no. 4, 287–308.

[28] D. Y. Gao, *Duality, triality and complementary extremum principles in non-convex parametric variational problems with applications*, IMA J. Appl. Math. **61** (1998), no. 3, 199–235.

[29] ———, *Duality-mathematics*, Wiley Encyclopedia of Electronical and Electronical Engineering **6** (1999), 68–77.

[30] ———, *General analytic solutions and complementary variational principles for large deformation non-smooth mechanics*, Meccanica **34** (1999), no. 3, 169–198.

[31] ———, *Analytic solutions and triality theory for non-convex and non-smooth variational problems with applications*, Nonlinear Anal. **42** (2000), no. 7, Ser. A: Theory Methods, 1161–1193.

[32] ———, *Canonical dual transformation method and generalized triality theory in non-smooth global optimizaton*, J. Global Optim. **17** (2000), no. 1-4, 127–160, Dedicated to the memory of Professor P. D. Panagiotopoulos.

[33] ———, *Duality principles in non-convex systems: Theory, methods and applications*, 1st edition ed., Kluwer Academic Publishers, Dordrecht/Boston/London, 2000 (English).

[34] ———, *Finite deformation beam models and triality theory in dynamical post-buckling analysis*, Internat. J. nonlinear Mech. **35** (2000), no. 1, 103–131.

[35] ———, *Complementarity, polarity and triality in non-smooth, non-convex and non-conservative Hamilton systems*, R. Soc. Lond. Philos. Trans. Ser. A Math. Phys. Eng. Sci. **359** (2001), no. 1789, 2347–2367, Non-smooth mechanics.

[36] ———, *Non-convex semi-linear problems and canonical duality solutions*, Advances in mechanics and mathematics. Vol. II, Adv. Mech. Math., vol. 4, Kluwer Acad. Publ., Boston, MA, 2003, pp. 261–312.

[37] ———, *Perfect duality theory and complete solutions to a class of global optimization problems*, Optimization **52** (2003), no. 4-5, 467–493, Theory, methods and applications of optimization.

[38] ———, *Canonical duality theory and solutions to constrained non-convex quadratic programming*, J. Global Optim. **29** (2004), no. 4, 377–399.

[39] D. Y. Gao (ed.), *Complementarity, duality and symmetry in nonlinear mechanics*, Advances in Mechanics and Mathematics, vol. 6, Boston, MA, Kluwer Academic Publishers, 2004.

[40] ———, *Complementary principle, algorithm, and complete solutions to phase transitions in solids governed by Landau-Ginzburg equation*, Math. Mech. Solids **9** (2004), no. 3, 285–305.

[41] ———, *Sufficient conditions and perfect duality in non-convex minimization with inequality constraints*, J. Ind. Manag. Optim. **1** (2005), no. 1, 53–63.

[42] ———, *Solutions and optimizality criteria to box constrained non-convex minimization problems*, J. Ind. Manag. Optim. **3** (2007), no. 2, 293–304.

[43] ———, *Dual extremum principles in finite deformation theory with applications to post-buckling analysis of extended nonlinear beam theory*, Applied Mechanics Reviews **50** (November 1997), 64–71.

[44] D. Y. Gao, J.-F. Li, and D. Viehland, *Tri-duality theory in phase transformations of ferroelectric crystals with random defects*, Complementarity, duality and symmetry in nonlinear mechanics, Adv. Mech. Math., vol. 6, Kluwer Acad. Publ., Boston, MA, 2004, pp. 67–84.

[45] D. Y. Gao and R. W. Ogden (eds.), *Advances in mechanics and mathematics 2002*, Advances in Mechanics and Mathematics, vol. 1, Kluwer Academic Publishers, Dordrecht, 2002.

[46] ———, *Complete solutions to the azimuthal shear problem in finite elasticity*, Technical Report, Department of Mathematics, Virginia Tech, 2006.

[47] ———, *Multiple solutions to non-convex variational problems with implications for phase transitions and numerical computation*, Q J Mechanics Appl Math **4** (2008), no. 61.

[48] D. Y. Gao, R. W. Ogden, and G. E. Stavroulakis (eds.), *Non-smooth/non-convex mechanics*, Non-convex Optimization and its Applications, vol. 50, Kluwer Academic Publishers, Dordrecht, 2001, Modeling, analysis and numerical methods, A volume dedicated to the memory of Professor P. D. Panagiotopoulos, Including papers from the minisymposium within the ASME Mechanics and Materials Conference held in Blacksburg, VA, June 27–30, 1999.

[49] D. Y. Gao and G. Strang, *Dual extremum principles in finite deformation elastoplastic analysis*, Acta Appl. Math. **17** (1989), no. 3, 257–267.

[50] ———, *Geometric nonlinearity: potential energy, complementary energy, and the gap function*, Quart. Appl. Math. **47** (1989), no. 3, 487–504.

[51] D. Y. Gao and H. Yu, *Multi-scale modeling and canonical dual finite element method in phase transitions of solids*, International Journal of Solids and Structures **45** (2008), 3660 3673.

[52] R. N. Gasimov, *Augmented Lagrangian duality and nondifferentiable optimization methods in non-convex programming*, J. Global Optim. **24** (2002), no. 2, 187–203.

[53] W. Gautschi, *Numerical analysis: an introduction*, Birkhauser, 1997.

[54] E. Giusti, *Direct methods in the calculus of variations*, World Scientific, Singapore, 2003.

[55] J. Giusti, *Numerical methods for engineers and scientists*, McGraw-Hill, New York, 2001.

[56] C. J. Goh and X. Q. Yang, *Duality in optimization and variational inequalities*, Optimization Theory and Applications, vol. 2, Taylor & Francis Ltd., London, 2002.

[57] G. H. Golub and C. F. Van Loan, *Matrix computations*, vol. 3, Johns Hopkins Univ Pr, 1996.

[58] R. Horst, P. M. Pardalos, and N. V. Thoai, *Introduction to global optimization*, second ed., Non-convex Optimization and its Applications, vol. 48, Kluwer Academic Publishers, Dordrecht, 2000.

[59] ———, *Introduction to global optimization*, second ed., Non-convex Optimization and its Applications, vol. 48, Kluwer Academic Publishers, Dordrecht, 2000.

[60] E. Infeld and G. Rowlands, *Nonlinear waves, solitons and chaos*, second ed., Cambridge University Press, Cambridge, 2000.

[61] R. James and D. Kinderlehrer, *Theory of diffusionless phase transitions*, PDEs and continuum models of phase transitions (Nice, 1988), Lecture Notes in Phys., vol. 344, Springer, Berlin, 1989, pp. 51–84.

[62] R. D. James, *Co-existent phases in the one-dimensional static theory of elastic bars*, Arch. Rational Mech. Anal. **72** (1979/80), no. 2, 99–140.

[63] C. Johnson, *Numerical solution of partial differential equations by the finite element method*, vol. 32, Cambridge university press Cambridge, 1987.

[64] C. T. Kelley, *Iterative methods for linear and nonlinear equations*, Frontiers in Applied Mathematics, vol. 16, Society for Industrial and Applied Mathematics (SIAM), Philadelphia, PA, 1995, With separately available software.

[65] R. V. Kohn, *The relaxation of a double-well energy*, Contin. Mech. Thermodyn. **3** (1991), no. 3, 193–236.

[66] K. A. Lurie and A. V. Cherkaev, *On a certain variational problem of phase equilibrium*, Material instabilities in continuum mechanics (Edinburgh, 1985–1986), Oxford Sci. Publ., Oxford Univ. Press, New York, 1988, pp. 257–268.

[67] R. J. Meziat and J. Villalobos, *Analysis of microstructures and phase transition phenomena in one-dimensional, nonlinear elasticity by convex optimization*, Struct. Multidiscip. Optim. **32** (2006), no. 6, 507–519.

[68] B. Noble and M. H. Sewell, *On dual extremum principles in applied mathematics*, Transactions of the Seventeenth Conference of Army Mathematicians (U.S. Army Missile Command, Redstone Arsenal, Ala., 1971), U.S. Army Res. Office-Durham, Durham, N.C., 1972, pp. 615–737. U.S. Army Research Office (Durham, N.C.), Report No. 72–1.

[69] J. Nocedal and S. J. Wright, *Numerical optimization*, second ed., Springer Series in Operations Research and Financial Engineering, Springer, New York, 2006.

[70] J. T. Oden and J. N. Reddy, *Variational methods in theoretical mechanics*, second ed., Universitext. [University Textbook], Springer-Verlag, Berlin, 1983.

[71] Pedregal P., *Equilibrium conditions for Young measures*, SIAM J. Control Optim. **36** (1998), no. 3, 797–813.

[72] K. C. Patidar, *On the use of nonstandard finite difference methods*, J. Difference Equ. Appl. **11** (2005), no. 8, 735–758.

[73] A. C. Pipkin, *Relaxed energy densities for small deformations of membranes*, IMA J. Appl. Math. **50** (1993), no. 3, 225–237.

[74] R. T. Rockafellar, *Convex analysis*, Princeton University Press., 1970.

[75] R. T. Rockafellar and Roger J.-B. Wets, *Variational analysis*, Grundlehren der Mathematischen Wissenschaften [Fundamental Principles of Mathematical Sciences], vol. 317, Springer-Verlag, Berlin, 1998.

[76] R. Rogers and L. Truskinovsky, *Discretization and hysteresis*, Physica B **233** (1997), 370–375.

[77] A. Rubinov and X. Yang, *Lagrange-type functions in constrained non-convex optimization*, Applied Optimization, vol. 85, Kluwer Academic Publishers, Boston, MA, 2003.

[78] A. M. Rubinov, X. Q. Yang, and B. M. Glover, *Extended Lagrange and penalty functions in optimization*, J. Optim. Theory Appl. **111** (2001), no. 2, 381–405.

[79] Y. Saad and Y. Saad, *Iterative methods for sparse linear systems*, PWS Pub. Co., 1996.

[80] E. K. H. Salje, *Phase transitions in ferroelastic and co-elastic crystals*, Cambridge University Press, Cambridge, United Kingdom, 1993.

[81] M. J. Sewell, *Maximum and minimum principles*, Cambridge Texts in Applied Mathematics, Cambridge University Press, Cambridge, 1987, A unified approach, with applications.

[82] I. Singer, *Duality for optimization and best approximation over finite intersections*, Numer. Funct. Anal. Optim. **19** (1998), no. 7-8, 903–915.

[83] D. J. Steigmann and R. W. Ogden, *Plane deformations of elastic solids with intrinsic boundary elasticity*, Proc. Roy. Soc. London Ser. A **453** (1997), no. 1959, 853–877.

[84] G. Strang, *Introduction to applied mathematics*, Wellesley-Cambridge Press, Wellesley, MA, 1986.

[85] G. Strang and R. Kohn, *Fibered structures in optimal design*, Ordinary and partial differential equations (Dundee, 1986), Pitman Res. Notes Math. Ser., vol. 157, Longman Sci. Tech., Harlow, 1987, pp. 205–216.

[86] W. G. Strang and G. J. Fix, *Analysis of the finite element method*, Prentice-Hall, 1973.

[87] J. C. Strikwerda, *Finite difference schemes and partial differential equations*, Society for Industrial Mathematics, 2004.

[88] R. Temam and G. Strang, *Duality and relaxation in the variational problems of plasticity*, J. Mécanique **19** (1980), no. 3, 493–527.

[89] P. T. Thach, *Global optimality criterion and a duality with a zero gap in non-convex optimization*, SIAM J. Math. Anal. **24** (1993), no. 6, 1537–1556.

[90] M. Tinkham, *Introduction to superconductivity, 2nd edition*, McGraw-Hill, New York, 1996.

[91] J. F. Toland, *Duality in non-convex optimization*, J. Math. Anal. Appl. **66** (1978), no. 2, 399–415.

[92] E. Tonti, *A mathematical model for physical theories. I, II*, Atti Accad. Naz. Lincei Rend. Cl. Sci. Fis. Mat. Natur. (8) **52** (1972), 175–181; ibid. (8) 52 (1972), 350–356.

[93] L. N. Trefethen and D. Bau, *Numerical linear algebra*, no. 50, Society for Industrial Mathematics, 1997.

[94] L. Truskinovsky and G. Zanzotto, *Ericksen's bar revisited: energy wiggles*, J. Mech. Phys. Solids **44** (1996), no. 8, 1371–1408.

[95] H. Tuy, *D.C. optimization: theory, methods and algorithms*, Handbook of global optimization, Non-convex Optim. Appl., vol. 2, Kluwer Acad. Publ., Dordrecht, 1995, pp. 149–216.

[96] A. Vainchtein, *Dynamics of phase transitions and hysteresis in a viscoelastic Ericksen's bar on an elastic foundation*, J. Elasticity **57** (1999), no. 3, 243–280 (2000).

[97] D. Zwillinger, *Handbook of differential equations*, second ed., Academic Press Inc., Boston, MA, 1992.